Application of Adaptive Trusses to Vibration Isolation in Flexible Structures

by

William Walker Clark

Dissertation submitted to the Faculty of the

Virginia Polytechnic Institute and State University

in partial fulfillment of the requirements for the degree of

Doctor of Philosophy

in

Mechanical Engineering

APPROVED:

Harry H. Robertshaw, Committee Chairman
Mechanical Engineering Department

Robert G. Leonard
Mechanical Engineering Department

Alfred L. Wicks
Mechanical Engineering Department

Scott L. Hendricks
Engineering Science and Mechanics Department

William T. Baumann
Electrical Engineering Department

December 5, 1991
Blacksburg, Virginia

Application of Adaptive Trusses to Vibration Isolation in Flexible Structures

by

William Walker Clark

Committee Chairman: Harry H. Robertshaw
Mechanical Engineering

Abstract

This dissertation presents techniques for using adaptive trusses for active vibration isolation in flexible structures. Passive methods have been used almost exclusively in the past for vibration isolation, although in the more recent literature active techniques have been proposed in an attempt to achieve greater isolation performance. Most of the active techniques, however, require either detailed knowledge of the system or of the disturbance to be isolated. This work focuses on techniques in which knowledge of the disturbance is minimal, and in some cases, knowledge of the system is not necessary. Two new active vibration isolation methods are presented which are based on feedback of transmitted forces in the system. The methods include force feedback through a high gain, and state feedback using the LQR method with disturbance modelling. A third method which has been demonstrated in the literature, force feedback through a classical compensator, is also presented for comparison. For the purpose of discussion, each of the methods is applied to a system which includes a single active mount. The methods are then applied analytically to an adaptive truss, which essentially contains multiple mounts, to demonstrate multi-degree-of-freedom active vibration isolation. It is shown that

force feedback provides two-way isolation, and its effects are independent of the type of active mount used (whether it is a force- or displacement-commanded mount). The most promising technique proves to be the simplest, the high-gain feedback method. This technique is a stable, model-free method of vibration isolation which places no restrictions on the type of system disturbance, other than that it must be within the actuator's bandwidth. The high-gain approach is applied experimentally and shown to agree with the simulated results.

Acknowledgements

I would first like to thank Harry Robertshaw for his encouragement and wealth of good ideas throughout the progress of this work. When I think back over the past few years, I can think of many words to describe Harry. The printable ones include "friend" and "coach", but more than anything I consider him to be my mentor from whom I have learned and will continue to learn much.

I would also like to thank the other members of my committee, Drs. Baumann, Hendricks, Leonard, and Wicks, for their guidance, and for always setting me straight when my grand ideas proved not to be so grand.

There were many people who provided assistance along the way, if not in the technical areas, then through motivational discussions (otherwise known as gripe sessions) and general good fun, including Dan Cole, Ken Ellis, Babak Kimiavi, Steve Rubenstein, Will Saunders, Bob Salerno, Paul Tidwell, Carmel Villiger, Tom Warrington, and Robert & Carol Wynn.

A special thanks goes to my parents and family who not only provided me with a place to go to keep it all in perspective, but they also always provided encouragement for me to pursue my individual interests.

I don't think I will ever be able to fully express my thanks to my wife, Laura, for her understanding during this work. Her willingness to endure the long nights when I was away and the times when I was there without really being there, all of which are hours that cannot be given back, is very much appreciated.

Contents

List of Figures

List of Tables

Nomenclature

Symbol	Definition	Unit
c	damping coefficient	kg/sec
D	transfer function denominator polynomial	
E	Young's modulus	N/m^2
f	force	N
f_c	control force	N
f_d	disturbance force	N
f_t	transmitted force	N
F_o	harmonic force amplitude	N
g	mode participation factor	1/kg
GF	generalized force	
GM	generalized mass	kg
G_l	lead screw gain	m/rad
G_m	motor gearhead gain	rad/rad
i_a	motor armature current	A
I	mass moment of inertia	$kg - m^2$
J	cost functional	
J_a	motor armature inertia	$kg - m^2$
J_{eq}	equivalent motor/leadscrew inertia	$kg - m^2$
J_{ls}	leadscrew inertia	$kg - m^2$
k	stiffness	N/m
k_b	motor back emf constant	V-s/rad
k_c	force feedback gain	V/N, N/N
k_t	motor torque constant	N-m/A
l	actuator link length	m
L_1, L_2, L_3, L_4	truss nominal link length	m
m	mass	kg
N	transfer function numerator polynomial	
q	mode displacement	m
Q_i	generalized force	

Symbol	Definition	Unit
R_a	motor armature resistance	Ω
s	Laplace variable	1/sec
S	sensitivity transfer function	
t	time	sec
T	kinetic energy	N-m
T_m	motor output torque	N-m
V	potential energy	N-m
V_{in}	motor input voltage	V
w	displacement	m
x	displacement	m
z	discrete time delay	
$\hat{\mathbf{a}}$, $\hat{\mathbf{b}}$, $\hat{\mathbf{c}}$, $\hat{\mathbf{d}}$, $\hat{\mathbf{e}}$	coordinate system unit vectors	
$\mathbf{A}$	system dynamics matrix	
$\mathbf{B}$	input dynamics matrix	
$\mathbf{C}$	damping matrix	
$\mathbf{C}_o$, $\mathbf{D}_o$	output dynamics matrices	
$\mathbf{d}$	disturbance input	
$\mathbf{F}$	forcing matrix	
$\mathbf{G}$	system open-loop transfer function matrix	
$\mathbf{H}$	feedback compensator matrix	
$\mathbf{I}$	identity matrix	
$\mathbf{K}$	stiffness matrix	
$\mathbf{K}_c$	feedback gain matrix	
$\mathbf{L}$	disturbance input matrix	
$\mathbf{M}$	mass matrix	
$\mathbf{P}$	modal transformation matrix	
$\mathbf{q}$	modal vector	
$\mathbf{Q}$	state cost matrix	
$\mathbf{R}$	control cost matrix	
$\mathbf{R}_i$	displacement vector	
$\mathbf{T}$	system dynamics matrix	
$\mathbf{u}$	control input	
$\mathbf{w}$	disturbance state vector	
$\mathbf{x}$	state vector	
$\mathbf{y}$	output vector	
$\mathbf{z}$	output vector	

Symbol	Definition	Unit
α	truss angular displacement	rad
β	truss top-link angular displacement	rad
δ	actuator displacement	m
ϵ	strain	m/m
ζ	damping ratio	
η	measurement noise	
θ_m	motor angular displacement	rad
ϕ	mode shape function	
ψ	truss link angular displacement	rad
ω_d	disturbance frequency	rad/sec
ω_n, ω_i	system natural frequency	rad/sec
ξ	stochastic disturbance	

Chapter 1

Introduction

There are many systems in our world in which proper performance depends on isolation of vibrations. Examples are wide ranging, but perhaps the most well-known is that shown in Fig. 1.1a, where an unbalanced machine places unwanted forces on its support. The frequency with which this example appears in textbooks has led to the phrase "vibration isolation" being most commonly associated with the problem of "mounting a machine in such a manner that no vibrations will appear in the structure to which it is attached" [Den Hartog, 1985]. The work presented in this dissertation addresses the vibration isolation problem; however, it is defined on a broader scale.

Figures 1.1b and 1.1c provide two more examples of vibration isolation; preventing vibrations arising in one part of a space structure from affecting another part, or reducing the effects of ground inputs on vehicles and their passengers, a problem more generally known as "support motion." These examples may also be considered vibration isolation problems if we allow our definition to read something like "vibration isolation is the minimization of transmitted vibrations between components of a system." The term "vibrations" in the preceding definition is somewhat vague, because it could represent, among other measures, displacements, velocities, or forces. All these measures are, of course, related and one cannot be changed

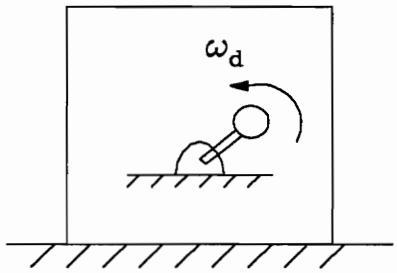

a. Unbalanced machine.

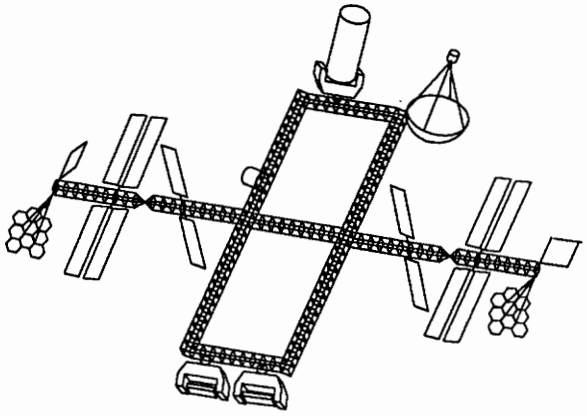

b. Large flexible space structure.

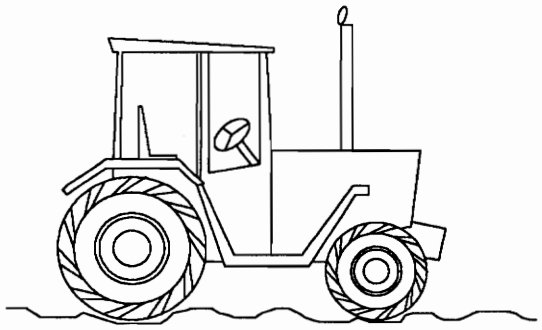

c. Ground input to vehicle.

Figure 1.1: Examples of systems which contain vibration isolation problems.

without affecting the others.

In the past, vibration isolation problems have been solved primarily with passive methods, such as the mounts which support machinery on a plant floor, or the seat suspension which carries a tractor operator and separates him from unwanted ground inputs. The primary role of these mounts is to support the static loads. Many times these static loads are large, which requires the stiffness of the mount to be high. As a mount becomes stiffer, however, its transmission of vibration becomes more complete (consider that a rigid connection passes all frequencies at the same magnitude), meaning that the static load specifications of a mount place a limit on the achievable passive vibration isolation.

A good example of where this idea arises in a day-to-day application are the engine mounts in a car. They are designed to be flexible to isolate high-frequency engine disturbances from the car's frame, but stiff enough to hold the engine in place, maintaining required clearances, as the car travels around turns and over hills. These stiffness characteristics cause the mount to act as a low-pass filter. At low engine speeds (when the car is idling, for example) significant forces may be transmitted from the engine. At high speeds, however, these transmitted forces are attenuated.

Understanding the performance requirements of passive vibration isolation systems helps us to envision the characteristics of an ideal mount. The stiffness of such a mount would behave as shown in Fig. 1.2, where it is very high at low frequencies (to meet the static load requirements), but falls off very quickly as we approach higher frequencies where transmitted forces may be undesirable [von Flotow, 1988]. There are limits to how closely a real system can approach those characteristics. An important consideration becomes what happens when the two regions in Fig. 1.2 overlap. In those cases, the passive approaches may not prove to be adequate, and

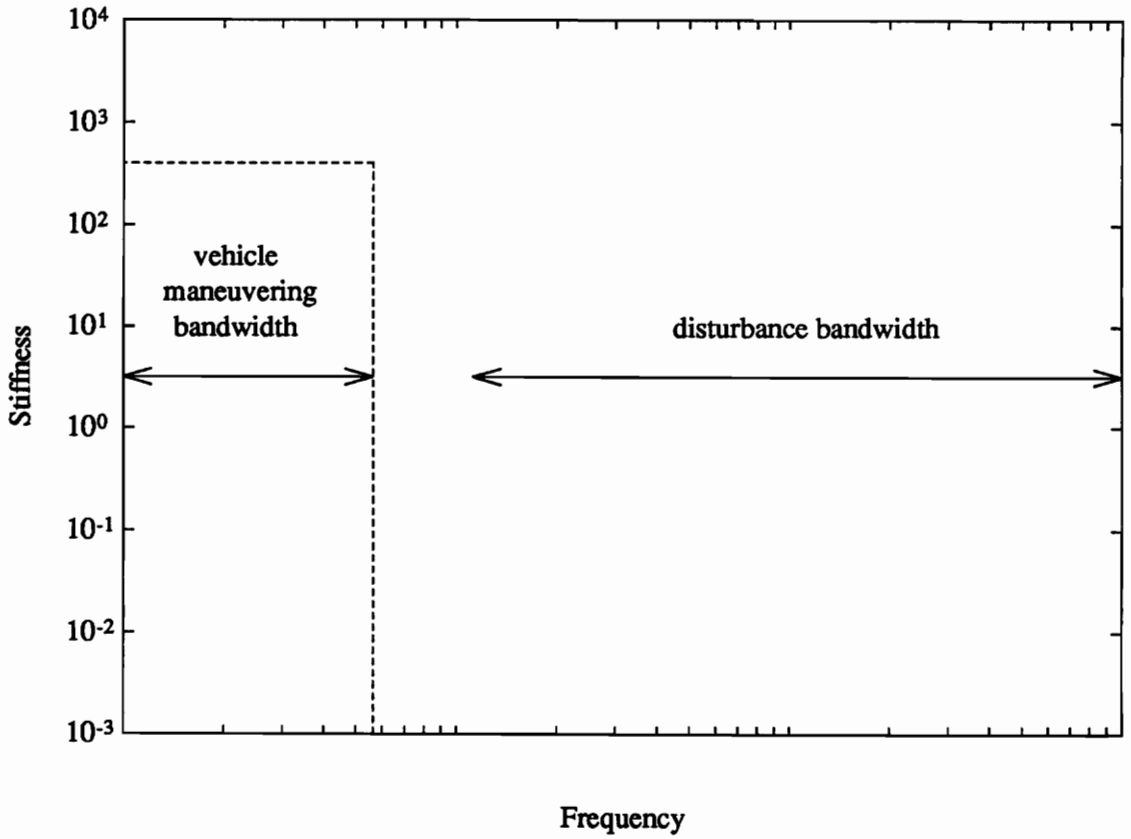

Figure 1.2: Ideal mount stiffness vs. frequency for vibration isolation (von Flotow [1988]).

alternative methods of vibration isolation may be required.

The approach taken in this work to solving the vibration isolation problem is to extend the historical passive techniques by activating the connecting mount. Passive techniques attempt to minimize the transmitted force in such a connecting mount, so it is reasonable to design active systems to do the same. Following this approach addresses the problem at the so-called vibration "bottleneck" [von Flotow, 1988], since all vibrations must pass through this hardware. This approach localizes the vibration problem, which is an alternative to many vibration suppression methods which address the problem "on the structure."

This brings us to the heart of the vibration isolation problem. The elimination of unwanted vibrations from a mechanical system may be addressed in two ways: 1) the vibrations may be suppressed in the system through the use of a vibration control scheme, or 2) they may be inhibited from entering the system through a vibration isolation scheme. This work addresses the latter.

We will follow the philosophy introduced by Kaplow [1980], in which the system is divided into a "dirty" side, the subsystem which sees the disturbances, and a "clean" side, the subsystem which is to be free from disturbances. The mount, of course, will be located between those two sides, and will be active. The purpose of the active mount will be to operate such that we are allowed to choose the forces that are transmitted from one side to another (for example, allow static loads to be carried, but inhibit high frequency loads, or inhibit regions below the passive roll-off frequency). This will do nothing to suppress the vibrations on the dirty side, but we are assuming that such vibrations either are not a problem or will be addressed through another control scheme.

Consider what happens when the two structures are ideally isolated from one another; no vibrations from either structure are passed to the other. In other words,

a free body diagram of either the clean or the dirty side would contain no force at the point of connection. So, if our control system is designed to always maintain the forces within the connector at zero, isolation will be achieved. A passive system does this, but only in a certain frequency range. Our concern here will be how to get an active mount to eliminate these connection forces.

Some of the questions that arise when we consider employing an active mount include the configuration of the mount itself, the actuation technique (does the mount effect a control force or a change in length, for example), and the required sensed variables (do we sense mount forces, positions, or accelerations, and do we use absolute or relative measurements?).

Control methods could be developed around the sensing of displacements, velocities, and accelerations, either absolute, at locations on the clean and dirty sides, or relative across the connector. Relative measurements will be difficult to implement. During isolation, either or both structures may be in motion, meaning that the relative displacements (and velocity and accelerations) across the connector will be constantly changing. Using a relative measurement, we could not design our control to drive the output to zero, and it would certainly be difficult to track the necessary displacement (or velocity or acceleration) paths over time, even if those paths could be determined. (Relative displacement measurements may still be necessary in order to maintain a nominal orientation of the structure, or to keep our mount "centered".)

Of the absolute measurements, accelerations and forces are the easiest to attain. It is possible to perform isolation using either of these measurements. Kaplow [1980] presents a technique for using acceleration measurements for active isolation, but it is clear that the purpose is "one-way" isolation. It is assumed that no vibrations originate on the clean side of the system. This work addresses the more general case

where vibrations occur on both sides of the system, and must be separated from one another. It is shown that force measurements can be used to achieve the necessary "two-way" isolation required in this case.

As for the mount configuration and its principle of actuation, these ideas will be discussed in detail in later chapters. It is interesting to note, though, that many isolation problems are not one-dimensional as Figs. 1.1a and 1.1c imply. Many times the mount transmits forces through several degrees of freedom. A particular case of interest is a large space structure, such as that in Fig. 1.1b. The mount used in this work is directed toward such a system.

Future space structures will be made up of trusses. The possibility of activating part of the truss (resulting in an "adaptive truss") and using it for vibration or motion control has been investigated in the past [Clark, 1989, 1990, Wynn, 1990, Warrington, 1990]. This work looks into using the same adaptive truss hardware for vibration isolation. By doing this we can localize the multiple-degree-of-freedom isolation problem to the individual links of the truss. These same techniques can then be applied to any multiple-degree-of-freedom isolation problem, be it a space structure or not. By sorting out the issues of single-degree-of-freedom active isolation and isolation with an adaptive truss, the foundation can be laid for addressing vibration isolation techniques which are distributed in nature, such as bearings which transmit forces in an infinite number of directions to their supporting structure.

Presented here are two new methods for active vibration isolation utilizing adaptive trusses. The first method involves a simple, local control law for each active link of an adaptive truss, where force feedback is used. This method is shown to be stable and to provide two-way isolation for wideband disturbances. The second method is an extension of LQG optimal control techniques for steady-state vibration control in which the cost is developed to achieve isolation, but to add no damping

to the system. Also presented are simple, classical control techniques which have been used in the literature for active isolation. Their performance provides a basis for comparison to the new methods. These methods are implemented analytically in flexible structures to highlight their strengths and weaknesses. Experimental results are also provided for simple force-feedback applied to an adaptive truss.

The following Chapters provide a review of the techniques, active and passive, which have been used in the past for vibration isolation, as well as other general control techniques which may be considered for active vibration isolation. Chapter 3 follows with a discussion of active force feedback, where we consider what it means to use feedback of the transmitted force for vibration isolation, and what can be achieved with this method. Chapter 4 contains a discussion of the possible active mount configurations, including their mathematical models, along with a description of the active mount used in this work. A discussion of three methods for active vibration isolation is taken up in Chapter 5, including their application to a simple system with a one-degree-of-freedom mount. Chapter 6 describes the analytical and experimental application of these techniques to a system with multiple mounts (an adaptive truss). Chapter 7 provides a wrap-up with conclusions that may be made from this work along with extensions in the way of recommendations for further work in the area of active vibration isolation.

Chapter 2

Literature Review

Many different techniques have been applied to the vibration isolation problem in the past. For years, only passive techniques were used, but with advancements in control theory and vibration control hardware, active techniques are becoming more popular. This chapter presents an overview of the vibration isolation field, starting with the well-established passive techniques, then moving on to the relatively newer active methods. The reader will then have a foundation from which to see the extensions made here in the active isolation arena and also see how those extensions relate to the passive methods.

2.1 Passive Techniques for Vibration Isolation

By far, the most widely used techniques for vibration isolation are passive. The following sections present three passive methods, altering a system's mass, stiffness, and damping, to achieve vibration isolation.

2.1.1 Designing Mount Stiffness and Damping

The most common method of passive vibration isolation is designing the stiffness and damping of a machinery mount so that very little force is passed in the frequency range of the disturbance. Figure 2.1 shows the system of Fig. 1.1a with a flexible

mount placed between the machine and its support. As mentioned before, this is a fundamental example of vibration isolation [Thomson, 1981, Den Hartog, 1985 James, 1989], in which the goal is to minimize the force transmissibility; the ratio of applied force to transmitted force (transmitted force being that force which is applied to the support). The transmissibility is plotted as a function of frequency for this system in Fig. 2.2. Note that a consequence of introducing flexibility in the mount is that a resonance is produced which must be avoided. We see that isolation is achieved as long as $\omega_d > \sqrt{2}\omega_n$, where ω_n is the system's natural frequency. This figure reiterates two important points about passive vibration isolation which were mentioned earlier. First, as the stiffness increases, ω_n increases, which means that for the same disturbance frequency, ω_d, we are operating at a higher point on the transmissibility curve. As the stiffness goes to infinity, the transmissibility goes to 1, after passing through the resonant peak, and the mount is rigid.

We also mentioned earlier that the characteristics of a good connecting mount are high stiffness at low frequencies (for vehicle maneuvering) and rapidly decreasing stiffness as ω_d increases, so that disturbances cannot be transmitted. This can be addressed in terms of transmissibility with Fig. 2.2. For any amount of damping the transmissibility approaches 1 as ω_d aproaches zero, which is desirable. For no damping, transmissibility falls off very quickly with frequency, but the uncapped resonant peak may be a problem. To reduce the effect of resonance, damping may be added, but this also serves to reduce the isolation achieved (as ζ approaches ∞, we get no resonant peak, but we also get no isolation at any frequency). The best case will be a tradeoff between the amount of damping needed at resonance and that allowed for effective isolation.

A summary of the results of designing passive spring/damper mounts, along with the ideal case, can be seen in Fig. 2.3, which plots transmissibility as a function of

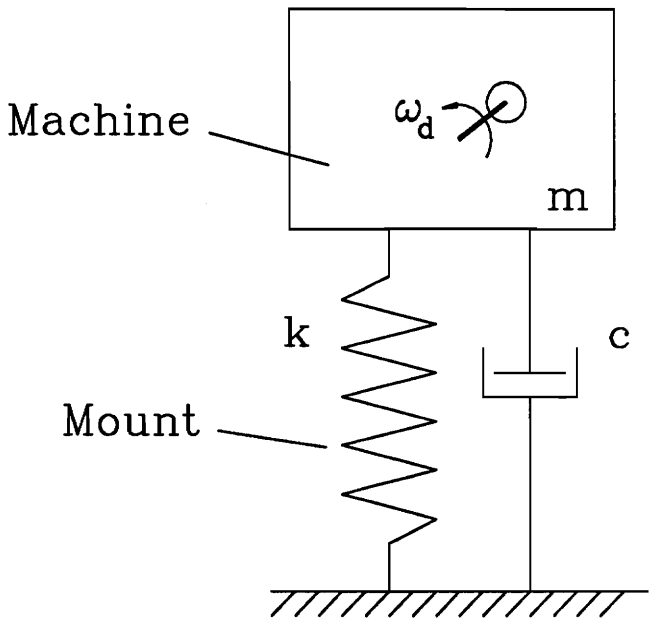

Figure 2.1: Unbalanced machine on flexible mounts.

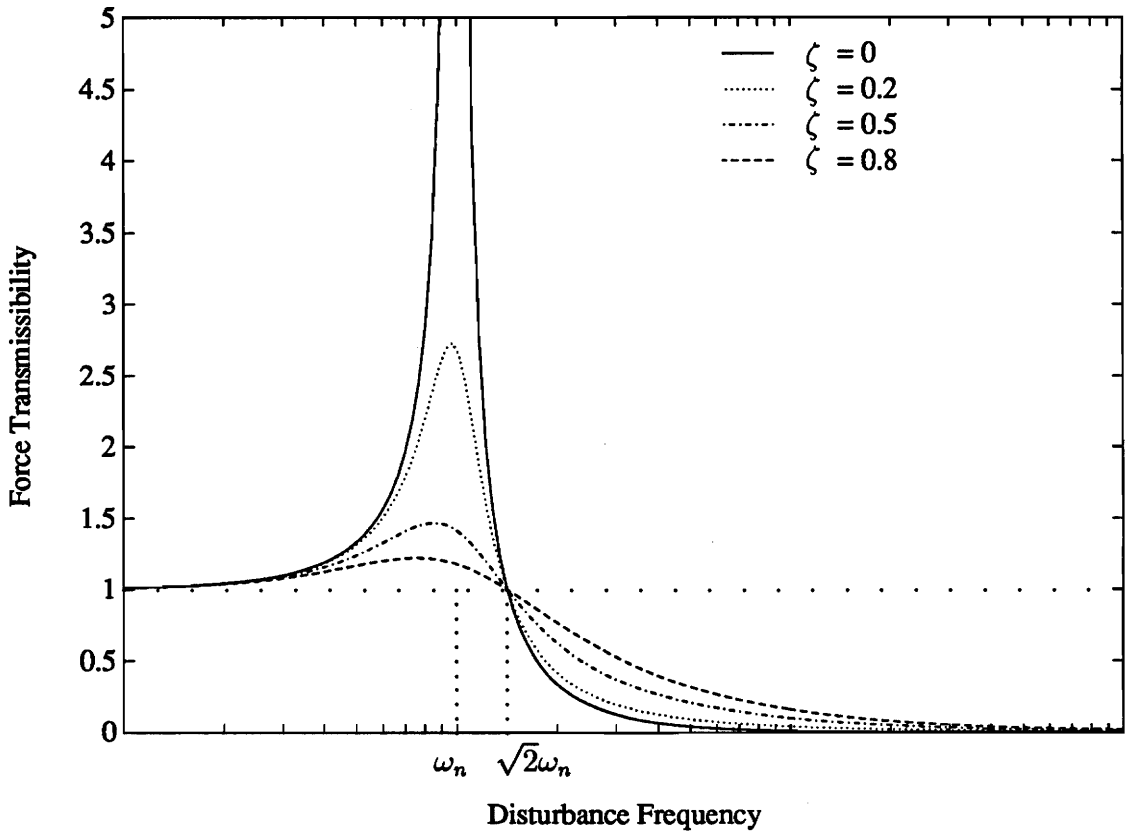

Figure 2.2: Force transmissibility for $\zeta = 0$, 0.2, 0.5, and 0.8 for system shown in Fig. 2.1.

frequency. This plot is similar to ones shown in Scribner, Eyerman [1990], and Sievers. Shown along with this are the regions of vehicle maneuver inputs which must be transmitted, and disturbance inputs which must be minimized.

2.1.2 Passive Tuned Vibration Absorber

A typical solution to the vibration isolation problem, although usually not intended for that purpose, is to design a vibration absorber [James, 1989, Thomson, 1981]. Consider again the single-degree-of-freedom system shown in Fig. 2.1 (let $c = 0$ to simplify the discussion). Transmitted force is equal to the spring force, which exists only if the mass is away from its equilibrium position. So, if the mass can be held at its equilibrium position, the transmitted force can be eliminated. The purpose of a tuned vibration absorber is to hold the mass motionless, so it can be thought of as a tuned isolator in this context.

The idea behind a vibration absorber is to add a second-order system to the existing system whose dynamics are such that the original mass remains motionless. Figure 2.4a illustrates such a system, where k_1 and m_1 comprise the original system and k_2 and m_2 the absorber. The amplitude of the response, $x_1(t)$, to input $F(t)$, can be written as

$$X_1 = \frac{\left(\frac{k_2}{m_2} - \omega_d^2\right)\frac{F_o}{m_1}}{\left(\frac{k_2}{m_2} - \omega_d^2\right)\left(\frac{k_1+k_2}{m_1} - \omega_d^2\right) - \frac{k_2^2}{m_1 m_2}} \tag{2.1}$$

which becomes zero for $\omega_d = \sqrt{\frac{k_2}{m_2}}$. The absorber parameters can then be chosen to "tune" the absorber to ω_d. The resulting transmissibility plot is shown in Fig. 2.5a.

2.1.3 Passive Tuned Mount

A tuned vibration isolation mount can be thought of as an "inversion" of the tuned absorber. Here, rather than adding a free-standing second-order system to the

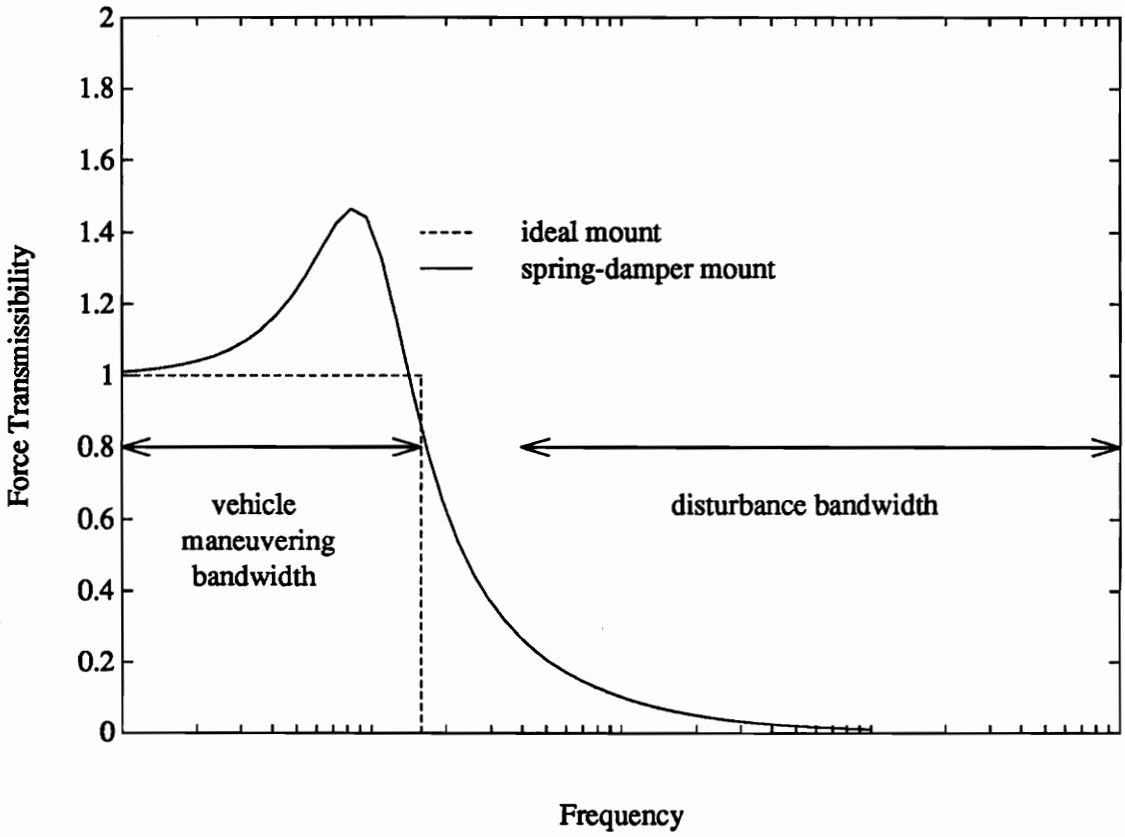

Figure 2.3: Transmissibility for spring/damper mount compared to that for ideal mount.

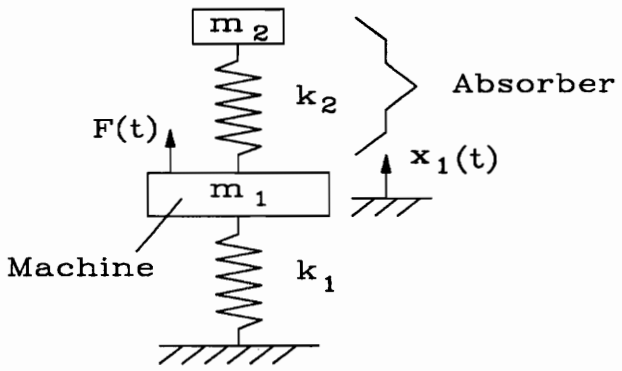

a. Tuned absorber.

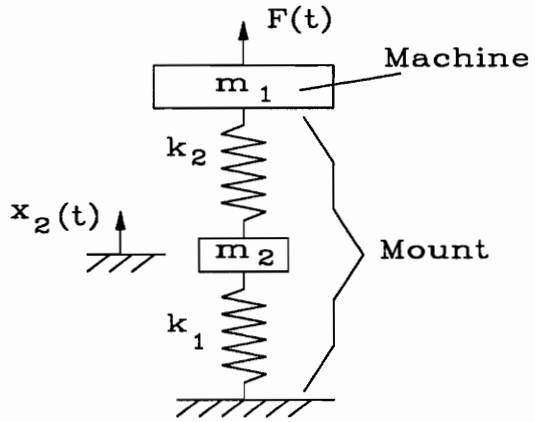

b. Tuned mount.

Figure 2.4: Illustration of tuned absorber and tuned mount.

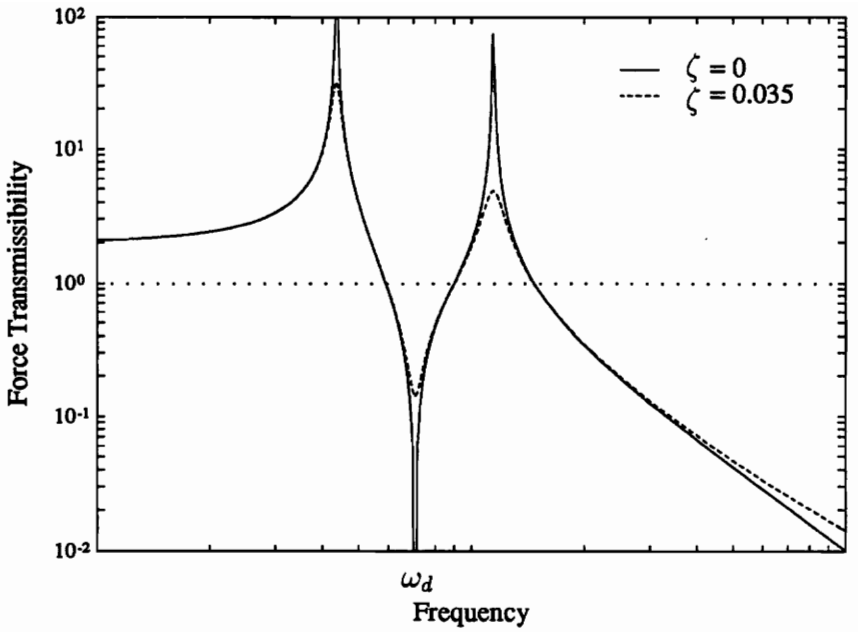

a. Transmissibility for tuned vibration absorber.

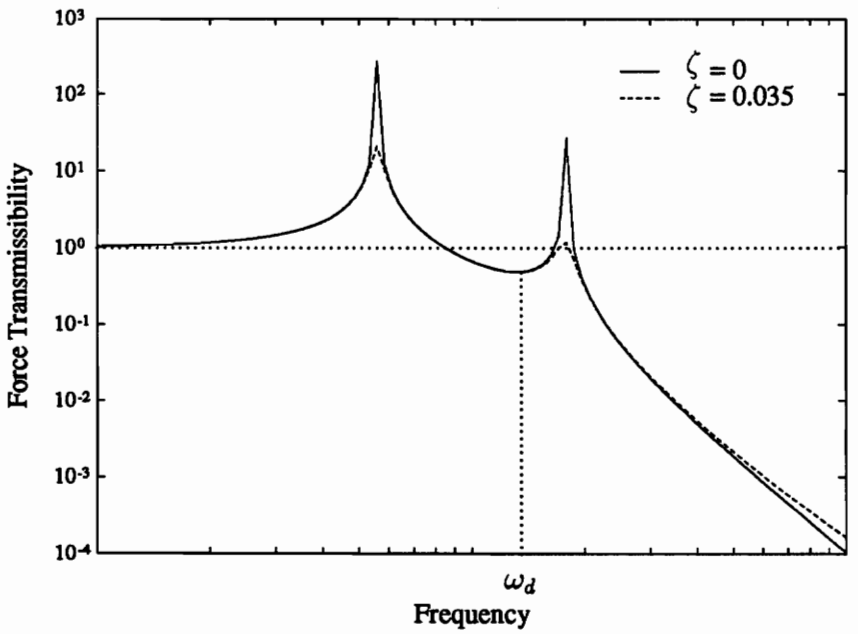

b. Transmissibility for tuned mount.

Figure 2.5: General transmissibility plots for tuned absorber and tuned mount.

machine, second-order dynamics are included in the mount, as shown in Fig. 2.4b. In this case, in order to eliminate transmitted force, we wish to maintain $x_2(t)$ at zero. The amplitude of the response, $x_2(t)$, to input $F(t)$ is slightly different than before and can be written as

$$X_2 = \frac{\frac{k_2}{m_1 m_2} F_o}{\left(\frac{k_2}{m_1} - \omega_d^2\right)\left(\frac{k_1+k_2}{m_2} - \omega_d^2\right) - \frac{k_2^2}{m_2 m_1}} \tag{2.2}$$

The parameters, k_1, k_2, and m_2 can now be used to design a mount which provides transmissibility less than one at the disturbance frequency, as shown in Fig. 2.5b.

Before leaving tuned absorbers and mounts, a few observations are appropriate. Note that each of these passive techniques is good for only one disturbance frequency. Each additional disturbance frequency which is to be minimized requires another degree-of-freedom to be added to the mount or absorber. These degrees-of-freedom, of course, consist of hardware, which may not be feasible in terms of space and weight.

The resonant peaks in Figs. 2.5a and 2.5b may be a problem if the disturbance frequency, ω_d, is not stationary, or if the absorber or mount is not properly tuned. These peaks can be spread apart by adjusting the ratio $\frac{m_1}{m_2}$, but this approach may not be practical if the other design parameters are constrained. Proper tuning is not as important for tuned mounts as for absorbers, though, because of the difference in "notch" shapes. The absorber's notch is much more severe. There is a tradeoff, though, in that the mount's notch cannot reach zero, while the absorber's can.

The resonant peaks can also be limited in magnitude by adding damping. The dashed lines in Figs. 2.5a and 2.5b show cases where slight damping (3.5% of original critical) is added in parallel with the springs. Both figures show the resonant peaks being reduced, but for the absorber, the notch is reduced as well. Adding damping in parallel with k_1 only (in the absorber) provides the best of both worlds in that it

reduces the peaks, but does nothing to the notch.

The types of tuned mounts presented here are restricted in their capabilities, and must be tuned properly, but they are often used in isolating ship-borne guns and machinery [Scribner, 1990, Eyerman, 1990].

2.2 Active Techniques for Vibration Isolation

We have seen that passive vibration isolation can be effective in some cases, but it does have limitations. Many times passive systems prove to be too restrictive either in their operating bandwidth or in their ability to attenuate amplitude of vibration. They are also limited in the instances where it is desirable to have the characteristics of the isolating system change during certain operating schemes (such as for disturbances with time-varying frequency content).

With the inherent limitations of passive systems, and with improvement of sensor and actuator technology and, to a great extent, computing power, active vibration isolation has become more popular. Active isolation allows much more flexibility than does passive isolation. The frequency response of an isolated system can be shaped more effectively, allowing wider bands of frequencies (or maybe more individual frequencies) to be isolated and, in some cases, more amplitude reduction. These benefits, however do not come about without expense. Active vibration isolation has its drawbacks, the most obvious of which are the need for actuators and sensors, computing hardware, and of course a source of power. These extras are in many cases in addition to passive isolation hardware which is used in mounting the active system to the structures or machines, or to "supplement" the active system [Laskin, 1988]. The drawbacks mentioned above are physical requirements of the system, but there are also "operational" considerations such as stability and robustness which may or may not make an active system feasible. These issues can be

adressed through control theory.

Many of the earlier methods for active vibration isolation are so-called "semi-active," which involve changing the passive system dynamics, or are active in the sense that they effectively place the system poles to provide a system with a more desirable response [Crosby, 1973, Karnopp, 1973, Thompson, 1976]. In either case, feedback is used to alter the stiffness and damping of a mount so that certain disturbances are isolated more effectively.

The most recent active techniques are those that use control forces within a mount in such a way that the resulting system is no longer restricted to the passive characteristics (with a damping-dependent resonant peak and roll-off) shown in Fig. 2.2. Kaplow's [1980] work, which has already been mentioned, is such a method. In that work, active mounts are used to apply forces between two structures based on acceleration measurements. The techniques to be discussed in the following sections are also those that fall into this category.

It has been mentioned that vibration isolation can be approached much the same as the suppression of steady-state disturbances in a mechanical system. The focus, however, is not on eliminating the structural response, but rather, the transmitted forces within connecting mounts. Many schemes have been developed with which to attack the disturbance rejection problem. The following pages provide a general discussion of each of those schemes, indicating the similarities and differences between them as well as examples of their use in vibration isolation.

We will begin our discussion with a development of the disturbance rejection problem from a controls standpoint. This will lead into a classical controls approach for solving the problem where some ideas will be introduced which have been shown to be a common thread throughout all active disturbance rejection techniques.

2.2.1 The Classical Disturbance Rejection Problem

A problem common to many systems can be described by Fig. 2.6a, where the plant can be represented by its transfer function $\mathbf{G}(s)$ (we will be concerned only with linear systems throughout this work, but will allow multi-input, multi-output systems, thus $\mathbf{G}(s)$ is, in general, a matrix), which describes the relationship between the system's output $\mathbf{y}$ to its input $\mathbf{u}$. Typical feedback control theory is concerned with affecting the way the system's output behaves for various inputs. Many systems, however also see a disturbance, shown as $\mathbf{d}$, which alters the output from its desired response. The object of disturbance rejection is to design a control system which rejects or eliminates $\mathbf{d}$ from the total response, $\mathbf{z}$. If $\mathbf{z}$ provides a measure of the vibration of the clean side of the system (acceleration or transmitted force, for example) then minimizing $\mathbf{z}$ will cause the clean side to be isolated with respect to the disturbance. This section gives a general overview of the disturbance rejection problem from the classical feedback standpoint, and it will be shown later that many other approaches can be viewed similarly.

The block diagram in Fig. 2.6a shows the disturbance entering the system at the output. In reality the disturbance could enter at the input, $\mathbf{u}$, or somewhere within the plant. With some modification of the block diagram, each of these situations can be represented by Fig. 2.6a [Maciejowski, 1989]. The output can be written as

$$\mathbf{z}(s) = \mathbf{y}(s) + \mathbf{d}(s) \tag{2.3}$$

or

$$\mathbf{z}(s) = \mathbf{G}(s)\mathbf{u}(s) + \mathbf{d}(s) \tag{2.4}$$

Recall that the goal of disturbance rejection is to eliminate that portion of $\mathbf{z}(s)$ which arises from $\mathbf{d}(s)$. In other words, we wish to modify the transfer function from $\mathbf{d}(s)$ to $\mathbf{z}(s)$ so as to minimize its response. To do this with feedback, we must

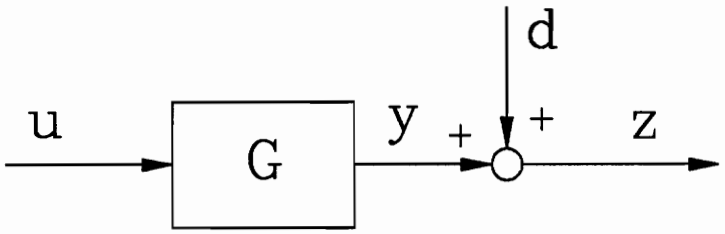

a. Typical plant on which disturbance acts.

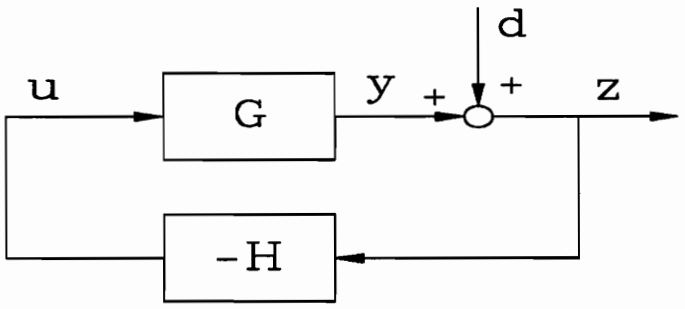

b. Illustration of feedback approach to disturbance rejection.

Figure 2.6: Block diagrams illustrating the classical disturbance rejection problem.

design a compensator so the control is of the form

$$\mathbf{u}(s) = -\mathbf{H}(s)\mathbf{z}(s) \tag{2.5}$$

The resulting closed-loop block diagram is shown in Fig. 2.6b. The transfer function from $\mathbf{d}(s)$ to $\mathbf{z}(s)$ becomes

$$\mathbf{z}(s) = [\mathbf{I} + \mathbf{G}(s)\mathbf{H}(s)]^{-1}\,\mathbf{d}(s) \tag{2.6}$$

or

$$\mathbf{z}(s) = \mathbf{S}(s)\mathbf{d}(s) \tag{2.7}$$

where $\mathbf{S}(s)$ is called the sensitivity transfer function. A magnitude plot of this function describes the amount of disturbance rejection achieved at various frequencies. In the regions where $\mathbf{S}(s)$ is small, very little disturbance shows up in the output.

The discussion may be simplified by addressing the single-input, single-output case. Here the sensitivity transfer function becomes

$$S(s) = \frac{1}{1 + G(s)H(s)} \tag{2.8}$$

From Eq. 2.8 it is easy to see that in order to make $S(s)$ small, we must make $G(s)H(s)$ large. Since, in most cases, $G(s)$ is fixed, we must design our compensator, $H(s)$, to achieve that goal. A typical Bode magnitude plot for such a plant and compensator is shown in Fig. 2.7, along with the resulting sensitivity magnitude plot. By designing the compensator such that the peak of the open-loop magnitude plot lies in the vicinity of the disturbance frequency, we get disturbance rejection to the degree shown in the closed-loop (sensitivity) magnitude plot. We have freedom to choose characteristics of the compensator such as the location and height of its magnitude peak and its bandwidth.

The freedom of design is limited by power requirements and available bandwidth of the controller, as well as stability considerations. In designing any compensator

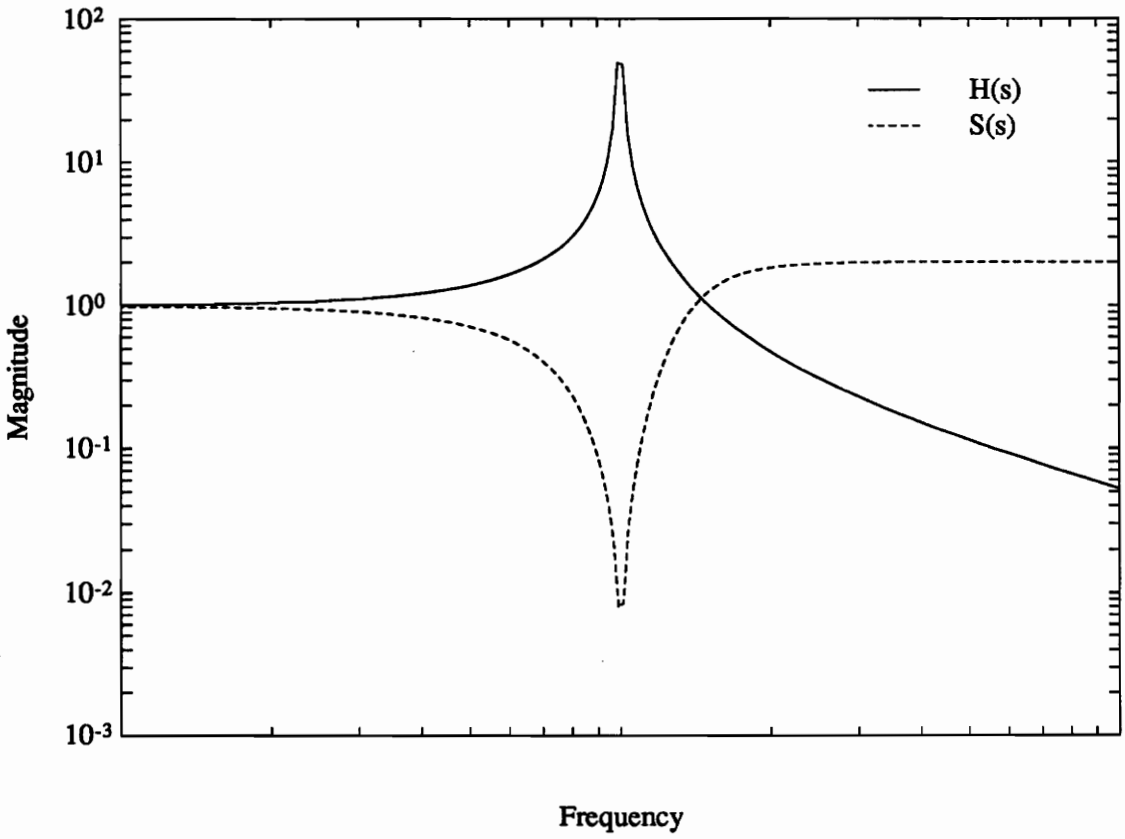

Figure 2.7: Typical Bode magnitude plot and resulting sensitivity plot for classical feedback compensator.

for this task, it is important to always insure that the resulting closed-loop system is stable. This is sometimes difficult to do considering uncertainities of the plant. Performance of the controller will most likely be compromised for stability [Hall, 1989, Sievers, 1990].

An example of a compensator designed to reject a pure harmonic disturbance can be written as

$$H(s) = \frac{c_1(s + c_2)}{s^2 + w_d^2} \tag{2.9}$$

where w_d is the disturbance frequency, and c_1 and c_2 are chosen to adjust the compensator's bandwidth as well as insure stability [Hall, 1989, Sievers, 1990]. Substituting this expression into Eq. 2.8, we see that since $H(s)$ is infinite at $s = j\omega_d$, the sensitivity is zero for a disturbance of that frequency, and the disturbance is rejected completely.

The reason for this rejection is that the poles of the compensator which form the open-loop peak become closed-loop zeros which form the notch in Fig. 2.7. We will see that each of the disturbance rejection methods to be discussed below in some way produce these closed-loop zeros, and can be related to the classical approach shown here.

Classical techniques have been used for active vibration isolation [Scribner, 1990, Sievers, 1990] in systems whose structural resonances are far from the disturbance frequencies. Their implementation has been through the use of the Higher Harmonic Control method, which will be discussed later.

2.2.2 Modern Controls–Stochastic Linear Quadratic Regulator

The Linear Quadratic Regulator (LQR) method is a full-state, optimal, feedback control method which is based on a linear plant model and a quadratic cost index.

Discussion of this technique is well-documented [Stengel, 1986, Kwakernaak, 1972]. This method has been studied extensively for its potential use in active (transient as well as steady-state) vibration control, however its use in vibration isolation has been limited. When optimal control methods such as this are used for vibration isolation [Thompson, 1976], the approach is to change the system response (effectively changing the passive isolation characteristics by altering the system stiffness and damping) rather than directly addressing the transmitted vibrations. An approach will be presented later which does address the transmitted vibrations, and thus the isolation problem.

The LQR method is a model-based, modern controls approach, so the system model is written as

$$\dot{\mathbf{x}} = \mathbf{A}\mathbf{x} + \mathbf{B}\mathbf{u} + \mathbf{L}\xi \tag{2.10}$$

$$\dot{\mathbf{y}} = \mathbf{C}_o\mathbf{x} + \mathbf{D}_o\mathbf{u} \tag{2.11}$$

where $\mathbf{x}$ is the state vector, $\mathbf{u}$ is the control, and ξ is the disturbance input. The feedback gains, $\mathbf{K}$, for this approach are determined by minimizing the cost functional

$$J = \int_0^{t_f} (\mathbf{x}^t\mathbf{Q}\mathbf{x} + \mathbf{u}^t\mathbf{R}\mathbf{u})dt \tag{2.12}$$

The control can then be written as

$$\mathbf{u} = -\mathbf{K}_c\mathbf{x} \tag{2.13}$$

If the disturbance can be described as uncorrelated, white noise, then the LQR method provides a stable closed-loop system whose response is optimally regulated as defined by the cost functional. If, however, the disturbance is "colored" noise, either narrow band or a broad spectrum of spikes, then the LQR method must be extended. The idea is to change the system representation so that its disturbance

input appears to be white noise. This, of course, is not the true disturbance input, so the difference is accounted for by altering the system model or the cost function. There are two common approaches found in the literature for handling a colored noise disturbance; disturbance modelling and frequency shaping of the cost functional.

Disturbance Modelling

First we will assume that the disturbance signal can be described by passing white noise through a filter such that the output is harmonic or is a narrow band of frequencies. This can be described by

$$\dot{\mathbf{w}} = \mathbf{A}_d\mathbf{w} + \mathbf{B}_d\xi \tag{2.14}$$

where $\mathbf{w}$ are the disturbance states, ξ is again a white noise input (note that in this case ξ is actually a fictitious white noise signal which is used only to help us formulate the problem, since the disturbance input to the LQR problem must be of this form), and $\mathbf{A}_d$ and $\mathbf{B}_d$ are the disturbance dynamics and input matrices, respectively. With this knowledge of the disturbance dynamics, the original state vector can be augmented to include the disturbance states, so that we have a new system which is of the same form as Eq. 2.10, where the disturbance input is white noise.

$$\begin{bmatrix} \dot{\mathbf{x}} \\ \dot{\mathbf{w}} \end{bmatrix} = \begin{bmatrix} \mathbf{A} & \mathbf{L} \\ \mathbf{0} & \mathbf{A}_d \end{bmatrix} \begin{bmatrix} \mathbf{x} \\ \mathbf{w} \end{bmatrix} + \begin{bmatrix} \mathbf{B} \\ \mathbf{0} \end{bmatrix} \mathbf{u} + \begin{bmatrix} \mathbf{0} \\ \mathbf{B}_d \end{bmatrix} \xi \tag{2.15}$$

This set of equations now describes a system which can be controlled using the standard LQR approach as described above. The resulting control law has two parts,

$$\mathbf{u} = -\begin{bmatrix} \mathbf{k}_c & \mathbf{k}_d \end{bmatrix} \begin{bmatrix} \mathbf{x} \\ \mathbf{w} \end{bmatrix} \tag{2.16}$$

The first part of the gain set, $\mathbf{k}_c$, are the feedback gains applied to the original system states, while the second part, $\mathbf{k}_d$, are gains applied to the disturbance states. Since the disturbance dynamics are uncontrollable, $\mathbf{k}_d$ should not be considered feedback gains in that they cannot change the eigenstructure of the disturbance. Rather, we should see $\mathbf{k}_d$ as feedforward gains which provide information about the disturbance to the controller so that it may be rejected. They are used to alter the control input in such a way as to cancel the disturbance from the output. Figure 2.8a shows a block diagram of the controlled system where this architecture is illustrated. When the control law of Eq. 2.16 is implemented, the system's frequency response is changed so that a notch is formed at each disturbance frequency. This effect is very similar to the sensitivity magnitude plot shown in Fig. 2.7.

Up to now we have seen how the LQR approach can be modified to handle colored disturbance inputs, but we have maintained the assumption of full state measurement, and we have also assumed that the disturbance states can be measured. In many cases all of the states cannot be measured, and none of the disturbance states are available. In addition the available measurement is taken from the system output where the disturbance and plant are combined. When this happens, an estimate of the system states and disturbance can be used in the control law.

Assume the measured variables can be written as

$$\begin{bmatrix} \mathbf{z} \\ \mathbf{z}_d \end{bmatrix} = \begin{bmatrix} \mathbf{H} & \mathbf{0} \\ \mathbf{0} & \mathbf{H}_d \end{bmatrix} \begin{bmatrix} \mathbf{x} \\ \mathbf{w} \end{bmatrix} + \eta \tag{2.17}$$

where η is gaussian, zero mean, white noise. This information can be used to form an estimate of the system and disturbance states by the equation

$$\begin{bmatrix} \dot{\hat{\mathbf{x}}} \\ \dot{\hat{\mathbf{w}}} \end{bmatrix} = \begin{bmatrix} \mathbf{A} & \mathbf{L} \\ \mathbf{0} & \mathbf{A}_d \end{bmatrix} \begin{bmatrix} \hat{\mathbf{x}} \\ \hat{\mathbf{w}} \end{bmatrix} + \begin{bmatrix} \mathbf{B} \\ \mathbf{0} \end{bmatrix} \mathbf{u} + \mathbf{K}_f \left(\begin{bmatrix} \mathbf{z} \\ \mathbf{z}_d \end{bmatrix} - \begin{bmatrix} \mathbf{H} & \mathbf{0} \\ \mathbf{0} & \mathbf{H}_d \end{bmatrix} \begin{bmatrix} \hat{\mathbf{x}} \\ \hat{\mathbf{w}} \end{bmatrix} \right) \tag{2.18}$$

where $\mathbf{K}_f$ are estimator gains found by minimizing the expression

$$E\left\{\left(\begin{bmatrix}\mathbf{x}\\ \mathbf{w}\end{bmatrix}-\begin{bmatrix}\hat{\mathbf{x}}\\ \hat{\mathbf{w}}\end{bmatrix}\right)\left(\begin{bmatrix}\mathbf{x}\\ \mathbf{w}\end{bmatrix}-\begin{bmatrix}\hat{\mathbf{x}}\\ \hat{\mathbf{w}}\end{bmatrix}\right)^t\right\} \tag{2.19}$$

This estimation approach is the standard Linear Quadratic Gaussian (LQG) method [Stengel, 1986, Kwakernaak, 1972] with the disturbance model augmenting the system equations. The modified block diagram for estimating the plant and disturbance states is shown in Fig. 2.8b. The estimates are obtained from the available system output (not necessarily including disturbance measurements), and the same LQR feedback gains are applied to form the control. The resulting notch is again much the same as that shown in Fig. 2.7.

Frequency Shaping of the Cost Functional

There is another popular method of disturbance rejection, known as "Frequency Shaping of the Cost Functional," which also utilizes the LQR approach. This method is based on the idea of penalizing the system states as a function of frequency, rather than as a constant across the frequency spectrum. In the typical LQR approach, the penalty matrices, $\mathbf{Q}$ and $\mathbf{R}$ in Eq. 2.12, are constant, therefore every frequency in the response is penalized equally. Since the objective in disturbance rejection (at least in the narrow band case we are dealing with) is to eliminate individual bands of frequencies from the system response, it seems reasonable to formulate the penalty as a function of frequency so that the narrow disturbance bands may be penalized more severely. The resulting cost function would look like

$$J=\int_{-\infty}^{\infty}\left(\mathbf{x}^*(j\omega)\mathbf{Q}(j\omega)\mathbf{x}(j\omega)+\mathbf{u}^*(j\omega)\mathbf{R}(j\omega)\mathbf{u}(j\omega)\right)d\omega \tag{2.20}$$

where * denotes complex conjugate. Gupta [1980] developed a method to implement the frequency dependent costs of Eq. 2.20. This amounts to posing the frequency

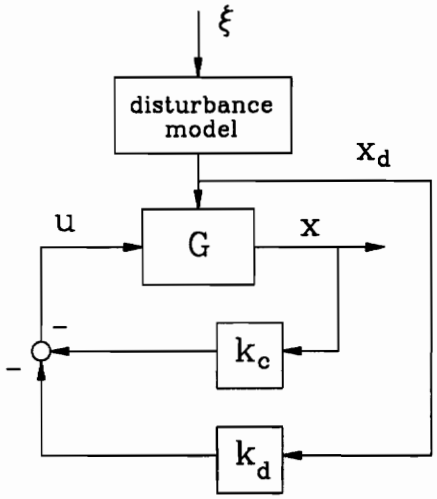

a. Full state LQR.

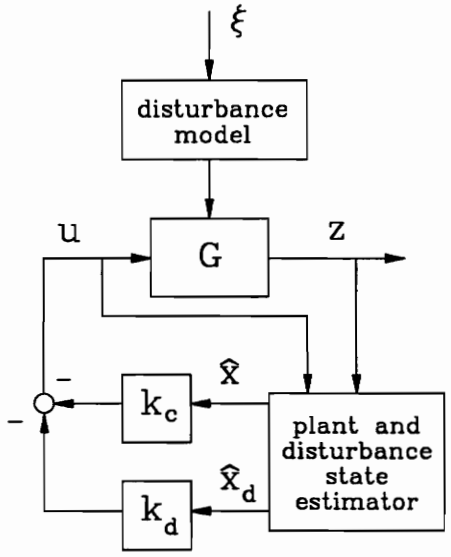

b. LQR with estimated states.

Figure 2.8: Block diagram illustrating LQR control with disturbance modelling (Sievers [1990]).

dependent cost matrix as a constant matrix but with new states added to the system description. First assume the cost matrix can be written as a rational function of frequency squared, ω^2.

$$\mathbf{Q}(j\omega) = \mathbf{P}^*(j\omega)\mathbf{P}(j\omega) \tag{2.21}$$

The matrix $\mathbf{P}$ can be defined by

$$\mathbf{P}(jw)\mathbf{z} = \mathbf{z}_f \tag{2.22}$$

where $\mathbf{z}$ is the system output and $\mathbf{z}_f$ is the "filtered" output. If $\mathbf{P}$ is a ratio of polynomials where the number of zeros does not exceed the number of poles, then Eq. 2.22 can be written as a system of differential equations whose input is the output of the original system, and whose outputs are contained in the vector $\mathbf{z}_f$.

$$\dot{\mathbf{x}}_f = \mathbf{A}_f\mathbf{x}_f + \mathbf{B}_f\mathbf{z} \tag{2.23}$$

$$\mathbf{z}_f = \mathbf{C}_f\mathbf{x}_f \tag{2.24}$$

We now have additional states with which the original system representation may be augmented to form a new set of system equations,

$$\begin{bmatrix} \dot{\mathbf{x}} \\ \dot{\mathbf{x}}_f \end{bmatrix} = \begin{bmatrix} \mathbf{A} & \mathbf{0} \\ \mathbf{B}_f\mathbf{C}_o & \mathbf{A}_f \end{bmatrix} \begin{bmatrix} \mathbf{x} \\ \mathbf{x}_f \end{bmatrix} + \begin{bmatrix} \mathbf{B} \\ \mathbf{0} \end{bmatrix} \mathbf{u} + \begin{bmatrix} \mathbf{L} \\ \mathbf{0} \end{bmatrix} \xi \tag{2.25}$$

and the extended cost functional becomes

$$J = \int_0^{t_f} \left(\begin{bmatrix} \mathbf{x}^t & \mathbf{x}_f^t \end{bmatrix} \begin{bmatrix} \mathbf{0} & \mathbf{0} \\ \mathbf{0} & \mathbf{C}_f^t\mathbf{C}_f \end{bmatrix} \begin{bmatrix} \mathbf{x} \\ \mathbf{x}_f \end{bmatrix} + \mathbf{u}^t\mathbf{R}\mathbf{u} \right) dt \tag{2.26}$$

Equations 2.25 and 2.26 are now in standard LQR form, where the cost functional contains constant penalty matrices, and may be solved to find optimal feedback gains. The block diagram representation for this method is shown in Fig. 2.9.

Note that this approach has allowed us to represent a frequency dependent cost function with constant matrices by augmenting the system states with appropriate

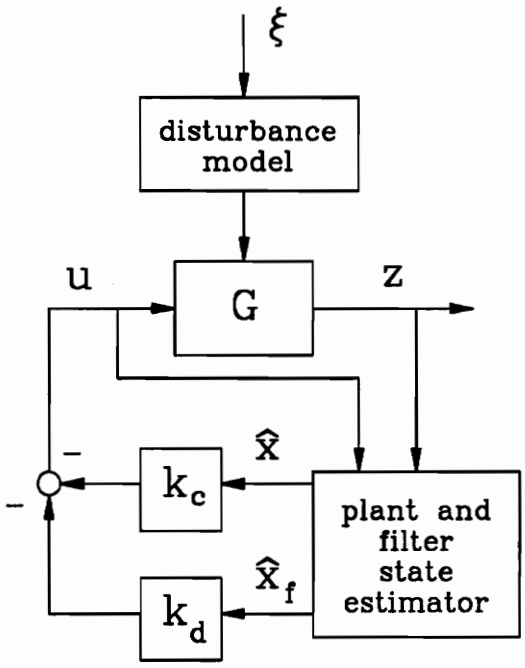

Figure 2.9: Block diagram illustrating LQR with frequency shaping of the cost functional (Sievers [1990]).

filter dynamics. By penalizing the filter states, we shape the cost as a function of frequency. If the filter is chosen such that it has poles at the disturbance frequencies, the penalty is higher at those frequencies, rather than being constant across the spectrum. Now, the filter output can be used in feedback so that the filter dynamics create the necessary zeros at disturbance frequencies, and notches are formed in the system's frequency response.

A typical filter shape may look like

$$P(s) = \frac{w_d^2}{s^2 + w_d^2} \tag{2.27}$$

which itself has a resonant peak at the frequency w_d, and works well for a sinusoidal (or narrowband) disturbance [Sievers, 1990]. By augmenting these dynamics to the system model, and filtering the system output before applying the feedback gains, we effectively penalize the region nearby w_d more than any other.

Gupta [1982] demonstrates linear quadratic regulator control with frequency shaping of the cost functional in a helicopter application. The control is implemented on an analytical model of a helicopter to reduce vibrations caused by the rotor. Cheok [1989] uses frequency-shaping LQ control in an active seat suspension control problem similar to that shown in Fig. 1.1c, where the operator must be isolated from ground inputs. Frequency shaping is utilized in this application by providing more disturbance rejection effort over the band of frequencies that cause the most discomfort to the operator, particularly the operator's resonant frequencies.

It is clear that the two LQ methods discussed here are similar (Sievers [1990] shows that they are the same), they each augment the system model with dynamics that describe frequency regions requiring increased control effort. The motivation for each method, however, is entirely different. In disturbance modelling an effort is made to model the dynamics of the unwanted disturbance to aid in rejection,

whereas in frequency shaping of the cost functional, no attention need be paid to the disturbance, the focus is placed on rejecting disturbances in the frequency regions where the most harm is done.

2.2.3 Higher Harmonic Control

Higher Harmonic Control (HHC) or Multicyclic Control describes a collection of active disturbance rejection techniques developed in the helicopter industry for suppressing the vibrations resulting from rotor dynamics. The purpose of these methods is to suppress vibrations due to periodic aerodynamic effects of the main rotor which increase maintenance requirements of the aircraft in the long term, and can reduce passenger comfort and pilot effectiveness in the short term. The unwanted vibrations occur at the rotor frequency and at integer multiples thereof, thus the reference to harmonics in the name.

This technique is well-suited for vibration isolation, because it effectively produces a classical compensator in the feedback loop which has complex poles centered at the frequency of the disturbance. If the disturbance signal (or a correlated signal) is available, then this compensator can be implemented to provide a self-tuning, narrowband, vibration isolation method. This technique is demonstrated for single-degree-of-freedom vibration isolation by Scribner [1990].

The HHC method discussed below is based on that developed by Shaw [1981, 1989], and is closely related to many in the literature [Hall, 1989, Johnson, 1982]. In this approach, the dynamics of the helicopter are described by a matrix, $\mathbf{T}$, called the control response matrix, which relates certain harmonics of the input to those same harmonics in the output. $\mathbf{T}$ is derived from a model of the helicopter, $\mathbf{G}(j\omega)$, evaluated at the disturbance frequency. The matrix $\mathbf{T}$, for a single input/single

output system can be written as

$$\mathbf{T} = \begin{bmatrix} a & b \\ -b & a \end{bmatrix} \tag{2.28}$$

where

$$\begin{aligned} a &= \text{Real}\,\{G(j\omega_d)\} \\ b &= \text{Imag}\,\{G(j\omega_d)\} \end{aligned} \tag{2.29}$$

Using this description for the plant, the sine and cosine components of the vibration output at the modelled disturbance frequency can be written as (for SISO system)

$$\mathbf{z} = \mathbf{T}\mathbf{u} + \mathbf{z}_d \tag{2.30}$$

where $\mathbf{z}$ is the vector of vibration amplitudes of the output, $\mathbf{u}$ is the vector of input amplitudes, and $\mathbf{z_d}$ is that part of the output which arises from the disturbance. Shaw's method involves cancelling the disturbance from the output with the control input, $\mathbf{u}$. Since $\mathbf{z}_d$ is unknown, the approach is to multiply the output by $\mathbf{T}^{-1}$, which will provide the control necessary to exactly cancel $\mathbf{z}_d$, from Eq. 2.30. The resulting control law, for the continuous-time case, is

$$\mathbf{u} = \mathbf{T}^{-1}\mathbf{z} \tag{2.31}$$

Figure 2.10 shows a block diagram which illustrates how such a controller would work. The forward loop contains the plant, whose output receives the disturbance, $\mathbf{d}$, to form the measured output, $\mathbf{z}$. The measurement is multiplied by $sin(\omega_d)$ and $cos(\omega_d)$ (ω_d is relatively easy to measure in a helicopter) and each branch is integrated to determine the sine and cosine components at the disturbance frequency. By multiplying these signals by the inverted plant, $\mathbf{T}^{-1}$, the necessary control signal is found which will cancel the disturbance from the output. The control signals are then modulated by $sin(\omega_d)$ and $cos(\omega_d)$ and added to form the command signal to the system.

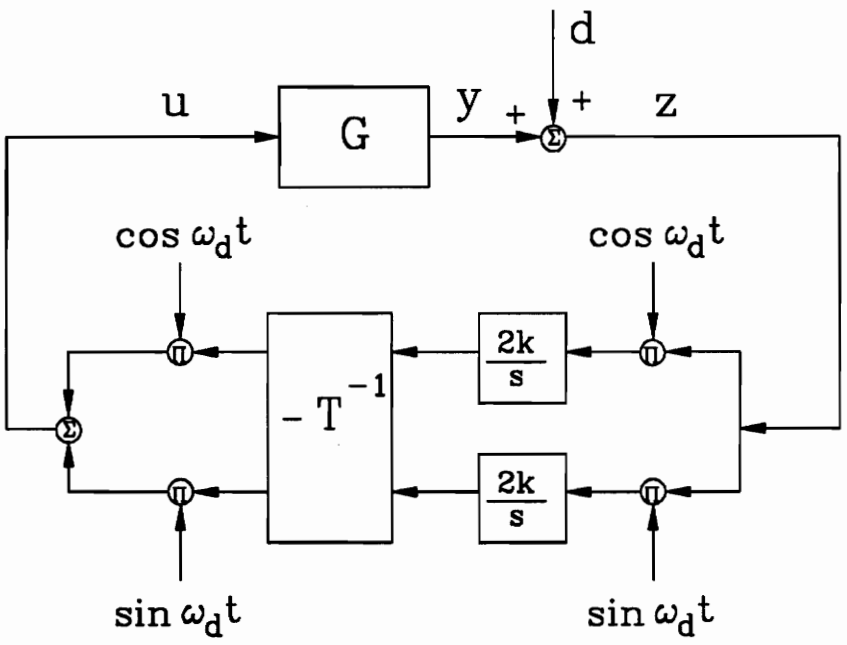

Figure 2.10: Block diagram representation of Shaw's Higher Harmonic Control method (Hall [1989]).

It will now be shown that this approach provides a controller which is very similar to the classical feedback controller shown previously. To do this, we will derive the transfer function for the feedback compensator [Hall and Werely, 1989] for the SISO case.

The system output, $z(t)$, is first modulated by $cos(w_d t)$ and $sin(w_d t)$ to form two terms which may be written as

$$\begin{aligned} z(t)cos(w_d t) &= z(t)\tfrac{e^{j\omega_d t}+e^{-j\omega_d t}}{2} \\ z(t)sin(w_d t) &= z(t)\tfrac{e^{j\omega_d t}-e^{-j\omega_d t}}{2j} \end{aligned} \tag{2.32}$$

Laplace transforming both sides, recalling that $\mathcal{L}\{f(t)e^{at}\} = F(s-a)$, and then integrating the result as shown in Fig. 2.10, leads to

$$\begin{aligned} z_c(s) &= \tfrac{2k}{2s}\left(z(s-j\omega_d) + z(s+j\omega_d)\right) \\ z_s(s) &= \tfrac{2k}{2js}\left(z(s-j\omega_d) - z(s+j\omega_d)\right) \end{aligned} \tag{2.33}$$

These terms are then multiplied by $\mathbf{T}^{-1}$ to provide two components of the control,

$$\begin{aligned} u_c(s) &= -\tfrac{1}{G_{\omega_d}}\left[az_c(s) - bz_s(s)\right] \\ u_s(s) &= -\tfrac{1}{G_{\omega_d}}\left[bz_c(s) + az_s(s)\right] \end{aligned} \tag{2.34}$$

where $G_{\omega_d} = a^2 + b^2$. The control components are again modulated by $cos(\omega_d t)$ and $sin(\omega_d t)$, and added, to form

$$u(t) = u_c(t)cos(\omega_d t) + u_s(t)sin(\omega_d t) \tag{2.35}$$

or, as in Eq. 2.33,

$$u(s) = \frac{1}{2}\left(u_c(s-j\omega) + u_c(s+j\omega)\right) + \frac{1}{2j}\left(u_s(s-j\omega) - u_s(s+j\omega)\right) \tag{2.36}$$

Substituting for u_s and u_c,

$$\begin{aligned} u(s) = &-\tfrac{1}{2}\left\{\tfrac{1}{G_{\omega_d}}\left[az_c(s-j\omega_d) - bz_s(s-j\omega_d)\right] + \tfrac{1}{G_{\omega_d}}\left[az_c(s+j\omega_d) - bz_s(s+j\omega_d)\right]\right\} \\ &+\tfrac{1}{2j}\left\{\tfrac{1}{G_{\omega_d}}\left[-bz_c(s-j\omega_d) + az_s(s-j\omega_d)\right] + \tfrac{1}{G_{\omega_d}}\left[-bz_c(s+j\omega_d) + az_s(s+j\omega_d)\right]\right\} \end{aligned} \tag{2.37}$$

Substituting for $z_c(s)$ and $z_s(s)$ evaluated at $s \pm j\omega_d$, the only terms which remain are those containing $z(s)$, resulting in

$$u(s) = -\frac{2k}{G_{\omega_d}} \frac{as + b\omega_d}{s^2 + \omega_d^2} z(s) \tag{2.38}$$

This describes the compensator transfer function, so

$$H(s) = \frac{2k}{G_{\omega_d}} \frac{as + b\omega_d}{s^2 + \omega_d^2} \tag{2.39}$$

which is the same as the classical compensator in Eq. 2.9 if we let $c_1 = \frac{2ka}{G_{\omega_d}}$ and $c_2 = \frac{b\omega_d}{a}$.

2.2.4 Adaptive Filtering

Another class of disturbance rejection methods which have gained popularity over the last few years are adaptive filtering techniques. Adaptive filtering is a feed-forward technique which involves cancelling a disturbance from a system's response with a reference input. Cancellation is achieved by first passing the reference input through a filter whose parameters are adjusted in such a way that the disturbance is eliminated from the system's response. The following sections will describe the basics of adaptive filtering, and will discuss their use in disturbance rejection.

Adaptive filters are typically finite impulse response (FIR) digital filters and can be implemented as shown in Fig. 2.11a which is a discrete implementation where z^{-1} indicates a delay of one time step. The transfer function for the block diagram shown in this figure can be written as

$$H(z) = w_0 + z^{-1}w_1 + \cdots + z^{-1}w_L \tag{2.40}$$

The character of this transfer function, and thus the filter's response for a given input can be altered by changing the parameters, w_i, of equation 2.40. By adapting

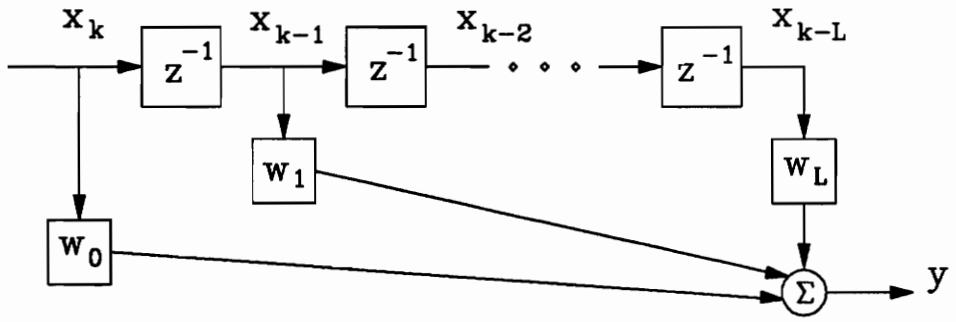

a. Digital filter block diagram.

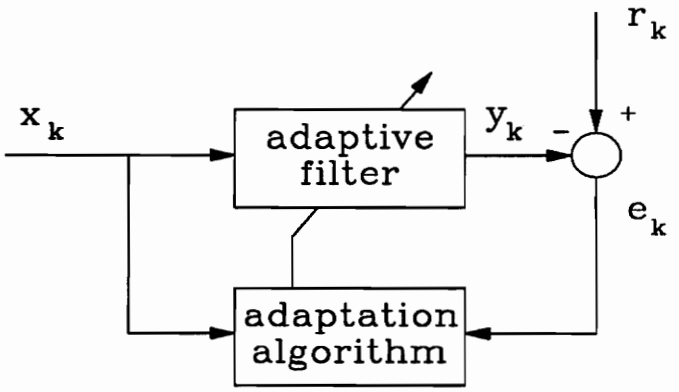

b. Standard use for an adaptive filter [Widrow, 1985].

Figure 2.11: Schematics for adaptive filtering.

these parameters we can no longer represent the filter as a transfer function, but we can express the output as a function of the input by

$$y_k = \mathbf{X}_k^t \mathbf{W}_k \tag{2.41}$$

where

$$\begin{aligned} x_k &= \left[\; x_k, \;\; x_{k-1}, \;\; . \;\; . \;\; . \;\; x_{k-L} \; \right]^t \\ w_k &= \left[\; w_{0_k}, \;\; w_{1_k}, \;\; . \;\; . \;\; . \;\; w_{L_k} \; \right]^t \end{aligned} \tag{2.42}$$

A typical use for such an adaptive filter can be illustrated by Fig. 2.11b. This figure shows a system in which an adaptation algorithm adjusts the structure of a filter so that its output, y, is equal to a desired output, r. This example is representative of many adaptive filtering processes, so it will be briefly discussed to introduce the concepts involved in adaptive filtering. First the underlying idea will be introduced, followed by a description of the various adaptation algorithms used. Following this will be a discussion of how this technique is used in disturbance rejection, focusing on the least-mean-square (LMS) algorithm.

The adaptation algorithms discussed here are based on minimizing the error signal, e, shown in Fig. 2.11b. The error can be written as (the following development can be found in Widrow [1985])

$$e_k = r_k - y_k \tag{2.43}$$

where the subscript, k, is a time index. If $e_k = 0$, then $r_k = y_k$, and the objective of matching the output with the desired response is met. From Eq. 2.41 the error can be written as

$$e_k = r_k - \mathbf{X}_k^t \mathbf{W}_k \tag{2.44}$$

Typically, the squared error is chosen as a performance measure, so

$$e_k^2 = r_k^2 + \mathbf{W}_k^t \mathbf{X}_k \mathbf{X}_k^t \mathbf{W}_k - 2 r_k \mathbf{X}_k^t \mathbf{W}_k \tag{2.45}$$

If we assume that $\mathbf{W}_k$ is constant (or slowly changing compared to the other variables) and e_k, x_k, and r_k are statistically stationary, the expected value of the squared error is found to be

$$E\left[e_k^2\right] = E\left[r_k^2\right] + \mathbf{W}^t E\left[\mathbf{X}_k \mathbf{X}_k^t\right] \mathbf{W} - 2E\left[r_k \mathbf{X}_k^t\right] \mathbf{W} \tag{2.46}$$

By defining the "input correlation matrix," $\mathbf{R}$, as

$$\mathbf{R} = E\left[\mathbf{X}_k \mathbf{X}_k^t\right] \tag{2.47}$$

and the vector of cross correlations between the inputs and the desired response as P,

$$\mathbf{P} = E\left[r_k \mathbf{X}_k\right] \tag{2.48}$$

The mean-square error can now be expressed as

$$MSE = \xi = E\left[e_k^2\right] = E\left[r_k^2\right] + \mathbf{W}^t \mathbf{R} \mathbf{W} - 2\mathbf{P}^t \mathbf{W} \tag{2.49}$$

Equation 2.49 is quadratic in the filter weights so the surface defined by the mean-square error as a function of the filter weights is a paraboloid (or a hyperparaboloid for a filter with more than two weights). The purpose of the adaptation algorithm, then, in Fig. 2.11b is to adjust the filter weights so that system operates at the "bottom of the mean-square error bowl."

LMS Algorithm

There are several methods used for finding the filter weights which minimize the mean-square error. Two popular methods, Newton's Method and the Method of Steepest-Descent, discussed in chapters 4 and 5 of Widrow [1985], involve searching the parabolic performance surface defined by Eq. 2.49 for its minimum using gradient approaches. The LMS algorithm is developed by taking e_k^2 itself as an estimate

for the mean-square error. A gradient estimate of ξ can now be formed at each time step by

$$\hat{\nabla}_k = \begin{bmatrix} \frac{\partial e_k^2}{\partial w_0} \\ \cdot \\ \cdot \\ \cdot \\ \frac{\partial e_k^2}{\partial w_L} \end{bmatrix} = 2e_k \begin{bmatrix} \frac{\partial e_k}{\partial w_0} \\ \cdot \\ \cdot \\ \cdot \\ \frac{\partial e_k}{\partial w_L} \end{bmatrix} = -2e_k \mathbf{X}_k \tag{2.50}$$

The last step of the above equation follows from Eq. 2.44. With this estimate of the error, a steepest-descent type of adaptation algorithm can be formed. A general steepest-sescent method can be written as

$$\mathbf{W}_{k+1} = \mathbf{W}_k + \mu(-\nabla_k) \tag{2.51}$$

and involves moving in the direction of the negative of the gradient at each time step. The speed with which this process unfolds depends on μ. Substituting for the gradient in Eq. 2.51 with the estimate shown in Eq. 2.50, we have

$$\mathbf{W}_{k+1} = \mathbf{W}_k + 2\mu e_k \mathbf{X}_k \tag{2.52}$$

This is the LMS algorithm [Widrow 1960, 1970].

Use of LMS Algorithm for Disturbance Rejection

Figure 2.12a shows how the LMS algorithm can be used to cancel a disturbance signal applied to the plant. This particular block diagram arrangement is called the "filtered-x" LMS algorithm because the reference input, x, is first filtered by a model of the plant before entering the LMS algorithm. This change was necessary for disturbance cancelling applications because without it the adaptive filter may be unstable or converge to an irrelevant solution [Widrow, 1985]. Consider the block diagram in Fig. 2.12a without the plant model in the loop which enters the LMS block. The reference and error signals both enter the LMS algorithm to form the

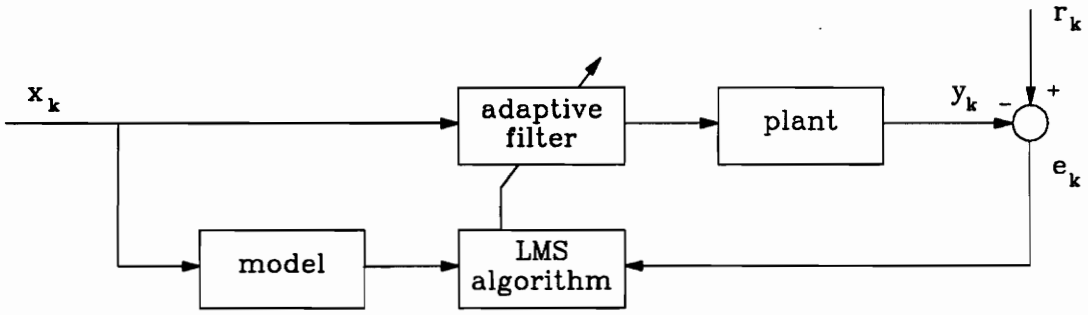

a. The filtered-x LMS algorithm used for disturbance cancelling (Miller [1988]).

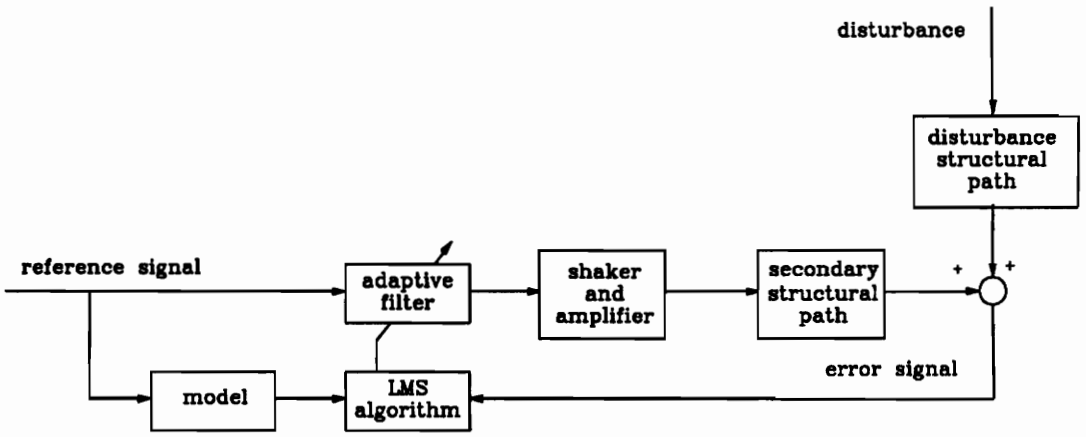

b. A detailed block diagram of the filtered-x LMS algorithm used for disturbance rejection (Miller [1988]).

Figure 2.12: The filtered-x LMS algorithm.

new adaptive filter weights. The reference signal is also applied to the adaptive filter which applies an input to the plant, and thus causes a disturbance cancelling response. There is a delay in that process as the reference signal makes its way from the adaptive filter to the plant output where it shows up in the error signal. If the plant model is not in the lower loop, then the error signal entering the LMS block is not properly phased with the reference input at any instant in time. This leads to improper adjustment of the adaptive filter.

Fig. 2.12b shows a more detailed block diagram illustrating how the procedure of Fig. 2.12a is used to cancel a disturbance in a vibrating system. This figure shows a disturbance entering the plant and causing an unwanted response. To cancel that response, a reference signal (correlated with the disturbance) is passed through an adaptive filter and applies a second input to the structure whose response adds to that of the original disturbance. The LMS algorithm adapts the filter parameters such that the two responses add destructively, and neither appear in the end. In this system, the model represents those blocks from the output of the adaptive filter to the response of the "secondary structural path." In practice, the model itself is a filter whose weights have been found by an adaptive modelling process described in Widrow [1985].

The method described in Fig. 2.12b is widely used for disturbance rejection. Elliot [1987] presents an algorithm for incorporating multiple error signals into the adaptation process and demonstrates the method by attenuating low-frequency sound. Fuller [1989] uses the multiple-error filtered-x LMS algorithm in actively controlling sound transmission through an elastic plate using point force actuators on the plate for control inputs. Microphones are used as the error sensors in one experiment and accelerometers mounted on the plate are used in another. In further work Fuller [1989] examines the use of piezoceramic actuators mounted to the

surface of an elastic plate for controlling certain vibrational modes. Miller [1988] presents an analytical work in which the filtered-x LMS algorithm is used for vibration isolation in a three degree-of-freedom lumped-mass system and in a flexibly mounted plate. The disturbances were a sum of two sinusoids for the former system and a single sinusoid for the latter, while the reference signals were taken to be similar to the disturbance, shifted in amplitude or phase. Control forces were applied in parallel with the mounts, and error signals were taken to be the response of each flexible support just below the mount. Vibration isolation was, of course, achieved when the error signals (and thus the support motion) were maintained near zero. Plant models used to filter the reference input were assumed to be available from previous work. Simulations showed that vibration isolation was achievable using the filtered-x LMS algorithm in this manner. Convergence rates were, in general, good, unless disturbance frequencies were in the neighborhood of structural resonances, in which case stability concerns dictated that convergence rates be small.

Comparison to Classical Method

An analog implementation of the filtered-x LMS algorithm was used by Scribner [1990] to perform vibration isolation. This technique was analyzed by Sievers [1990] to show that it has the characteristics of the classical disturbance rejection method described by Eq. 2.9. A block diagram representing an analog SISO implementation of the filtered-x LMS algorithm is shown in Fig. 2.13. This figure, and the following derivation, is similar to that given in Sievers work.

To show that the system in Fig. 2.13 is similar to the classical approach, we will derive the transfer function, $H(s)$, from the error signal, $E(s)$, to the control input, $U(s)$. The reference signal, $x(t)$, is assumed to be sinusoidal of the same frequency as the disturbance. For this derivation the reference signal is assumed to be $cos(\omega_d t)$

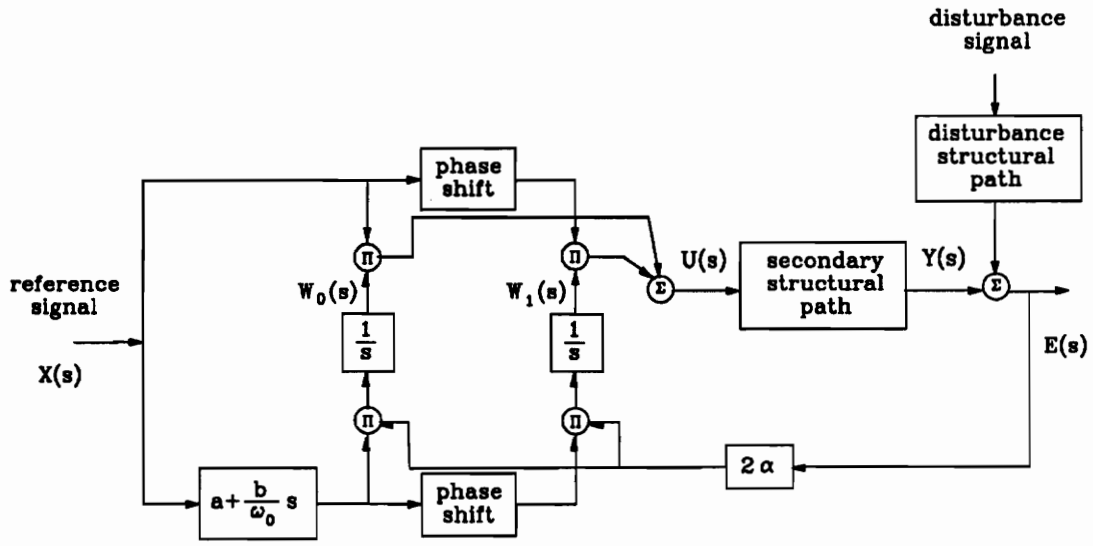

Figure 2.13: Analog single-input single-output implementation of filtered-x LMS algorithm for disturbance rejection (Sievers [1990]).

and the phase shift equal to 90°. The control input, as a function of time is

$$u(t) = w_0(t)cos(\omega_d t) + w_1(t)cos(\omega_d t - 90°) \tag{2.53}$$

where w_0 and w_1 are the adaptive filter weights. In the Laplace domain, this becomes (using the same approach as in Eq. 2.33 and 2.32)

$$U(s) = \frac{1}{2}\left[W_0(s - j\omega_d) + W_0(s + j\omega_d) - jW_1(s - j\omega_d) + jW_1(s + j\omega_d)\right] \tag{2.54}$$

By the same token, the expressions for the filter weights can be written as

$$\begin{aligned} W_0(s) &= \tfrac{\alpha}{s}\left[aE(s - j\omega_d) + aE(s + j\omega_d) + bjE(s - j\omega_d) - bjE(s + j\omega_d)\right] \\ W_1(s) &= \tfrac{\alpha}{s}\left[-ajE(s - j\omega_d) + ajE(s + j\omega_d) + bE(s - j\omega_d) + bE(s + j\omega_d)\right] \end{aligned} \tag{2.55}$$

Substituting the expressions of Eq. 2.55 into Eq. 2.54 leads to

$$\begin{aligned} U(s) \;=\; & \tfrac{\alpha}{2}\tfrac{1}{s^2+\omega_d^2}\left[(s + j\omega_d)(a - bj) + (s - j\omega_d)(a + bj)\right]E(s) \\ & -\tfrac{j\alpha}{2}\tfrac{1}{s^2+\omega_d^2}\left[(s + j\omega_d)(aj + b) - (s - j\omega_d)(-aj + b)\right]E(s) \end{aligned} \tag{2.56}$$

where all the terms containing $E(s \pm 2j\omega_d)$ cancel after the substitution. This equation can be reduced to form the transfer function

$$H(s) = \frac{U(s)}{E(s)} = \frac{2\alpha(as + b\omega_d)}{s^2 + \omega_d^2} \tag{2.57}$$

which is the same as the classical compensator in Eq. 2.9 if we let $c_1 = 2\alpha a$ and $c_2 = \frac{b\omega_d}{a}$.

2.2.5 Adaptive Control

Adaptive control is a generalization of classical linear feedback control in which the controller characteristics are adapted based on measurements of the system inputs, outputs, and disturbances, with the intention of meeting some performance criteria. The field can generally be broken down into two classifications, model reference adaptive controllers and self-tuning regulators. Even though lately there has been

some discussion in the literature that these two distinct classes are in fact one, this survey will stick to the separate classification. The following sections will provide an overview of model reference adaptive control and self-tuning regulation and will give examples of their use in vibration isolation.

Model Reference Adaptive Control

Model reference adaptive control (MRAC) was introduced in 1958 for design of aircraft flight control systems [Chalam, 1987]. Since then, much research has been devoted to this technique, in applications and in developing design techniques and stability theory. The basic idea behind model reference adaptive control is shown in Fig. 2.14a [Jacobs, 1981, Chalam, 1987, Astrom, 1989]. The goal is to make the output of an unknown plant (or a plant with time-varying parameters) approach the output of a desired reference model. The input to the plant first passes through a controller whose characteristics are adjustable. The input also enters a reference model which gives a desired response. By comparing the desired response to the plant's response, a performance index (error signal) is obtained which becomes a driver for an adaptation mechanism that in turn adjusts the parameters of the controller. The adjustment continues until the error signal becomes zero, at which point the goal is achieved; the plant's output matches the desired output.

Model reference adaptive control has been applied to active vehicle suspension systems [Sunwoo, 1990a]. In this work the vibration isolation problem is inverted, the excitation is "support-motion" rather than excitation within the machine as in many of the previous examples, but this is vibration isolation nonetheless. The goal is to reduce the vehicle's response to road inputs in spite of changing vehicle and suspension characteristics (particularly vehicle mass).

Sunwoo's approach is to propose an ideal model for the vehicle and suspension

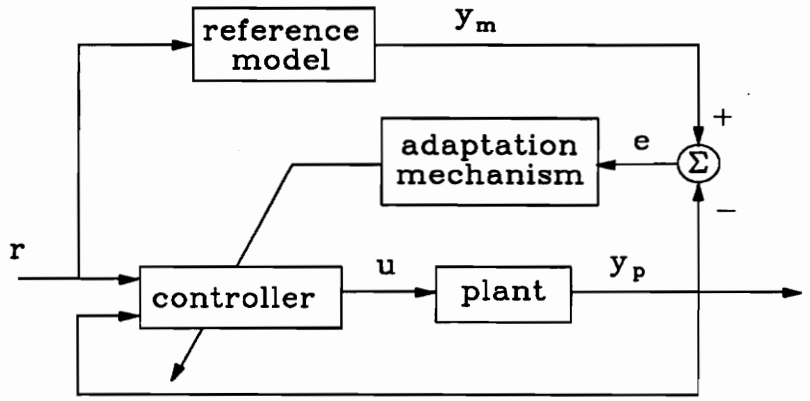

a. Model reference adaptive control system.

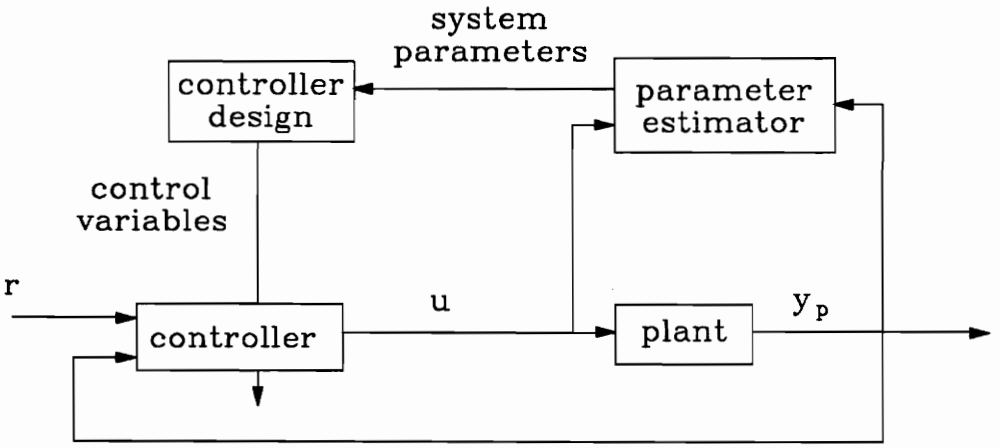

b. Typical control using a self-tuning regulator.

Figure 2.14: Schematic diagrams of model reference adaptive and self-tuning regulator control systems.

which has desirable response characteristics (called the skyhook damper suspension model because it inserts a damper between the vehicle and a fixed point in space). A feedback control law is derived such that the two systems can become identical if the gain set is properly chosen. Since the vehicle parameters are unknown, though, the proper gain set can not be determined a priori. The MRAC approach, then, is to apply the road input to both systems, the real system containing a control force actuator. The outputs of these systems are compared to form an error signal which can be used to adjust the controller's gain set to make the two systems converge. As the gains approach their proper values, the real system's response matches that of the ideal system, and the error signal approaches zero.

Self-Tuning Regulators

Self-tuning regulators were originally introduced by Astrom and Wittenmark in 1973. Even though model reference adaptive control has been around somewhat longer, self-tuning regulators are currently found to be more common in applications [Chalam, 1987]. This widespread use can be attributed to self-tuning regulators' versatility and ease of implementation (to which the boom in microprocessor technology can be given credit).

A typical self-tuning regulator is shown in Fig. 2.14b. This figure shows three functions common to most self-tuning regulators; on-line identification of unknown plant (and disturbance) parameters, on-line controller design, and on-line implementation of the adaptive controller. The underlying purpose of adaptive control is to account for unknowns in the plant or disturbances, so the first step in the process is to identify those unknowns. Once the plant is known, a relevant control design can be performed. The "controller design" block, then, contains the control strategy for the system. This strategy can follow any number of design rationales, thus the

versatility of self-tuning regulators. Finally, the results of the control design process (gain set or other controller parameters) are then implemented in the controller.

The self-tuning regulator shown in Fig. 2.14b and described above is classified as "explicit" because the control gains or parameters are explicitly determined by carrying out a design step (this class is also termed "indirect" from the standpoint of the identification step; the control gains are indirectly determined from the identification process). There is another class of self-tuning regulators in which the design step is bypassed and the control parameters are directly determined by the identification process, either by writing the identification process in terms of the control parameters or by choosing a controller which is amenable to such a process. This class, is called "implicit" (also called "direct") because the control gains are determined by an implied design process (the underlying strategy may still be pole-placement, for example) [Astrom, 1989, Jacobs, 1981].

A self-tuning regulator has been applied in active vehicle suspension systems [Sunwoo, 1990b]. The system in this case is the same as that described in the example above where model reference adaptive control was used. Sunwoo's approach here is to again propose an ideal model for the vehicle and suspension and design a feedback control law which makes the actual system respond like the ideal system. The controller gain set is written in terms of the actual and ideal system parameters, the actual parameters, of course, being unknown. By identifying the system parameters (by an on-line recursive least squares parameter estimation scheme), the necessary information was found with which to calculate the gains. This approach is essentially a pole-placement strategy, where the actual system poles are placed at the locations of the ideal system poles. The self-tuning regulator in this example is explicit because the gain set is explicitly derived and then implemented in the controller.

Chapter 3

Force Feedback for Vibration Isolation

From the discussions in Chapter 1, it is clear that vibration isolation can be achieved by eliminating the forces connecting two sides of a system. Perhaps the most effective means of eliminating these forces (while still maintaining necessary clearance or static loads) is to activate the mount which serves to connect the system. This chapter will discuss the details of applying force feedback within an active mount for vibration isolation. The approach will be to use general dynamic systems to address such issues as how much isolation can be expected with active force feedback and how force feedback provides two-way isolation, along with further discussions of passive vibration isolation.

The chapter will first provide a general analysis of a flexible dynamical system, breaking it up into clean and dirty sides. This will lead the way to an analysis of the effects of active force feedback in an active mount, assuming an ideal actuator. Following that will be a discussion of the effects of actuator, sensor, and compensator dynamics. Finally, there will be a section which considers some of the stability issues of each of the feedback cases covered in the chapter.

3.1 General Input/Output Description of a Flexible Mechanical System

The equations of motion for a flexible mechanical system are generally developed using a finite-element approach where the dependent variables are displacements within the system. Such an approach leads to a set of coupled, second-order differential equations of the form

$$\mathbf{M}\ddot{\mathbf{x}} + \mathbf{K}\mathbf{x} = \mathbf{F}f(t) \tag{3.1}$$

where the vector $\mathbf{F}$ describes how the force enters the system. These equations can be uncoupled so that the dependent variables become the normal modes [Thomson, 1981]. Using the transformation

$$\mathbf{x} = \mathbf{P}\mathbf{q} \tag{3.2}$$

where $\mathbf{P}$ is the matrix of system eigenvectors, Eq. 3.1 becomes

$$\mathbf{P}'\mathbf{M}\mathbf{P}\ddot{\mathbf{q}} + \mathbf{P}'\mathbf{K}\mathbf{P}\mathbf{q} = \mathbf{P}'\mathbf{F}f(t) \tag{3.3}$$

The eigenvectors in $\mathbf{P}$ are the mode shapes, ϕ_k, evaluated at the locations corresponding to the coordinates, $\mathbf{x}$. If we assume proportional damping, a damping term can be added which is also uncoupled, and a single equation from the above set can be written as

$$\ddot{q}_k + 2\zeta_k\omega_k\dot{q}_k + \omega_k^2 q_k = \frac{GF_k}{GM_k}f(t) \tag{3.4}$$

where ω_k is the natural frequency of the k'th mode, ζ_k is the corresponding damping ratio, and GF_k and GM_k are the mode's generalized force and mass, respectively. The generalized force is a function of the point of application of all the forces and torques applied to the structure.

$$GF_k = \sum_{i=1}^{n} \phi_k(x_i)F_i \tag{3.5}$$

The generalized mass is a constant which depends on the particular mode shape and the distribution of mass within the structure.

$$GM_k = \sum_{i=1}^{n} \phi_k(x_i) m_{ki} \phi_k(x_i) \tag{3.6}$$

For a single force input, these can be combined into one term which is dependent on the location, $\hat{x}$, of the applied force

$$g_k(\hat{x}) = \frac{GF_k}{GM_k} \tag{3.7}$$

and is called the "mode participation factor." If there are multiple inputs applied to the structure, then superposition allows $g_k(\hat{x})$ to become a row-vector of mode participation factors corresponding to each input, $f(t)$ will be a column containing the inputs, and the total force applied to each modal equation is the sum of all individual forces.

After substitution of Eq. 3.7, Eq. 3.4 can be transformed to give the response of a given mode of a flexible mechanical system to a force input,

$$q_k(s) = \frac{g_k(\hat{x})}{s^2 + 2\zeta_k \omega_k s + \omega_k^2} f(s) \tag{3.8}$$

In developing a feedback approach to the vibration isolation problem we will be less concerned with the response of any given structural mode than with the response of the structure at a particular location (that location being the point, or points, where the two sides of the system are connected). This information can be extracted from the structure's modes using the transformation in Eq. 3.2. For a single mode, the displacement, w, at some point, $\tilde{x}$, within the structure can be written as

$$w(\tilde{x}, t) = q_k(t) h_k(\tilde{x}) \tag{3.9}$$

where the constant, $h_k(\tilde{x})$, $(h_k(\tilde{x}) = \phi_k(\tilde{x}))$, describes the contribution of mode q_k to the displacement w.

Transforming Eq. 3.9 and substituting Eq. 3.8 gives the general relationship describing the contribution of a single mode to the response of a structure at a given point when a force is applied at any point.

$$w(\tilde{x}, s) = \frac{g_k(\hat{x})h_k(\tilde{x})}{s^2 + 2\zeta_k\omega_k s + \omega_k^2} f(s) \tag{3.10}$$

The notation of $\hat{x}$ and $\tilde{x}$ will now be dropped, because it is clear that their description of the input and output locations are contained solely in constants g and h. So, changing the location of applied force or measured response alters the transfer function only through the numerator constants.

If the structure is described by n modes, then displacement w becomes a sum of the contributions of the n mode shapes

$$w(s) = \sum_{k=1}^{n} \left(\frac{g_k h_k}{s^2 + 2\zeta_k\omega_k s + \omega_k^2} \right) f(s) \tag{3.11}$$

Equation 3.11, can be written in a transfer function representation of force to displacement as

$$\frac{w_i(s)}{f(s)} = G_i(s) = \frac{N_i(s)}{D_i(s)} = \sum_{k=1}^{n} \frac{g_k h_k}{s^2 + 2\zeta_k\omega_k + \omega_k^2} \tag{3.12}$$

By combining the right-hand-side of Eq. 3.12, the numerator and denominator of $G_i(s)$ are found to be

$$N_i(s) = \sum_{k=1}^{n} \left[g_k h_k \prod_{\substack{l=1 \\ l \neq k}}^{n} (s^2 + 2\zeta_l\omega_l + \omega_l^2) \right] \tag{3.13}$$

$$D_i(s) = \prod_{k=1}^{n} (s^2 + 2\zeta_k\omega_k + \omega_k^2) \tag{3.14}$$

where D_i is the characteristic polynomial of the structure, which describes the system's transient response.

3.1.1 Zeros of a Flexible Structure

Typically, in the analysis of flexible dynamic systems, much attention is given to the system poles, the damping and natural frequencies, because these characteristics describe how the system responds to various inputs. More recently, as interest has grown in controlling the vibrations of these flexible systems, more emphasis has been placed on the system zeros [Gevarter, 1970, Martin, 1978, Wie, 1981]. The zeros of a transfer function, which depend on the path from input to output, designate those points in the Laplace domain where a system's response is inhibited. Zeros play an important role in the control of flexible structures, and, as will be shown later, in active and passive vibration isolation. Before moving on to talk about active vibration isolation techniques, we will first wrap up this section about general characteristics of flexible structures with a discussion of flexible structure zeros, along with a derivation that makes clear their relationship with the locations of system inputs and outputs.

Given a force applied at some location on a structure, the response at any location is described by the transfer function in Eq. 3.12. The zeros of that transfer function (the roots of Eq. 3.13) are dependent on the locations of the input and the output. Not only do the values of the zeros change, but the number of calculated zeros may range from 0 to $2n-2$ as the input and output locations are changed (n is the number of modes retained in the model, for continuous systems with an infinite number of modes, there could be an infinite number of actual zeros).

The importance of zeros in flexible structures cropped up when engineers became interested in controlling the rigid-body motions of structures whose flexible modes were in the bandwidth of the control system [Gevarter, 1970, Wie, 1981]. It became readily apparent that a control system whose control force and measurement were

colocated on the structure could easily control the rigid-body motion in a stable manner. When the control force and measurement became separated, however, the process became more difficult, all a result of the numbers of and values for the system zeros. As we will see later, the vibration isolation problem is also dependent on the zeros of the structure.

From inspection of Eq. 3.13, it is not clear that the number of zeros of any given structural transfer function will change as the input/output locations are changed. That the values will change is apparent because the coefficients, $g_k h_k$ in Eq. 3.13, vary as input/output locations change, leading to different roots of the polynomial. The order of the polynomial, and thus the number of zeros, however, would appear to be constant from that representation. The following analysis will present the transfer function numerator in a manner which clearly shows the changes in number and value of a system's zeros.

Starting with Eq. 3.1 (with damping added), the transfer function matrix for force input to displacement output can be written as

$$\frac{\mathbf{x}(s)}{f(s)} = \left[\mathbf{M}s^2 + \mathbf{C}s + \mathbf{K}\right]^{-1}\mathbf{F} \tag{3.15}$$

The matrix in Eq. 3.15 that is inverted will be called the dynamic system matrix. Expanding the matrix inverse, Eq. 3.15 becomes

$$\frac{\mathbf{x}(s)}{f(s)} = \frac{\text{adj}\left[\mathbf{M}s^2 + \mathbf{C}s + \mathbf{K}\right]}{\det\left[\mathbf{M}s^2 + \mathbf{C}s + \mathbf{K}\right]}\mathbf{F} \tag{3.16}$$

The denominator of Eq. 3.16 is, of course, the characteristic polynomial, and determines the poles of the system. The adjoint matrix in the numerator determines the system zeros. Since, for any real system, the elements on the main diagonal of the mass matrix are all nonzero, the diagonal elements of the argument of the adjoint are of order s^2.

When the adjoint is performed, the off-diagonal terms become polynomials in s, but, depending on the degree of dynamic coupling, they may not be the highest order polynomials in the matrix. The diagonal terms, on the other hand, have the highest order polynomials possible (of order $2n-2$, see Eq. 3.13). This can be explained through the adjoint operation, which is the transpose of the cofactor matrix, or the transpose of the matrix of signed minors. Recall that a minor of an element is the determinant of the matrix that remains when the element's row and column have been removed. The minors of the diagonal elements contain the product of all remaining diagonal elements in the matrix, or, the terms $\prod_{\substack{i=1 \\ i\neq j}}^{n}(m_{ii}s^2 + c_{ii} + k_{ii})$, where j is the row or column of the diagonal element.

Consider the minor of a diagonal element, (k,k), of the dynamic system matrix. The matrix formed by removing the kth row and column will be called $\mathbf{A}$. The minor of element (k,k), then, is the determinant of $\mathbf{A}$, which can be formed by cofactor expansion [Anton, 1981]. Expanding along row i,

$$\det \mathbf{A} = a_{i1}C_{i1} + a_{i2}C_{i2} + \cdots + a_{in-1}C_{in-1} \tag{3.17}$$

The expansion of a diagonal element of $\mathbf{A}$ is

$$a_{ii}C_{ii} = a_{ii}M_{ii} = a_{ii}\det \mathbf{A}_{\substack{\text{row}\neq i \\ \text{col}\neq i}} \tag{3.18}$$

where M_{ii} is the minor of a_{ii}. (Note also that a_{ii} is a diagonal element of the dynamic system matrix.) The determinant in Eq. 3.18 can again be found by cofactor expansion, say along row j,

$$a_{ii}C_{ii} = a_{ii}(a_{j1}C_{j1} + a_{j2}C_{j2} + \cdots + a_{jn-2}C_{jn-2}) \tag{3.19}$$

In this expansion we get the term a_{jj}, which is also a diagonal term in $\mathbf{A}$, so one of the terms in the original expansion becomes $a_{ii}a_{jj}C_{jj}$. The expansion can be

repeated until the original minor is complete, and one of its terms will be a product of all the diagonal terms of **A**. Since the minor (Eq. 3.17) is actually a polynomial in s, its order is $2(n-1)$, where $(n-1)$ is the dimension of **A**.

The previous discussion can be summarized by an example. Consider a subset of the lumped-mass system of Fig. 3.1 (we will look at everything to the right of the force f_c, which leaves a three degree-of-freedom system). The dynamic system matrix can be written as (assuming all spring constants, damping coefficients, and masses to be equal)

$$\left[\mathbf{M}s^2 + \mathbf{C}s + \mathbf{K}\right] = \begin{bmatrix} ms^2+cs+k & -cs-k & 0 \\ -cs-k & ms^2+2cs+2k & -cs-k \\ 0 & -cs-k & ms^2+cs+k \end{bmatrix} \tag{3.20}$$

The adjoint of the dynamic system matrix is

$$\text{adj}\left[\mathbf{M}s^2 + \mathbf{C}s + \mathbf{K}\right] = \begin{bmatrix} (ms^2+2cs+2k)(ms^2+cs+k)-(cs+k)^2 & (ms^2+cs+k)(cs+k) & (cs+k)^2 \\ (ms^2+cs+k)(cs+k) & (ms^2+cs+k)^2 & (ms^2+cs+k)(cs+k) \\ (cs+k)^2 & (ms^2+cs+k)(cs+k) & (ms^2+cs+k)(ms^2+2cs+2k)-(cs+k)^2 \end{bmatrix} \tag{3.21}$$

Equation 3.21 shows clearly that the highest order polynomials occur on the main diagonal of the adjoint matrix, and are all of order $2n-2$ in s (which is 4 for this system). The off-diagonal terms are of lower order because of the dynamically uncoupled equations which are due to choice of coordinates for the problem.

The adjoint contains a matrix of possible numerator polynomials for the transfer function, the particular one chosen depends on the output (which chooses the row) and the force input (which, through **F**, chooses the column). It is clear that a colocated force/displacement pair will have a diagonal element of the adjoint for a numerator polynomial, and thus will have the most zeros possible. Any other input/output combination may result in fewer zeros, or even no zeros at all. Not only do colocated input/output pairs provide a full set of zeros, but Martin [1978] showed that the poles and zeros for this case alternate in location along the imaginary axis

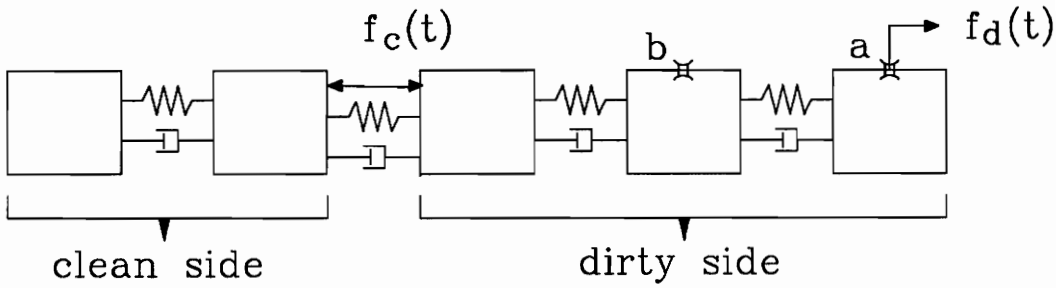

Figure 3.1: Example of an active mount applied to a flexible system.

in the Laplace plane. This result has implications in the stability of control systems applied to such a system.

By keeping the system equations in terms of displacement coordinates (rather than normal modes), and by looking at the adjoint in the transfer function, it was easy to see how colocation of input and output provides a "full set" of zeros, while any other combination may provide less than a full set. We must keep in mind, though, that this analysis was done using a finite-dimensional equation set for a (generally) infinite-dimensional system. The exact zeros will change in value somewhat (and in some cases, the number will change as well) from those found by a discrete model [Wie, 1981]. The fact that colocated input/output pairs give a full set of zeros that alternate with the poles is true for the discrete or continuous representation. The above argument applied to the adjoint matrix still holds, but the matrix dimension approaches infinity.

3.2 Force Feedback Applied to a Generic Flexible Structure

Given the discussion of the previous section we are now ready to analyze the effects of active force feedback within a flexible structure for vibration isolation. From Eq. 3.12, the input/output relationship for the general flexible structures shown in Fig. 3.2a can be written as

$$\frac{w_i(s)}{f_i(s)} = G_i(s) \tag{3.22}$$

where the two structures can represent the clean and dirty sides of our vibratory system, and the transfer functions describe the relationship between force input and displacement output. The force/displacement pair can occur anywhere on the structure. For the purposes of this discussion, however, they have been shown

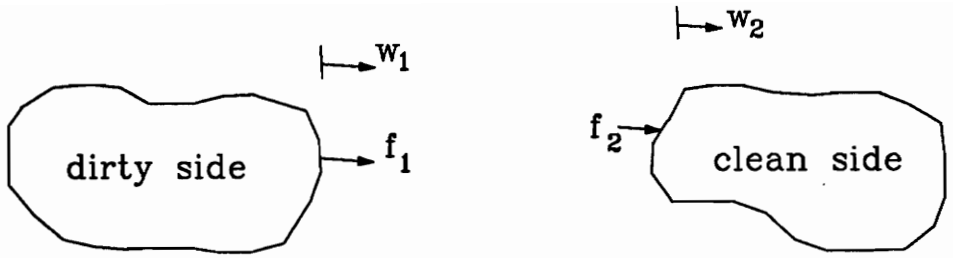

a. Colocated force/displacement pair for two generic flexible structures.

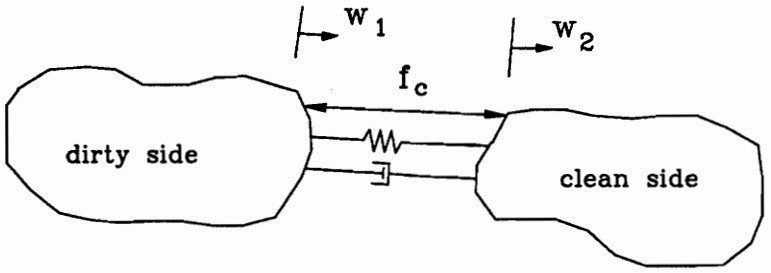

b. Generic flexible structure with an internal active mount.

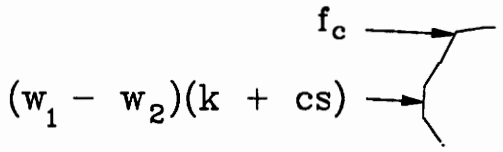

c. Transmitted forces in generic flexible structure.

Figure 3.2: Schematics of general flexible structure with an active mount.

to be colocated, because we will be concerned with forces being transmitted by a connecting mount and with the resulting displacements at that location.

By connecting the two structures we can begin to look at the effects of force feedback within a flexible structure joined by a connecting mount. This situation is represented in Fig. 3.2b. The mount will, in general, have some stiffness and damping characteristics (it is shown to be massless here, although the addition of mass does not change the outcome of this discussion), and will have the capability to apply an internal force to the structure, shown as f_c applied in parallel with the mount stiffness. A discussion of other mount configurations, and their mathematical implications, will be taken up in section 4.

In Chapter 1 it was explained that our approach to vibration isolation will be to minimize the forces transmitted from one side of a structure to another. For this work, the transmitted force will be defined as the force applied to the clean side by the mount. Fig. 3.2c illustrates the forces seen by the clean side, passive mount forces and actuator forces, the total being designated f_t, or

$$f_t = f_c + (w_1 - w_2)(k + cs) \tag{3.23}$$

The mount displacements, w_1 and w_2, have been previously defined in terms of the system transfer functions (Eq. 3.22), so, making those substitutions gives

$$f_t = f_c + (f_1 G_1 - f_2 G_2)(k + cs) \tag{3.24}$$

But, from Figs. 3.2a and 3.2c, f_2 is the transmitted force, and a force sum on the mount implies that f_1 is equal and opposite to f_2, so

$$f_2 = f_t \tag{3.25}$$

$$f_1 = -f_t \tag{3.26}$$

Substituting Eqs. 3.25 and 3.26 into Eq. 3.24 leads to

$$f_t = f_c + (-f_t G_1 - f_t G_2)(k + cs) \tag{3.27}$$

which describes the transmitted force as a function of only the applied force and the structure and mount dynamics. Equation 3.27 can be manipulated to give the transfer function from control force to transmitted force

$$\frac{f_t}{f_c} = \frac{1}{1 + (G_1 + G_2)(k + cs)} \tag{3.28}$$

We are now ready to see the effects of using the transmitted force in a feedback scheme for vibration isolation. The simplest approach will be to generate the control force, f_c by applying a feedback gain to f_t, as shown in Fig. 3.3. The resulting open- and closed-loop transfer functions are shown in Eqs. 3.29 and 3.30.

$$\frac{f_t}{f_c} = \frac{1}{1 + (G_1 + G_2)(k + cs)} \tag{3.29}$$

$$\frac{f_t}{f_{ref}} = \frac{1}{1 + (G_1 + G_2)(k + cs) + k_c} \tag{3.30}$$

By substituting Eq. 3.12, the open-loop transfer function shown in Eq. 3.29 can be transformed into a more meaningful form,

$$\frac{f_t}{f_c} = \frac{D_1 D_2}{D_1 D_2 + (N_1 D_2 + N_2 D_1)(k + cs)} \tag{3.31}$$

Recall from classical controls that root locus techniques can be used to determine a system's closed-loop response as parameters are varied. By choosing the parameter to be the feedback gain, as is typically done, we know that the closed-loop eigenvalues are equal to the open-loop eigenvalues when the feedback gain is zero, and they approach the open-loop zeros as the gain approaches infinity. Note that the zeros of the transfer function in Eq. 3.31 are the poles of the two unconnected sides of the system. This implies that if high-gain force feedback is used, the system begins to respond as if it were not connected by the mount.

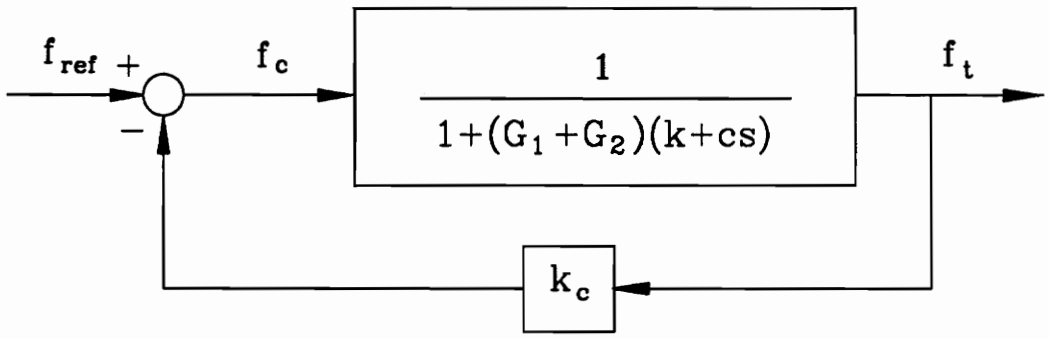

Figure 3.3: Block diagram of force feedback in a general flexible structure.

3.2.1 Illustration of System Separation by Root Locus Example

To illustrate the ability of high-gain, force feedback to separate the system eigenvalues back into their unconnected groups, we will look at an example. Figure 3.1 shows a one-dimensional, multi-degree-of-freedom, flexible system which contains an active mount. The mount is of the same arrangement (control force applied in parallel with the mount stiffness) as that shown in Fig. 3.2b. The root locus of this system, with transmitted-force feedback, is shown in Fig. 3.4 for varying feedback gain. The x's denote the open-loop eigenvalues and correspond to a zero-gain case, or a case where no control force is applied. The system responds as it's damped natural frequencies dictate. Note that one pair of open-loop eigenvalues lies at the origin, and corresponds to the rigid-body mode of the system. There is also a pair of zeros at the origin, which brings about a pole-zero cancellation that precludes the manifestation of the rigid-body mode in the response. The reason for the cancellation is, of course, the fact that the input, f_c, is an internal force, and cannot excite the system's rigid-body mode.

As the gain is increased, the eigenvalues approach the open-loop zeros, and we achieve perfect vibration isolation. This state of ideal eigenvalue placement has been called Fahrvagnügen by German engineers, which, roughly translated, means "nirvana in the Laplace domain."

As the gain is increased, the eigenvalues approach the open-loop zeros, which are denoted as o's in Fig. 3.4. Recall that the open-loop zeros are in fact the poles of the two independent sides of the system, so now the system's response is dictated by the damped natural frequencies of the two unconnected sides.

Note that as the gain approaches infinity, two new eigenvalues approach the origin to give the system an apparent rigid-body mode. This is expected if the

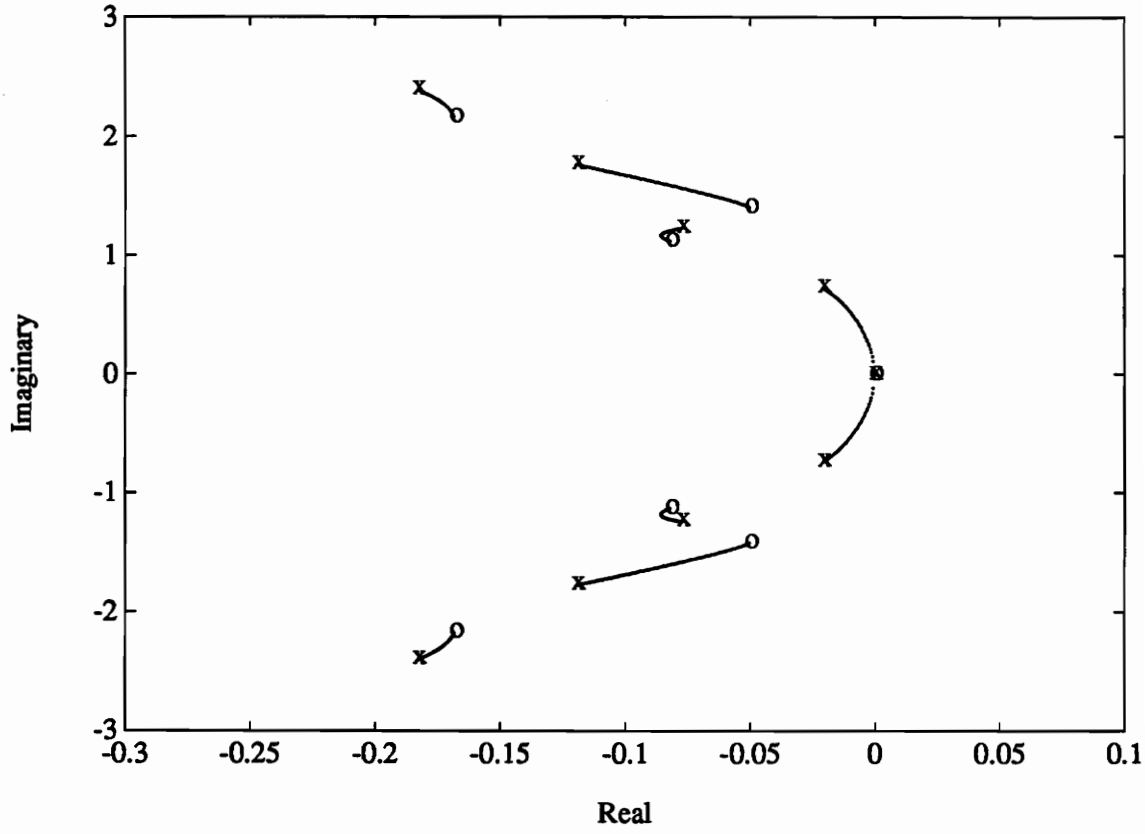

Figure 3.4: Root locus of flexible system with gain feedback of transmitted force.

two systems are completely isolated, because they are then free to move about independently of one another. This rigid-body mode is a result of the feedback not allowing a sustained (or dc-level) force to be transmitted in the mount. If such a force were applied, the controller would act to cause the two sides to drift apart (constantly driving the force to zero) and showing an apparent rigid-body mode. The center of mass of the total system would not move, but the relative displacement between the two sides would increase without bound.

A more likely scenario would be for an external dc force to be applied to the system. In this case, the total-system rigid-body mode would appear, (the center of mass would move), but the clean side would remain fixed. The root locus to describe this case would, of course, be different, because now we are allowing an external force, and the zeros of the transfer function from external force (disturbance) to transmitted force would be different from those shown in Fig. 3.4.

3.2.2 Illustration of Complete Isolation of Disturbances Through Frequency Response Examples

It has been shown above that when force feedback is implemented, the system will respond as the eigenvalues of the unconnected sides if the feedback gain is very high. It has not actually been shown, though, that this implies that a disturbance on the dirty side of the system will not produce a response in the clean side. This will be shown below with an analysis of the system transfer functions.

Consider the system shown in Fig. 3.5a. This is the same general system as that shown in Fig. 3.2b, with a disturbance force added. The transfer function from the disturbance input, f_d, to displacement output, w_1, can be written as (from Eq. 3.22)

$$\frac{w_1}{f_d} = G_{d_1} \tag{3.32}$$

The transmitted force in this situation still maintains the general form shown in Eq.

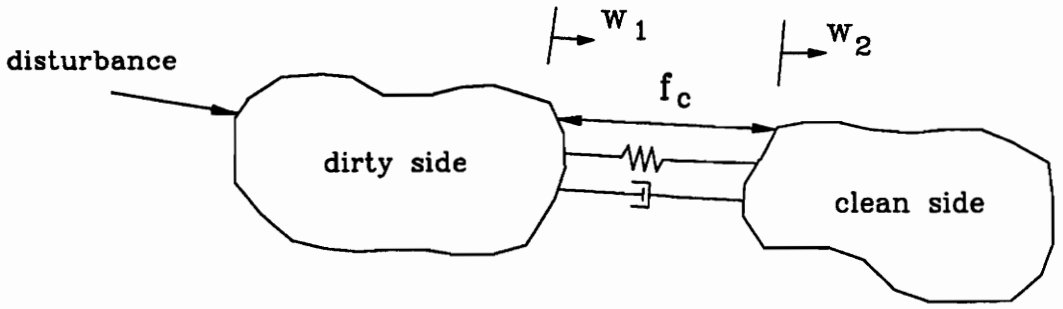

a. Flexible structure with disturbance applied to dirty side.

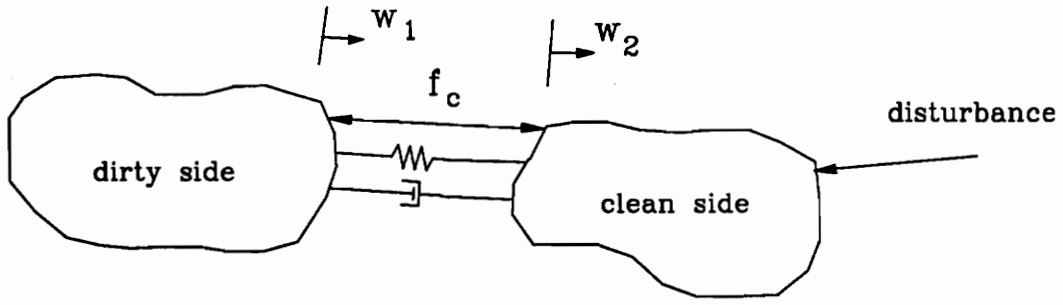

b. Flexible structure with disturbance applied to clean side.

Figure 3.5: General flexible structure with arbitrary disturbance force applied.

3.23,

$$f_t = f_c + (w_1 - w_2)(k + cs) \tag{3.33}$$

but a look inside shows that the details have changed. Displacement w_1 now contains two parts, that arising from the force in the mount (as before), and that which comes from the disturbance force. By the vector form of Eq. 3.10, we can apply superposition to this linear system and show that w_1 is sum of two responses

$$w_1 = G_1 f_1 + G_{d_1} f_d \tag{3.34}$$

Substituting Eq. 3.34 into Eq. 3.33 and recalling that $f_1 = -f_t$, $w_2 = f_2 G_2$, and $f_2 = f_t$ leads to

$$f_t = f_c + (-f_t G_1 + f_d G_{d_1} - f_t G_2)(k + cs) \tag{3.35}$$

If force feedback is applied, then

$$f_c = -k_c f_t \tag{3.36}$$

By substituting for f_c in Eq. 3.35 and rearranging, the transfer function from disturbance to transmitted force is found to be

$$\frac{f_t}{f_d} = \frac{G_{d_1}(k + cs)}{1 + k_c + (G_1 + G_2)(k + cs)} \tag{3.37}$$

or, in simplified form,

$$\frac{f_t}{f_d} = \frac{D_2 N_{d_1}(k + cs)}{D_1 D_2 + D_1 D_2 k_c + (N_1 D_2 + N_2 D_1)(k + cs)} \tag{3.38}$$

From Eq. 3.37 or Eq. 3.38, it is easy to see that as the feedback gain, k_c, is increased, the magnitude of the transfer function approaches zero. When this occurs, the disturbance, located anywhere on the dirty side of the system, produces no transmitted force, and thus brings about no response from the clean side of the system. Note also that this result is independent of the type of disturbance applied to the system.

As the feedback gain approaches infinity, complete vibration isolation is achieved, at all regions of the frequency domain.

To illustrate the isolation performance, Fig. 3.6 shows the frequency response of Eq. 3.38 as it pertains to the system shown in Fig. 3.1. The effect of feedback is to "roll off" the magnitude of the transmitted force at lower frequencies as the gain is increased. At low frequencies, the magnitude remains constant, but we see a resonant peak moving to the left as the gain is increased. This peak corresponds to the closed-loop poles approaching the origin in Fig. 3.4. The result of the constant low-end magnitude and the decreasing resonance is that for high gains, static loads can still be supported by the mount, but as the gain increases, a very lightly-damped, low-frequency mode appears which may be just as unacceptable as not being able to support a static load.

3.2.3 Two-Directional Isolation with Force Feedback

Up to this point, the isolation has been shown to occur "in one direction"; the disturbance enters the dirty side and is prevented from passing to the clean side. Using the same approach as above, it will be shown that force feedback results in isolation in both directions.

Consider again the general flexible structure connected by an active mount, but this time the disturbance force will enter what has been called the clean side (Fig. 3.5b). The transfer function from disturbance to displacement w_2 is

$$\frac{w_2}{f_d} = G_{d_2} \tag{3.39}$$

The transmitted force is the same as in Eq. 3.33, but now displacement w_2 (instead of w_1) is made up of two parts. Using superposition as before, w_2 can be written as

$$w_2 = G_2 f_2 + G_{d_2} f_d \tag{3.40}$$

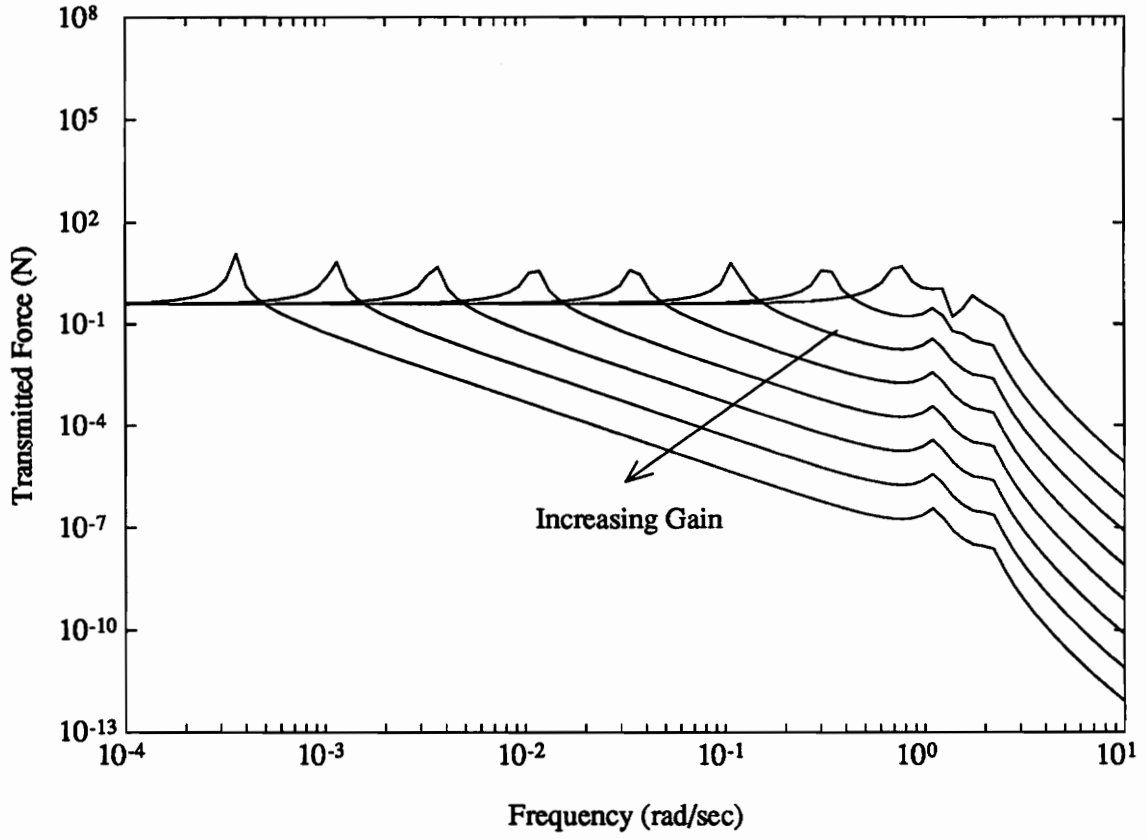

Figure 3.6: Frequency response of flexible system with feedback of transmitted force as feedback gain is increased.

Substituting Eq. 3.40 into Eq. 3.33 and making the proper substitutions for w_1, f_1, f_2, and f_c, as before, the transfer function from disturbance force to transmitted force can be derived for this situation as

$$\frac{f_t}{f_d} = \frac{G_{d_2}(k+cs)}{1+k_c+(G_1+G_2)(k+cs)} \tag{3.41}$$

or, again in simplified form,

$$\frac{f_t}{f_d} = \frac{D_1 N_{d_2}(k+cs)}{D_1 D_2 + D_1 D_2 k_c + (N_1 D_2 + n_2 D_1)(k+cs)} \tag{3.42}$$

Note that the characteristic polynomial for this case is the same as when the disturbance was applied to the other side of the system (as expected). It is also clear that as the feedback gain is increased, once again the transmitted force approaches zero. Our definition of f_t is the force applied from the mount to the clean side, but the implication here is that the dirty side is now isolated ($f_1 = -f_t$, and when $f_1 = 0$, no force enters the dirty side).

By using the same feedback control law, vibration isolation has been achieved in both directions across the mount. Force feedback simply minimizes the transmitted force in the mount, it matters not from which direction the force originates.

3.2.4 Relation to Classical Disturbance Rejection

A final word is due which relates what has been shown in this section to the methods of disturbance rejection of chapter 2. The transfer functions shown in Eqs. 3.37 and 3.41 are identical to (but more elaborate forms of) the plant of Fig. 2.6. In this chapter the feedback compensator, H, is simply the gain, k_c. The discussion of section 2.2.1 involved making H as large as possible at the frequencies of interest. We are following the same classical disturbance rejection approach here, making the denominator of the transfer function large, but the feedback gain does so at

all frequencies, so we achieve complete vibration isolation. Later discussions will involve the use of more sophisticated compensators, as implied in section 2.2.1, and how to suppress isolation at certain regions but leave static loads unaffected.

3.3 Effect of Actuator, Compensator, and Sensor Dynamics on Force Feedback

In applying force feedback through a gain, it was assumed that the actuator force was generated immediately, without any phase or magnitude shifts in the desired signal. In real applications, however, there will be actuator dynamics which will cause the control force to be delayed (or be applied at a different magnitude) from the control signal, and there will, in some cases, be additional terms in the feedback compensator (whether they are a result of sensor dynamics or compensator design) which will affect the form of the transfer functions developed in the preceding sections.

First, let's look at the case where the actuator contains significant dynamics. Assume the actuator can be described by the transfer function

$$\frac{f_c}{u} = G_a = \frac{N_a}{D_a} \tag{3.43}$$

where G_a is the transfer function containing the actuator dynamics. Whereas before the control force was directly proportional to the transmitted force ($f_c = -k_c f_t$), the proportionality factor is now tempered by the actuator dynamics.

If sensor and/or compensator dynamics are included in the feedback loop, then the control law can be considered to be changed as well. The relationship between control signal and transmitted force can be written as

$$\frac{u}{f_t} = G_c G_s = \frac{k_c N_c N_s}{D_c D_s} \tag{3.44}$$

Combining Eqs. 3.43 and 3.44, and substituting into the relationship for trans-

mitted force (Eq. 3.27) gives

$$f_t = -k_c G_a G_c G_s f_t + (-f_t G_1 - f_t G_2)(k + cs) \tag{3.45}$$

The resulting open-loop transfer function is shown below in simplified form

$$\frac{f_t}{u} = \frac{k_c N_a N_c N_s D_1 D_2}{D_a D_c D_s [D_1 D_2 + (N_1 D_2 + N_2 D_1)(k + cs)]} \tag{3.46}$$

Using the same reasoning as above, when the feedback loop is closed and the gain is increased, the closed-loop eigenvalues move from the open-loop poles to the open-loop zeros. From Eq. 3.46 it is clear that with the addition of actuator, compensator, and sensor dynamics, the open-loop zeros still contain the poles of the unconnected sides of the system, so we can achieve complete isolation.

We have now added zeros from the additional transfer functions. Some of the closed-loop eigenvalues approach the new zeros as $k_c \rightarrow \infty$. If the combined actuator-compensator-sensor transfer function is strictly proper, then m closed-loop eigenvalues will approach infinity, where m is the difference between the number of actuator poles and zeros. A minimum condition for high-gain force feedback, then, is that $m \leq 2$, or else the system will become unstable at high gains.

3.4 Stability of Force Feedback Techniques

An issue that is always of concern in designing a feedback controller is the stability of the resulting closed-loop system. In this section we will address the issue of stability when using force feedback control, starting with the case of strict gain feedback, then moving to the more complicated case where additional dynamics occur in the feedback loop.

3.4.1 Stability for High-Gain Force Feedback

Gevarter [1970] showed that a system whose open-loop transfer function can be represented by

$$G_i = \sum_{i=1}^{n} \frac{a_i}{s^2 + 2\zeta_i w_i s + w_i^2} \tag{3.47}$$

can be stably controlled by position or velocity feedback (or both) if all the a_i are the same sign. What this means physically is that the measurement and applied force are in phase for all modes, and by controlling the system based on the measurement, no single mode is driven unstable. Such a transfer function results when the force and measurement are colocated. Recall from section 3.1.1 that a colocated force/displacement also results in a full complement of zeros. Gevarter noticed, and Martin [1978] later proved, that these zeros are located between the poles along the imaginary axis in the complex plane. This helps explain why such a simple controller can be stable. Each pole has a corresponding zero, and it approaches that zero along a path that exists entirely in the left half of the complex plane. (For a force-to-displacement transfer function, there are two more poles than zeros, so two of the closed-loop poles approach asymptotes of $\pm 90°$.)

In this work, we also have a colocated input/output pair (we apply a control force through the mount, and measure the transmitted force at the same location, in the mount) but we do not have a position/force or velocity/force transfer function (so-called "dual" pairs [Sievers, 1989]). Our open-loop transfer function is force/force, so we need to show that we still attain the same stability results.

An interesting way to think of force feedback is that it amounts to the same thing as a combination of position and velocity feedback. Consider the system of Fig. 3.7a. Applying position and velocity feedback to this system results in the block diagram shown in Fig. 3.7b. If we let $k_v = c$ and $k_p = k$, then $y = f_t$, the

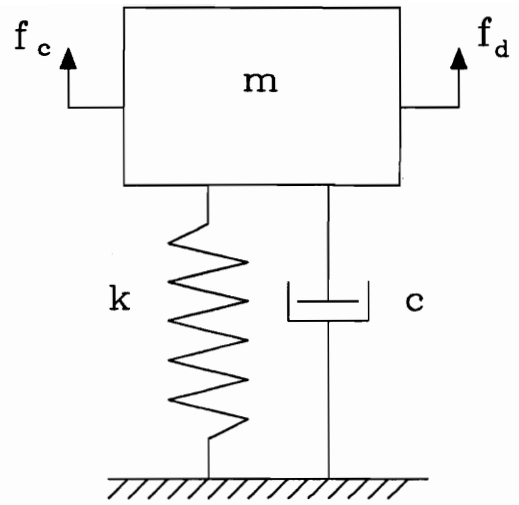

a. Single degree of freedom system with force feedback.

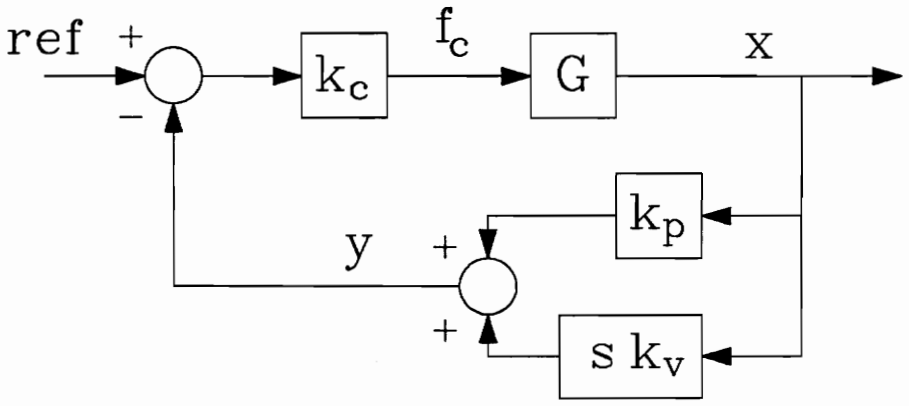

b. Block diagram for single degree of freedom system with position and velocity feedback.

Figure 3.7: Example of similarity between force feedback and position-velocity feedback.

transmitted force in the system. Feeding back y through the gain k_c, then gives us force feedback, which is no different than the combination of position-velocity feedback, which is guaranteed to be stable for a colocated actuator/sensor pair.

If the system becomes more complicated, such as that shown in Fig. 3.1, (and we apply the force across the mount), then we are effectively applying colocated position-velocity feedback in two locations, where the position and velocity measurements are relative.

Stability for simple force feedback can also be shown through the system equations. We will do this by first showing that our open-loop transfer function can be represented as shown in Eq. 3.47. This will be done for the undamped case. (The proofs in Martin are all done for undamped systems, and they do not extend directly to the damped case. The assumption used is that lightly-damped systems retain the same pole-zero patterns as the undamped systems, but are shifted slightly to the left in the complex plane.) Then we will show that all the a_i have the same sign. This will allow us to use Gevarter's results to say that we can achieve a stable system with gain feedback.

In general, the transfer function from active mount control force to transmitted force is shown in Eq. 3.31. The denominator of this expression is the characteristic polynomial for the entire structure, and it can be factored into the structural modes

$$D_1 D_2 + (D_1 N_2 + D_2 N_1)(k) = \prod_{l=1}^{m} (s^2 + \omega'^2_l) \tag{3.48}$$

where ω'_l are the natural frequencies of the connected structure. Using the factored form of the characteristic polynomial, Eq. 3.31 can be expanded using partial fractions to give

$$\frac{D_1 D_2}{D_1 D_2 + (D_1 N_2 + D_2 N_1)(k)} = s^2 \left(\frac{a_1 + b_1 s}{s^2 + \omega'^2_1} + \frac{a_2 + b_2 s}{s^2 + \omega'^2_2} + \cdots + \frac{a_m + b_m s}{s^2 + \omega'^2_m} \right) \tag{3.49}$$

The a_l and b_l terms can be found using the method of residues. Multiplying Eq. 3.49 by the denominator of the ith term and evaluating at $s = j\omega'_i$ gives

$$\left.\frac{D_1 D_2}{\prod_{l=1}^{m}(s^2+\omega'^2_l)}\right|_{s=j\omega'_i} = \left[s^2(a_i + b_i s)\right]_{s=j\omega'_i} + [\text{Remaining Terms}]_{s=j\omega'_i} \tag{3.50}$$

The left-hand-side becomes a constant, and the remaining terms in the expansion vanish, so Eq. 3.50 simplifies to

$$a_i + b_i j\omega'_i = \text{constant} \tag{3.51}$$

Since constant is real, a_i = constant and $b_i = 0$. So the open-loop transfer function, from control force to transmitted force, can be written as Eq. 3.47, or

$$\frac{D_1 D_2}{\prod_{l=1}^{m}(s^2+\omega'^2_l)} = s^2 \sum_{l=1}^{m} \frac{a_l}{s^2+\omega'^2_l} \tag{3.52}$$

To show that the transfer function in Eq. 3.52 has a pattern of alternating poles and zeros in the complex plane, we could use the results of Martin and Gevarter. Their work, however was done for force/displacement or force/velocity pairs. Using similar techniques, Sievers [1988] showed that a non-dual, colocated input/output pair (voltage input to force output) provides the same pole-zero pattern. In that work, the transfer function had the same form as that shown in Eq. 3.52, but there was only one pair of zeros at the origin. Here, we have two pairs of zeros at the origin, but there is also a pair of poles at the origin, which cancels two of the zeros. The resulting pattern along the imaginary axis, then, effectively starts with a pair of zeros, then alternates pole, zero, pole, zero, as frequency is increased, ending with a pole (the transfer function is proper). So, with gain feedback, each pole approaches a zero, and there are no asymptotes in the root locus.

It was shown by Martin that a system of the form of Eq. 3.47 has alternating poles and zeros along the imaginary axis in the complex plane if and only if the signs

of all the a_i are the same. Since we know that the transfer function for our plant can be written in terms of Eq. 3.47, and we also know that it has an alternating pattern of poles and zeros in the Laplace plane, then this theorem tells us that all the numerator coefficients in Eq. 3.52 have the same sign. Now we can say that, just as with colocated position and velocity feedback, we can use force feedback (with a simple gain) and be assured of a stable system.

3.4.2 Stability for More Complex Feedback Dynamics

As the dynamics in the feedback loop become more complex, the stability issues are no longer clear-cut. Added dynamics from the actuator, sensor, and compensator bring new poles and zeros into the system transfer function. The guaranteed patterns discussed in the previous section no longer hold, and stability is no longer guaranteed.

If the dynamics added to the system include only a first-order pole then the root locus remains simple. (In this work, the actuator is a dc motor, so if simple gain force feedback is used, a pole is added on the negative real axis.) Recall that the original transfer function had numerator and denominator of the same order, so there were no zeros at infinity. By adding a single pole, we get a single zero at negative infinity on the real axis, and as the feedback gain is increased, the system stays in the left-half plane.

Another simple compensator that has been considered for colocated, position feedback vibration control is a lead compensator [Martin, 1978]. Recall that for the undamped case, the alternating poles and zeros are all on the imaginary axis. For position feedback, as the poles approach the zeros, they do so along straight lines, not wandering off the axis. By adding lead compensation, the effect is to pull the eigenvalues slightly to the left, off the axis, and to add some damping to the system.

This is a desirable property in vibration control, but serves no purpose in vibration isolation (in fact, added damping can be counter to the goals of vibration isolation, see section 2.1.1).

More complicated compensators may include complex poles and zeros (as mentioned in the discussion of classical disturbance rejection, section 2.2.1. As soon as we introduce complex poles and zeros into the system transfer function, the guaranteed pole-zero pattern no longer holds, and we are no longer guaranteed to have the same sign on all the a_i in Eq. 3.52. So, the system may or may not be stable. Note from the discussion in section 3.3 that closed-loop eigenvalues still move from open-loop poles to open-loop zeros, which now include poles and zeros of the feedback dynamics. The endpoints of the locus are stable, (assuming we choose a stable compensator and there are no asymptotes which enter the right half-plane), but the question becomes whether or not the locus still exists entirely in the left-half plane.

That question is addressed by Sievers by looking at the system's phase margin. If the poles and zeros alternate along the imaginary axis, then the phase is bounded by 180° and 0° (the phase starts at 180° because of the two zeros at the origin). If poles are added, through feedback dynamics, which alter this pattern, then the phase margin may be reduced, and instabilities are possible. Sievers showed that as the system poles and zeros become more tightly spaced, the stability robustness increases for simple compensators of the kind shown in section 2.2.1. The reason for this can be stated heuristically by saying that as the pole-zero spacing decreases, the change in phase margin decreases from one pole or zero to the next. So, the chances decrease for lags in the feedback dynamics to cause the phase margin to approach zero.

A result of this idea, then, as mentioned by Sievers, is that a nice tradeoff may be made between model-based and non-model-based controllers. The non-model-

based controllers, such as the classical compensators discussed here, perform well in systems with tightly spaced modes, while the model-based controllers perform better in systems where the modes are more sparse (because the models can be more well-defined in those systems).

Chapter 4

Active Mount Configurations and Their Models

Up to this point, the discussion of active vibration isolation mounts has been directed toward a parallel arrangement, as that shown in Fig. 3.2b. This is not the only possibility for physically realizing an active mount, nor are the resulting equations of Chapter 3 the only possible mathematical models for such mounts. This chapter will discuss several different arrangements for active mounts, along with the physical and mathematical implications of each. Next, possible models will be presented for the various active mounts, and it will be shown that mathematically, the various choices for mounts affect the system the same way. The model for the active mounts used experimentally in this work will be presented. Finally, a few points on the simulation of these active links, and free-free systems in general will be presented.

4.1 Physical Arrangements for Active Mounts

As has been mentioned, the underlying reasoning behind connecting two vibrating systems is that there is either a static load which must be supported, or there are constraints on the relative motion which is allowed to take place between the two systems. It is the goal of a mount (whether active or passive) to meet those

constraints while allowing the minimum possible amount of interaction between the two systems. In the case of a static load, this implies the magnitude of the transmitted force frequency response to be unity at zero frequency, and to roll off at all other frequencies. In the case of space structures, the "load constraint" comes in the form of station-keeping forces, and may even be thought of as a relative-motion constraint. The ideal mount in this case would be one which could be made rigid while station-keeping forces were being applied to the entire structure, but would have zero stiffness at all other times, so that structural vibrations would not pass between the clean and dirty sides. Some capability would, of course, be required to maintain proper distances across the mount.

There are various methods for reaching the goals described above, and each method has its individual operational considerations which make it more suitable for certain applications. In general, there are two techniques for achieving an active mount, as shown in Fig. 4.1.

The parallel arrangement, the one most discussed up to this point, involves placing an actuator in parallel with the passive stiffness and damping of the mount. The idea behind this configuration is to use the passive characteristics of the mount to support any necessary static loads, and to maintain clearances. The actuator, then, acts to modify the frequency response, and improve on deficiencies in the passive design. If this arrangement is used, it is important that the actuator characteristics be compatible with those of the mount. For example, the actuator's stiffness must be somewhat less than that of the mount so that the passive system is allowed to perform as is should (if the actuator is rigid compared to the mount, then the mount serves no purpose).

Even though a parallel arrangement alleviates the need for the actuator to support static loads, it must be capable of overcoming the mount stiffness when the

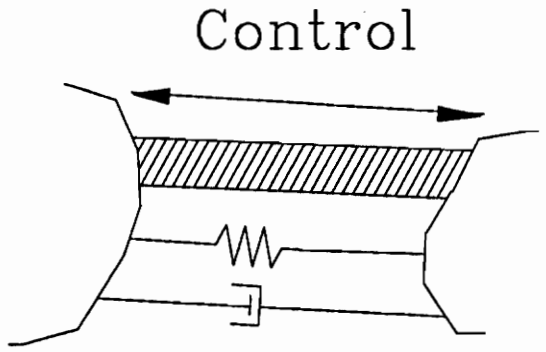

a. Parallel arrangement for active mount.

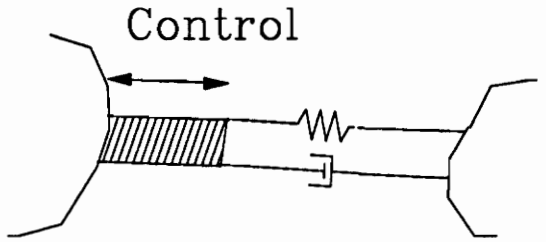

b. Serial arrangement for active mount.

Figure 4.1: Two general configurations for active mounts.

mount is activated. The result is an active mount capable of high forces, but low displacements. Applying a cancelling, isolation force in parallel with a steel support of a machine could require high forces (this depends upon the disturbance force) and small motions would be allowed in the elastic region of the support.

The serial arrangement, as shown in Fig. 4.1b, involves placing an actuator in series with the passive mount hardware. In this case, the passive mount may not actually be necessary, because any forces generated in the actuator would pass through the mount, directly to the structure. By the same token, the actuator must have sufficiently high stiffness to support static loads when used in this arrangement because the effective stiffness of a serial arrangement of springs is less than either individual stiffness. The usefulness of the passive mount in this case may be in providing mount compliance when the actuator is not operating.

Examples of serial active mounts could be hydraulic actuators or electric motor arrangements such as a linear dc motors or motor/leadscrews. The actuators used in this work are dc-motor/leadscrew pairs. These types of actuators can produce larger motions, but tend to have lower operating bandwidths than the piezoelectric or hydraulic actuators. Their configuration does not require them to overcome a high stiffness to be effective, and for that reason, large motions are more likely to be attained. This may be useful if we consider that a serial active mount's job is to "get out of the way" of the vibrating structure, rather than to produce a cancelling force as the parallel mount does.

4.2 Active Mount Models

Just as there are two different physical arrangements for active mounts, there are different possible mathematical descriptions for each active mount as well. Figure 4.2 shows several schematics, each representing possible mathematical models of the

parallel or serial mount configurations. Each figure shows a free-body diagram of a possible active mount as it would exist between two structures. Note that, for simplicity, the configurations discussed are considered to be undamped. The forces f_1 and f_2 are the forces applied to the mount by the structures, as shown in Fig. 3.2a. In this section we will derive the equations describing each schematic in Fig. 4.2, and in so doing, will show that the resulting transfer functions from control force to transmitted force have the same form, so the previous discussions involving force feedback characteristics hold for any mount configuration. The choice of mount model will then depend on the operational considerations of a particular case.

Figure 4.2a shows a schematic for an ideal active mount. In this mount, the force connecting the two systems is commanded by the controller, so that the transmitted force is $f_t = f_c$. (The serial spring, k_s, may or may not be present. It has no effect since the commanded force passes directly through it.) This is an ideal configuration, because the transmitted force can be chosen arbitrarily by the controller. If a static force, f_s, is required, then $f_c = f_s$, or if isolation between the two systems is desired, $f_c = 0$. The difficulty in this approach is in finding the hardware that can produce zero force (which implies zero stiffness and damping) upon command. In any physical implementation, there will always be some dynamics associated with the actuator, and, more importantly for this discussion, there will always be some residual stiffness and damping connecting the two systems when the commanded force is zero.

The configuration shown in Fig. 4.2b is a more realistic description of a parallel active mount. The control force is shown to be in parallel with some mount stiffness, which could be the stiffness of a passive mount or the residual stiffness mentioned above. The resulting transfer function from control force to transmitted force for

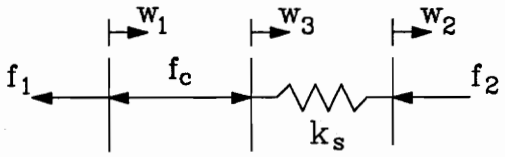

a. Force-commanded, serial mount.

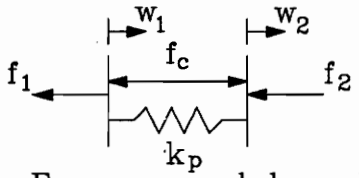

b. Force-commanded, parallel mount.

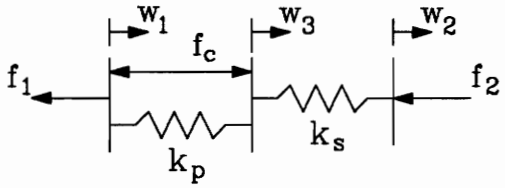

c. Force-commanded, hybrid mount.

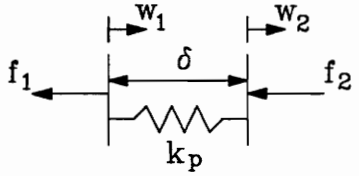

d. Position-commanded, parallel mount.

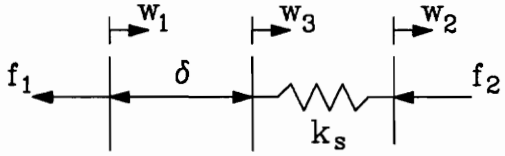

e. Position-commanded, serial mount.

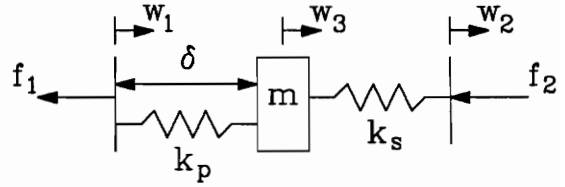

f. Position-commanded, serial mount, with mass.

Figure 4.2: Schematics of possible active mount models.

this case has been derived previously (Eq. 3.28), and is repeated here

$$\frac{f_t}{f_c} = \frac{1}{1 + k_p(G_1 + G_2)} \tag{4.1}$$

A more likely configuration would be for the active part of the mount to consist of only part of the entire passive length of the mount. For example, in the case of a piezoelectric actuator on a steel machine support, only part of the length of the support would be actuated. The rest of the support would be in series with the active portion of the mount. This configuration is represented in Fig. 4.2c. To derive the transfer function for this case, we start with force sums at points 2 and 3 in Fig. 4.2c.

$$\sum F_2 = -f_2 + k_s(w_3 - w_2) = 0 \tag{4.2}$$

$$\sum F_3 = f_c + k_p(w_1 - w_3) - k_s(w_3 - w_2) = 0 \tag{4.3}$$

These can be rearranged to give

$$f_t = \frac{k_s}{k_p + k_s} f_c + \frac{k_s k_p}{k_s + k_p}(w_1 - w_2) \tag{4.4}$$

where we used our previous definition for transmitted force, $f_t = f_2$. Applying the representations for w_1 and w_2 from Chapter 3, the transfer function becomes

$$\frac{f_t}{f_c} = \frac{\frac{k_s}{k_s+k_p}}{1 + \frac{k_s k_p}{k_s+k_p}(G_1 + G_2)} \tag{4.5}$$

Note that this is the same form as Eq. 4.1, with a slight difference in the representation of mount stiffness.

All the active mounts considered up to this point have included force-commanded actuators. Another possibility for actuator hardware is that for which the command is kinematic in nature (such as the desired length, velocity, or acceleration). Figures 4.2d–f illustrate possible active mount configurations in which the mount length is commanded. The actuators which make up these mounts could be stepper-motor

arrangements, where the commanded output is truely position, velocity, or acceleration, or they could be hydraulic cylinders or servo-motor arrangements which are controlled with a position loop.

The configuration shown in Fig. 4.2d is perhaps the simplest of such arrangements, where the active mount is shown in parallel with the mount stiffness. Note that the parallel stiffness need not exist if the actuator stiffness is high enough to support required static loads. By summing the forces at point 2 we get

$$\sum F_2 = -f_2 + k_p(w_1 - w_2) + f_\delta \tag{4.6}$$

where f_δ is the actuator force. The relative displacement between the two systems is the output of the actuator, $w_1 - w_2 = \delta$. So the transmitted force becomes

$$f_t = k_p\delta + f_\delta \tag{4.7}$$

This says that in order to drive f_t to zero, we must specify the displacement of the mount such that the force in the actuator is equal and opposite to the force in the "passive side" of the mount. The forward effect for this case, then, becomes the control force (not the control displacement), and this case is analogous to that in Fig. 4.2b.

The mount in Fig. 4.2e shows a commanded actuator displacement in series with a passive mount stiffness. Summing forces at point 2 for this case results in

$$\sum F_2 = -f_2 + k_s(w_3 - w_2) = 0 \tag{4.8}$$

But $w_3 = w_1 + \delta$, so Eq. 4.8 can be written as

$$f_2 = k_s\delta + k_s(w_1 - w_2) \tag{4.9}$$

which can be rearranged to give the transfer function

$$\frac{f_t}{\delta} = \frac{k_s}{1 + k_s(G_1 + G_2)} \tag{4.10}$$

Once again, the resulting transfer function is equivalent to that shown in Eq. 3.28. Note that in this case, the forward-effect is, indeed, the actuator length, while an unseen back-effect is the required actuator force. We are assuming that the actuator can supply any force required to provide the necessary motion. For a massless actuator, this is easy to do, since in theory we can achieve any acceleration (and thus any displacement) with no force. For a physical system, however, there is mass (and possibly other dynamics) in the actuator.

Figure 4.2f shows a serial, displacement-commanded active mount with mass included in the actuator. A force sum at point 2 will show that the added mass does not change the expression for transmitted force, and thus the transfer function from control displacement to transmitted force is unchanged. What has changed, however, is the expression for the required actuator force (the back-effect of the displacement-commanded actuator). A force sum at point 3 gives

$$\sum F_3 = f_\delta - k_s(w_3 - w_2) = m\ddot{w}_3 \tag{4.11}$$

Equation 4.11 contains the dynamics governing the motion of the actuator. The term f_δ contains some input command, along with actuator characteristics which dictate how it enters the equation. The above equation makes up the character of the "actuator dynamics" transfer function that was discussed in Chapter 3. As was shown here, the effects of mass (or actuator damping) can be included in those dynamics.

4.3 Active Link Model Used in This Work

Given the discussion of the previous section, we see that many different models for active mounts result in the same form of transfer function from control force to transmitted force. Choosing the proper model for an application depends on

the particular mount characteristics in that situation. The experimental hardware used in this work includes active mounts which are made up of dc-motor/leadscrew combinations. There is no parallel stiffness in the mount, so a serial model arrangement is warranted. When no control is applied to the actuator, it becomes essentially rigid in relation to the dynamics of the system to which it is attached (the leadscrew is not reversible). The implication here is that the active link is basically a length-commanded actuator. (We could model this as a force-commanded actuator arranged in parallel with a very high stiffness, but this would mean that actuation requires overcoming the parallel stiffness in order to provide any motion. The resulting control signals would be different from the actual ones by orders of magnitude.)

The model used for the active links in this work is shown in Fig. 4.3a. This is equivalent to that shown in Fig. 4.2e, and includes a length-commanded actuator in series with a mount stiffness. The stiffness is included so that, in simulations, we can have a measure of transmitted force (the force transmitted across the link is equal to the force in this serial stiffness). In the actual experiments a force transducer provides that measurement.

The equations of motion for the active mount for coordinates x_1 and x_3 shown in Fig. 4.3a are

$$\begin{aligned}(m_1 + m_2 + m_3)\ddot{x}_1 + (m_2 + m_3)\ddot{x}_2 + m_3\ddot{x}_3 &= Q_{x_1} \\ m_3\ddot{x}_1 + m_3\ddot{x}_2 + m_3\ddot{x}_3 + k_3 x_3 &= Q_{x_3}\end{aligned} \tag{4.12}$$

where Q_{x_i} are the generalized forces acting on the system. The third equation for this three degree-of-freedom system describes the motor/leadscrew dynamics, and govern coordinate x_2. Recall that the motor is not reversible, so its equation stands alone. The motor/leadscrew output, displacement x_2, is only dependent on the

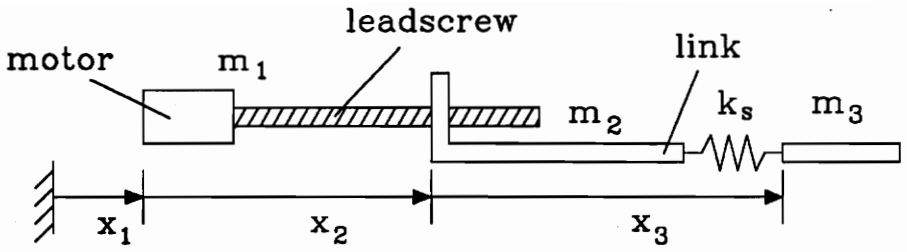

a. Active mount used experimentally and analytically in this work.

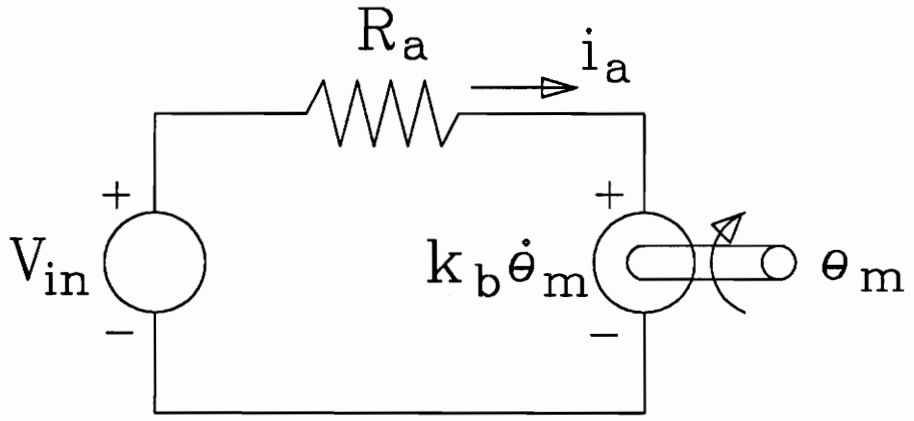

b. Electric circuit for motor of active mount.

Figure 4.3: Illustration of active mount and electrical circuit for its motor.

motor input voltage and the motor/leadscrew dynamics. It couples to the other equations by supplying a kinematic input through the $\ddot{x}_2$ terms in Eq. 4.12.

The motors used in this work are armature-controlled dc motors. The circuit from which the motor is modelled is shown in Fig. 4.3b. This model has been simplified by assuming the motor's armature inductance adds negligible dynamics (inductance adds an "electrical pole" to the system which is much faster than the "mechanical pole," so it is neglected) [Electro-Craft, 1980]. Applying Kirchoff's voltage law to the circuit in Fig. 4.3b gives

$$V_{in} - R_a i_a - K_b \dot{\theta}_m = 0 \tag{4.13}$$

where V_{in} is the input voltage, and θ_m is the motor shaft position. For a dc motor, the torque provided is proportional to the armature current

$$T_m = K_t i_a = J_{eq} \ddot{\theta}_m \tag{4.14}$$

With the leadscrew attached to the motor (with lead G_l), and assuming the motor output passes through a gear train (with ratio G_m), the link acceleration is related to motor shaft acceleration by

$$\ddot{x}_2 = \frac{G_l}{G_m} \ddot{\theta}_m \tag{4.15}$$

Substituting Eqs. 4.14 and 4.15 into Eq. 4.13 leads to the third equation of motion for the active mount

$$\ddot{x}_2 + \frac{K_b K_t}{R_a J_{eq}} \dot{x}_2 = \frac{G_l K_t}{R_a J_{eq} G_m} V_{in} \tag{4.16}$$

where J_{eq} is the equivalent inertial load seen by the motor. Note that the load is made up primarily of three parts: the armature moment of inerita, the leadscrew moment of inertia, and the link mass. These three inertial terms can be added to give the total equivalent inertia as

$$J_{eq} = J_a + J_{ls} \frac{1}{G_m^2} + m_{link} \frac{G_{ls}^2}{G_m^2} \tag{4.17}$$

As a result of the two gear ratios in the system, the armature moment of inertia is the dominant term in Eq. 4.17 by at least an order of magnitude.

Not shown in Eq. 4.14 is the structural loading on the motor. This loading couples the other equations through the acceleration terms, but it also sees the gear ratios of the third term in Eq. 4.17. With this in mind, we should feel confident that it is valid to ignore the structural loading and write the motor equation as independent of the rest of the system.

Another point to keep in mind when considering the "structural loading" term is that when the motor/leadscrew is being used as an actuator in an active vibration isolation mount, it is always being driven so as to "get out of the way of" the structure, so it doesn't see a load from the structure. If it does see a structural load, then this implies a transmitted force through the active mount, and the mount or the controller is not working effectively.

4.4 Considerations on Simulating Active Mounts and Free-Free Systems in General

During the course of this work there was a recurring problem whose origin was unexpected. Most of the systems dealt with throughout this work have free-free boundary conditions, so there is a rigid-body mode which may appear in the response (consider the systems shown in Figs. 3.2, 3.1, and 3.5). Since the disturbances seen in this work are almost exclusively zero-mean (sines and cosines or random signals), it was expected that only rigid-body motions which fluctuated about zero would be seen. This is not, however, what was found.

A periodic forcing function applied to a system whose type is greater than zero will produce a step or ramp term in its response. This can be seen by the following discussion.

Consider a system which can be described by the following type-two transfer function

$$\frac{x}{f} = G(s) = \frac{N(s)}{s^2 D(s)} \tag{4.18}$$

This could describe the force-to-displacement transfer function for a free-free flexible structure. If the force input is sinusoidal

$$f(t) = a \sin(\omega t) \tag{4.19}$$

then the Laplace-transformed output becomes

$$\begin{aligned} x(s) &= \frac{N(s)}{s^2 D(s)} \frac{a\omega}{s^2 + \omega^2} \\ &= (\text{transient dynamic terms}) + \frac{A}{s^2} + \frac{Bs + C}{s^2 + \omega^2} \end{aligned} \tag{4.20}$$

The second row of Eq. 4.20 is the partial fraction expansion of the output. The first term of this expansion contains the transient terms resulting from the system natural frequencies. The third term is the expected forced response. The second term, after applying the inverse-Laplace transform, becomes a ramp in the time domain. When this behavior appears in the response, it obscures the true picture by making the system appear to be unstable. (Note that a cosine forcing function also gives an unusual response term. Since its Laplace transform looks like $\frac{as}{s^2+\omega^2}$, the numerator s cancels with one of the free s's in $G(s)$, and we get a step in the response.)

There are several ways to get around this problem. One is to attach the system to ground with a simulated spring, which removes the rigid-body mode. This is unacceptable because it loses the point of simulating a free-free system in the first place. An alternative solution is to cancel the resulting ramp (or step) with an equal and opposite initial condition, a feasible solution for simulations. This can become complicated, though, if the disturbance contains multiple harmonics, or is

broadband in nature. Finally, the problem could be avoided altogether by applying an internal, rather than an external, disturbance force to the system. This may require the addition of a degree-of-freedom to the model to provide a proof-mass to react against. (Note that such a problem does not exist in the experiment, because there we use a proof-mass, or rotating unbalance forcing device, which provides an internal force to the system.)

If the problem were as simple as an external periodic force causing a ramp response in the free-free system, then it probably wouldn't be worth mentioning here. In a steady-state disturbance rejection problem, however, (as we have posed this vibration isolation problem) the character of the disturbance shows up indirectly as the character of the control signal. So, in this case, if the disturbance is sinusoidal, the motor input voltage is sinusoidal as well. Recall from Eq. 4.16 that the motor equation is second-order with no zeroth-order term. Its transfer function (from motor input to position output) is then type-one, and a harmonic input will cause a step in the motor response.

So, even if we have solved this step/ramp problem for the free-free system, it shows up again in the actuator. In this case, though, we cannot solve the problem by initial conditions, because the required initial condition would be unpredictable due to phase lags in the system, and due to the possibility of the controller and disturbance not starting simultaneously. The only choice in this case is to "tie the motor to ground", or to supply a spring term in the motor equation to remove the free integrator in its transfer function. This can be done through position feedback of the motor/leadscrew. It has been mentioned that position feedback may be desirable to avoid drift in the mount, or to maintain necessary clearances in the system, but now we see that is required to avoid a step response due to periodic control signals.

Chapter 5

Vibration Isolation With a Single Mount

This chapter demonstrates the use of active force feedback for vibration isolation by applying several control techniques to our lumped-mass system. This system is redrawn, with coordinates, in Fig. 5.1. The disturbance enters the system as shown in Fig. 5.1, and isolation occurs at the same location as before, however the mount arrangement is different. The active mount to be used in these simulations is the serial, length-commanded mount discussed in section 4.3. The system parameters are chosen so that the natural frequencies are within the bandwidth of the actuator.

The approach in this chapter will be to introduce the control methods to be used, then results of the application of those techniques on the system in Fig. 5.1 will be given.

5.1 Control Laws for Active Vibration Isolation

Three control schemes are used for active vibration isolation in this and the next chapter. In each case, force feedback will be the fundamental principle involved.

The first control law will be simple, high-gain force feedback which was discussed in Chapter 3. We know that this method provides a stable controller, and, given a

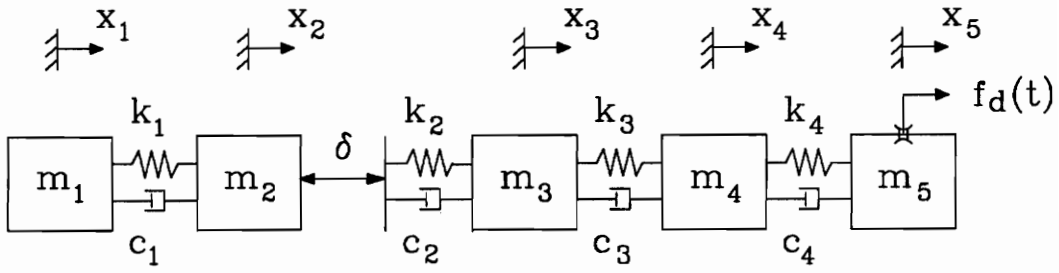

Figure 5.1: Lumped mass system shown with coordinates.

high enough gain, will produce complete isolation within the system.

The second control technique to be applied is force feedback through a classical compensator. The compensator will be chosen such that it has a pair of poles centered at the disturbance frequency. This technique, although it has the potential to destabilize the system, has an advantage over the gain-only controller in that a relatively low feedback gain is necessary to achieve a large decrease in transmitted force. The decrease comes about through the resulting closed-loop zeros which are centered at the disturbance frequency. The stability problem may be reduced by adding damping to the compensator (to keep the compensator poles from entering the right half-plane at low gains), or by including compensator zeros which are very near the poles (in an attempt to preserve the alternating pole-zero pattern of the system). Both of these techniques, however, can reduce the performance of the compensator.

The third control method employed here for vibration isolation is the linear quadratic regulator technique with disturbance modelling. In this approach, we assume we have an accurate model of the system and the disturbance dynamics, so the LQR method is applied to develop a controller with characteristics similar to those of the classical compensator, but one whose stability is guaranteed. It is important to realize that we only seek stability here, not increased damping as we would in a vibration control problem. By using an actuator to dissipate energy from a system, the actuator serves as a damping mechanism, and a damper can function only if there is a force applied across it. The damping force also becomes a transmitted force in the mount, which is counter to the goals of our isolation task. So, we cannot use the same actuator for vibration control and vibration isolation without compromising the performance of each. The approach for using the LQR method, then, will be to penalize the transmitted force in the system, but to leave

all other system states alone.

5.2 Results of Vibration Isolation with a Single Mount

5.2.1 High-Gain Force Feedback

We will begin our discussion with the case where high-gain feedback of the transmitted force is used for control. The first example involves a harmonic disturbance with amplitude of 1 Newton and frequency of 2 rad/sec. The results of this case are shown in Figs. 5.2-5.3. Figure 5.2a shows the force transmitted through the mount. It is clear that the high-gain control serves to immediately suppress the transmitted force. The control voltage required for this performance is shown in Fig. 5.2b. The gain in this case is 5000 V/N, and even though it does not produce excessive control voltage in steady-state, it is high enough to move the system eigenvalues very near their respective zeros, as shown in Table 5.1. We can see that we have effectively

Table 5.1: System eigenvalues for various cases of high-gain feedback.

Gain = 0	Gain = 5000	Gain = 250	Zeros
$-1.25 + 7.48j$	-180	$-13.47 + 8.59j$	$-\infty$
$-1.25 - 7.48j$	-32.1	$-13.47 - 8.59j$	-30
$-0.64 + 5.57j$	$-1.39 + 6.73j$	$-1.60 + 6.67j$	$-1.38 + 6.73$
$-0.64 - 5.57j$	$-1.39 - 6.73j$	$-1.60 - 6.67j$	$-1.38 - 6.73$
$-0.39 + 3.90j$	$-0.26 + 4.46j$	$-0.43 + 4.34j$	$-0.25 + 4.66$
$-0.39 - 3.90j$	$-0.26 - 4.46j$	$-0.43 - 4.34j$	$-0.25 - 4.66$
$-0.12 + 2.32j$	$-0.61 + 3.49j$	$-0.88 + 3.44j$	$-0.60 + 3.49$
$-0.12 - 2.32j$	$-0.61 - 3.49j$	$-0.88 - 3.44j$	$-0.60 - 3.49$
0	0	0	0
0	0	0	0
0	0	-1.41	0
-19.8	-0.38	-0.01	0

moved a pair of poles to the origin, and lost an oscillating mode of the system.

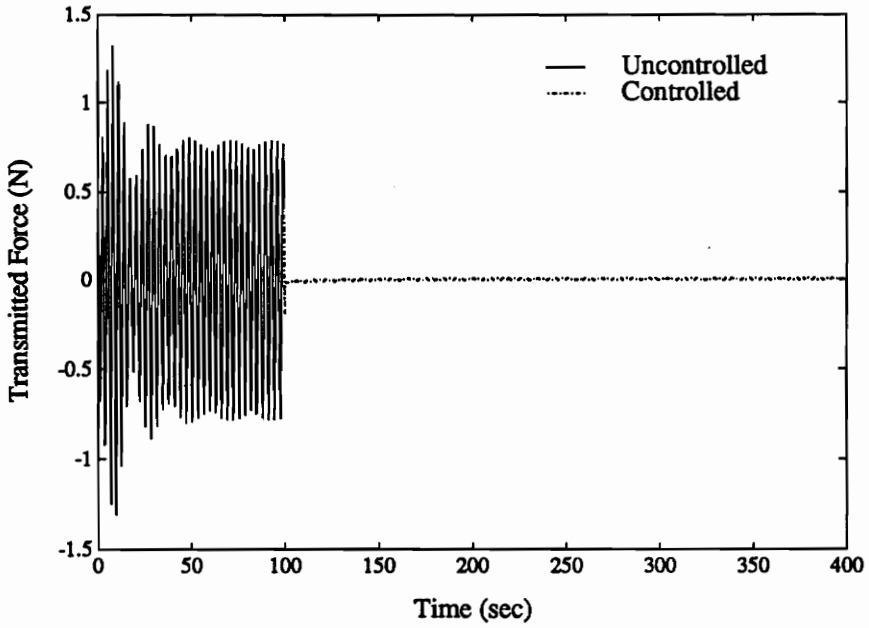

a. Transmitted force.

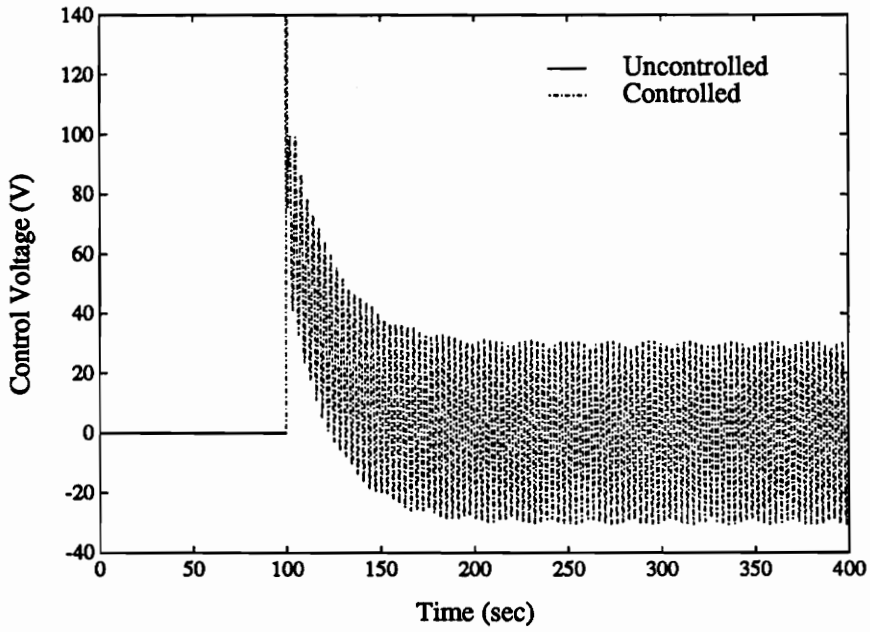

b. Control voltage.

Figure 5.2: Transmitted force and control voltage for high-gain ($k_c = 5000$) force feedback with no link control where disturbance is harmonic.

Remember that reduction of transmitted force only serves as a means to an end. The true goal is to reduce motions on the clean side of the system. Figure 5.3a shows the displacement amplitude of mass 1 (a clean-side mass), and it is clear that it is suppressed.

In reducing the transmitted force in the system, we have removed a significant portion of the mass from the part of the system affected by the disturbance. So in addition to decreasing the motions on the clean side of the system, we would expect to see an increase in motions of the dirty side. Figure 5.3b shows that the displacement amplitude of mass 3, a dirty-side mass, does, in fact, increase.

Note that the only control in this example is force feedback, which applies a harmonic input to the motors in the active mount. From Eq. 4.20 we know that such an input causes a step in the response of the motor output (since the motor transfer function from voltage to displacement is type-one). That step shows up in the displacements of Fig. 5.3, and also in the active link displacement shown in Fig. 5.4. To eliminate that offset, we must apply some low-authority control on the active link length. This is done (with a link-length gain of 5), and the results are shown in Fig. 5.5. Figure 5.5a shows that the added link gain causes the active link displacement to oscillate about zero in steady-state (we have changed the motor transfer function to type-zero). This is done with no noticeable degradation in the performance of the controller, as shown in Fig. 5.5b, where the transmitted force is suppressed just as before.

The explanation for how high-gain force feedback provides isolation has been that new rigid-body modes are created in the system, and the system eigenvalues are "separated." This condition, shown by Table 5.1, implies infinite (or at least very high) feedback gain. Such a gain may seem unreasonable in physical systems, primarily because of limitations such as saturation of the controller. It is important

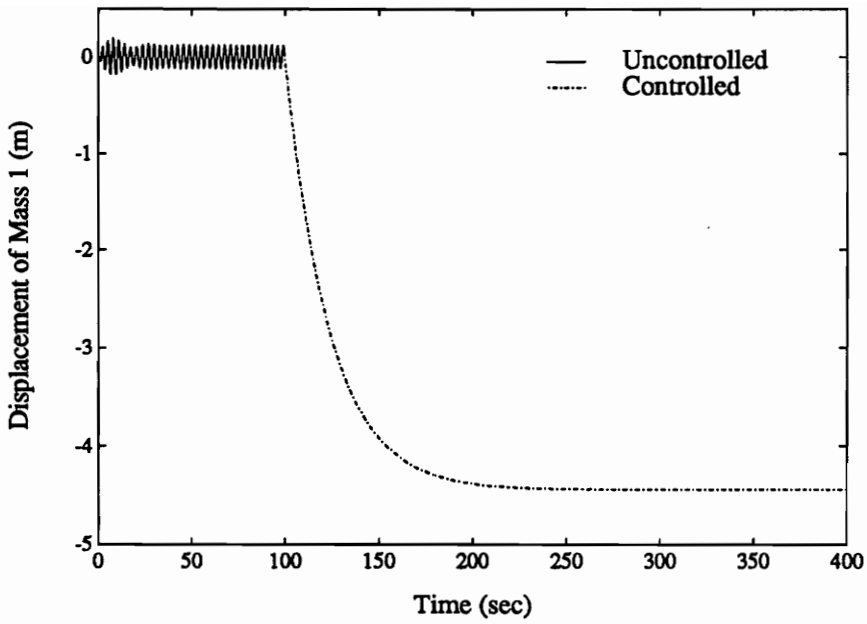

a. Displacement of mass 1.

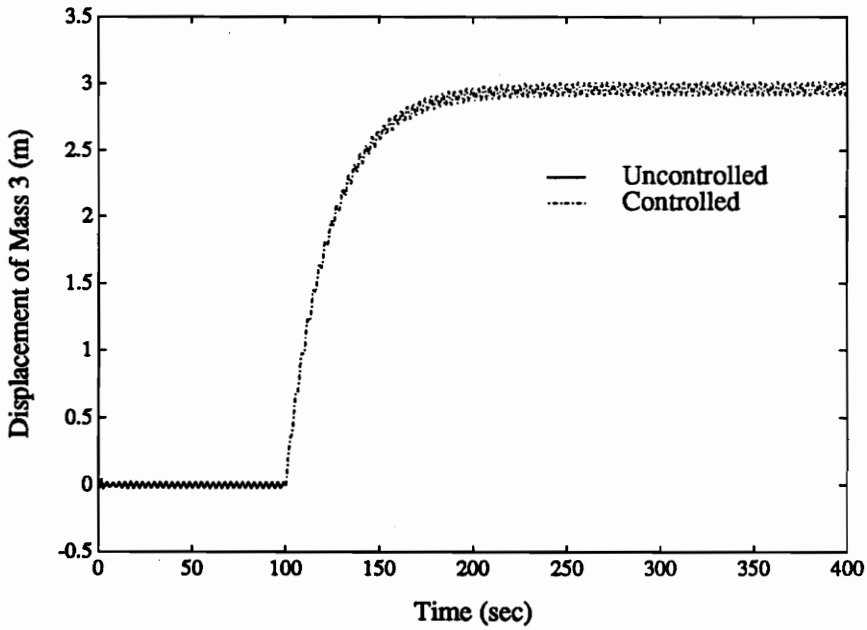

b. Displacement of mass 3.

Figure 5.3: Motions of masses within the isolated system.

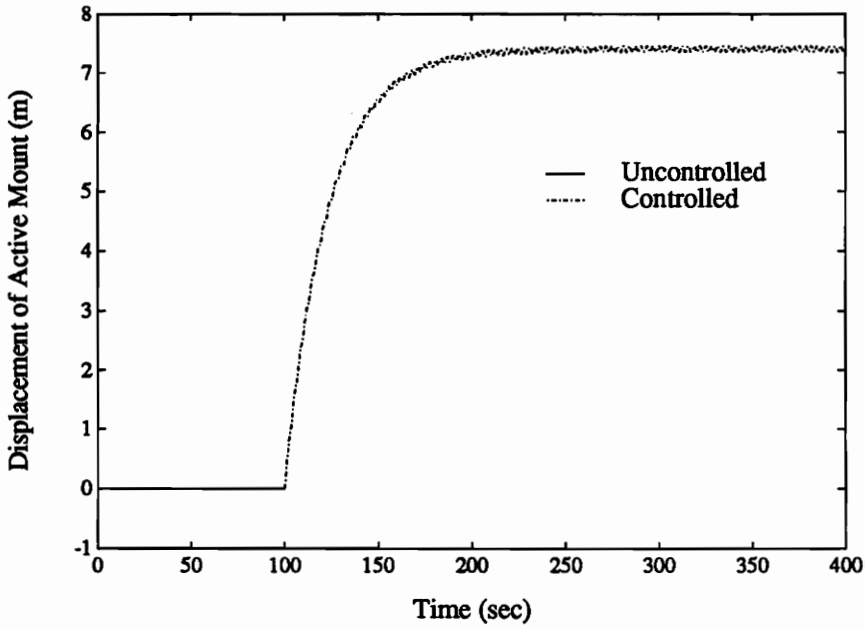

Figure 5.4: Displacement of active mount.

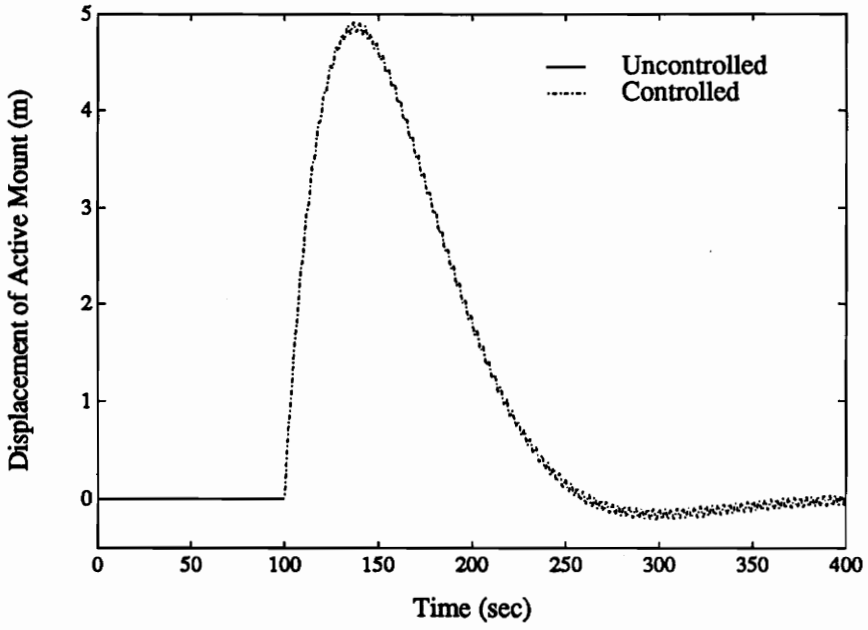

a. Displacement of active mount.

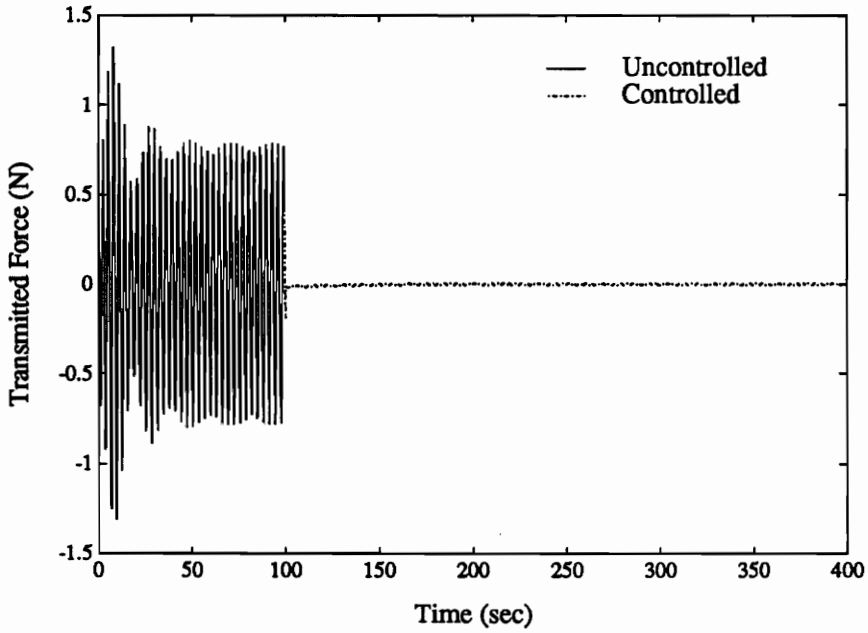

b. Transmitted force.

Figure 5.5: Active mount displacement and transmitted force for high-gain (k_c = 5000) force feedback with low-authority link control where disturbance is harmonic.

to note, however, that the gain does not have to be pushed to some critical value (where the poles are very near the zeros) before any performance is seen. We get some isolation for any amount of gain, as can be seen by Fig. 5.6, where the gain is 250. In this case, we get some isolation performance, however not as much as when the gain was much higher. The eigenvalues for this case (the third column of Table 5.1 are not moved nearly as far as before. We can also see that the required control for this case is lower, as expected. By comparing Figs. 5.2 and 5.6, we see that large increases in gain provide subsequently smaller increases in isolation, but the resulting increase in required control is almost insignificant.

A possible scenario in many vibration isolation problems is the case where the mount must sustain a static load (as discussed in Chapter 1). Such a load causes a dc offset in the transmitted force, and causes the active link to monotonically increase or decrease its length to try to eliminate the transmitted dc force. When there is feedback applied to the active link length, the active link changes its length to a point where the link control and the control due to the static component of the transmitted force cancel each other and the link displacement "levels off." This is shown in Fig. 5.7a where the disturbance force is harmonic (amplitude of 1 Newton) with a bias of 1 Newton. (In this example, in order to keep the static component of the force from exciting the system's rigid body mode, we have attached the system to ground through a spring on the left-hand-side. By doing this, a zero happened to be placed at approximately 2 rad/sec, so the disturbance frequency was shifted to 2.5 rad/sec in order to show an appreciable uncontrolled response.) Since the ratio of link-gain to force-gain is so low in this case (5:5000), the link length becomes extremely high before the two control effects cancel. Note from Fig. 5.7b that the controller attenuates the oscillatory transmitted force, but passes the static component. In order to decrease the dc offset of the active link length, it is possible

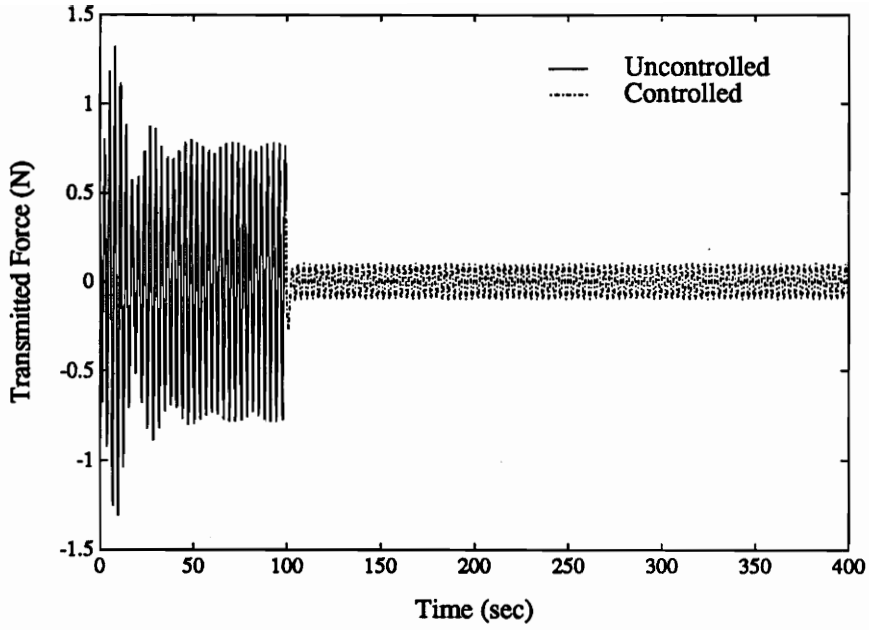

a. Transmitted force.

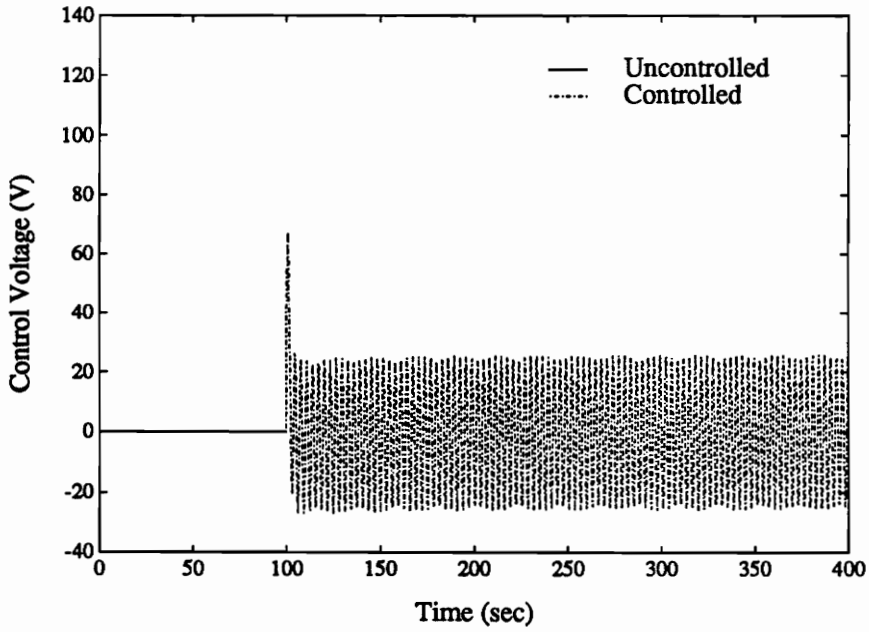

b. Control voltage.

Figure 5.6: Transmitted force and control voltage for "medium-gain" ($k_c = 250$) force feedback where disturbance is harmonic.

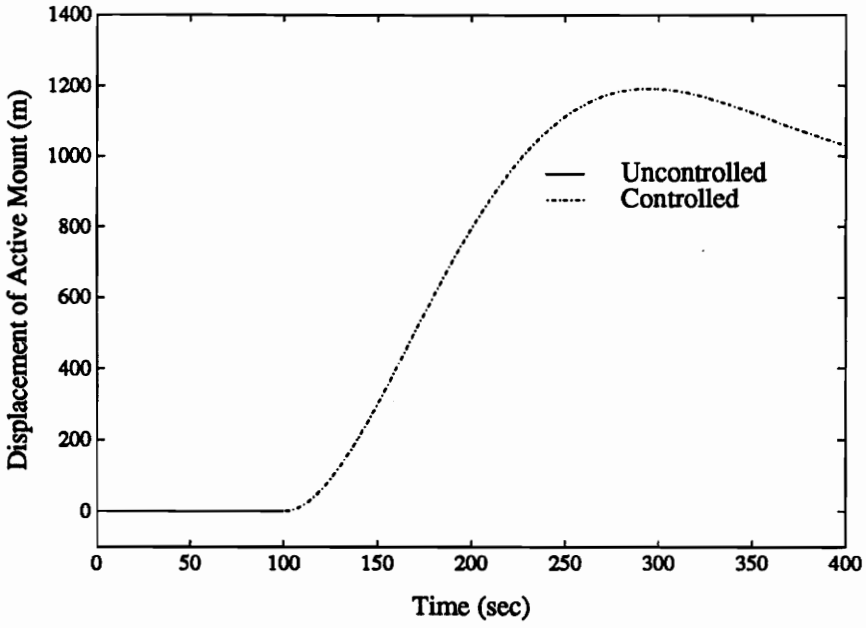

a. Active mount displacement.

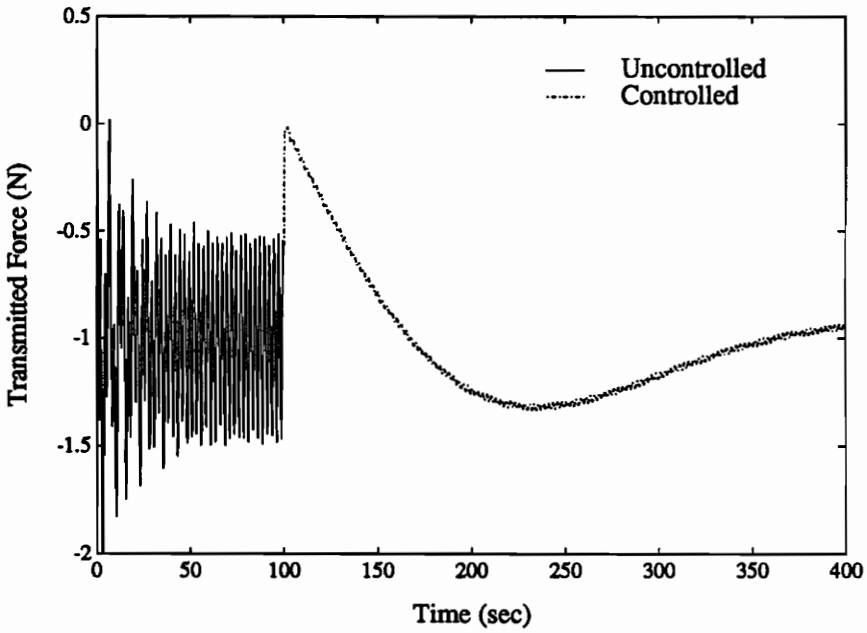

b. Transmitted force.

Figure 5.7: Transmitted force and active mount displacement for high-gain (k_c = 5000) force feedback where disturbance is harmonic with offset.

to increase the link gain. Figure 5.8a shows the resulting active link displacement when a link gain of 3000 is used. The offset of the link is more reasonable, but at the cost of decreased performance in isolation (Fig. 5.8b). The high link gain causes the motor/link poles to be underdamped, giving an oscillation in the response. In steady-state, the gain suppresses the dc offset, but it also hinders the mount's isolation performance. We have effectively penalized the control applied to the active mount.

The link gain applied to the active mount has the same effect as a spring in a passive mount. Low gains allow large static deflections, but provide good vibration isolation at higher frequencies, while high gains have the opposite effect.

Rather than applying a high link gain in cases where static loads exist, it is more desirable to remove the dc component of the transmitted force measurement before forming the control signal. This could be done by passing the measurement through a high-pass filter, or by simply adding or subtracting a constant to the force measurement in a manner which keeps the active link centered about its nominal length. By taking these measures, our active mount would then give us all the benefits of a passive mount, with the increased isolation performance that the control system can provide.

Before leaving the high-gain force feedback examples, recall that this method of isolation need not be restricted to a particular type of disturbance. Even though harmonic disturbances receive much attention in the literature, there are other types of disturbances which must be addressed, particularly transient inputs to the system which appear as oscillations at the system's natural frequencies. To address that situation, we apply a broadband disturbance to our system. The disturbance, shown in Fig. 5.9a, is actually random noise which has been filtered through a (100-order FIR) bandpass filter with break frequencies of 2 and 10 rad/sec. The frequency

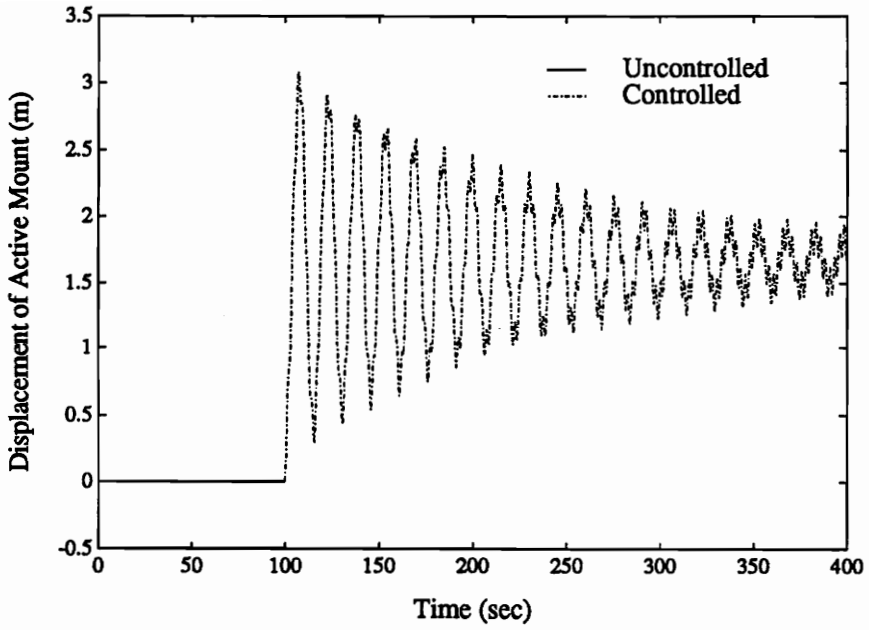

a. Active mount displacement.

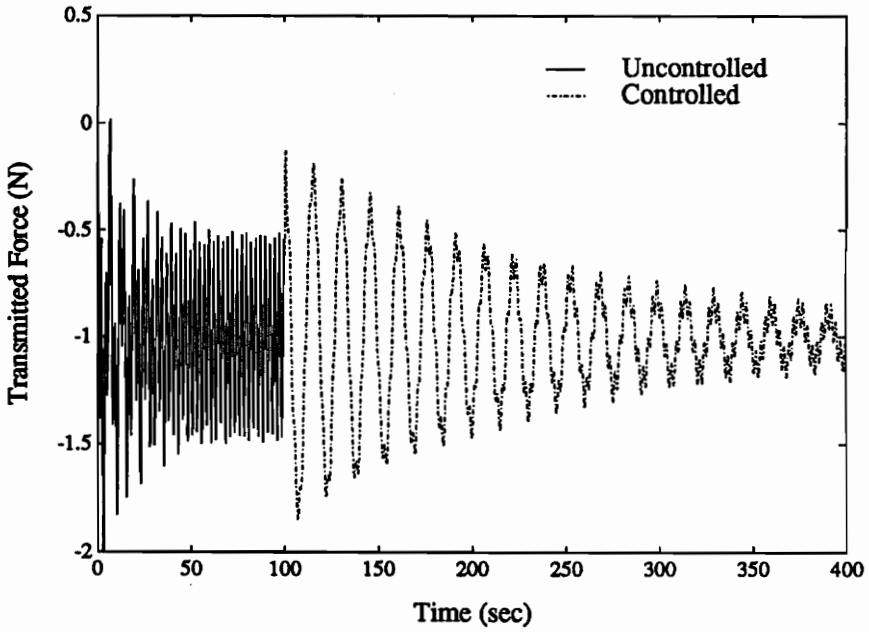

b. Transmitted force.

Figure 5.8: Transmitted force and active mount displacement for high-gain (k_c = 5000) force feedback and high link gain (k_l = 3000) where disturbance is harmonic with offset.

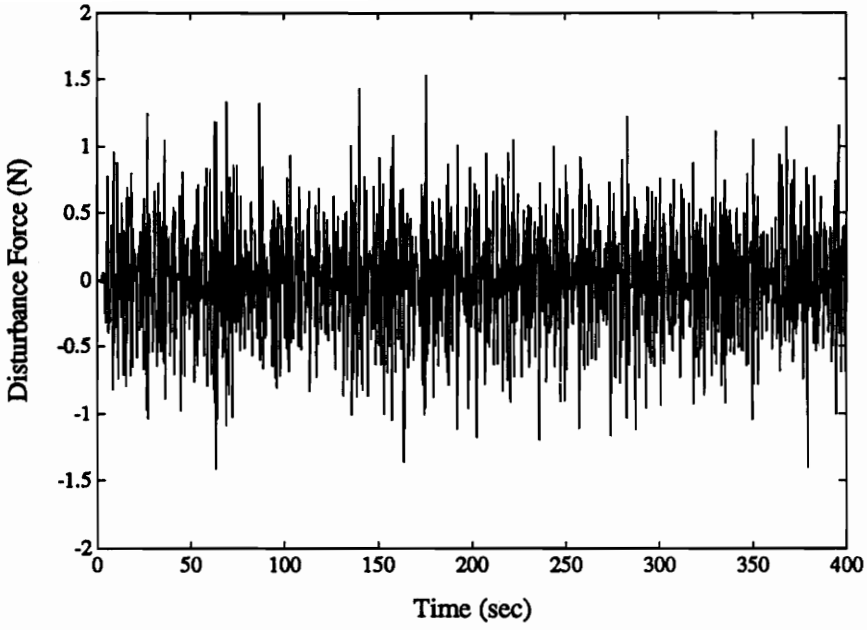

a. Broadband disturbance.

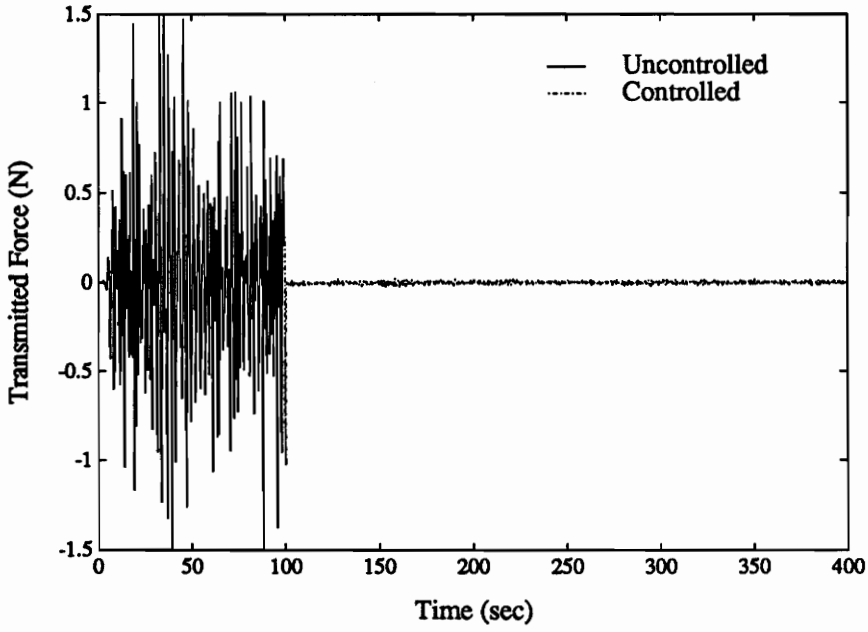

b. Transmitted force.

Figure 5.9: Transmitted force for high-gain ($k_c = 5000$) force feedback where disturbance is broadband.

content, then, is relatively flat between the break frequencies, with a magnitude of 1, and rolls off sharply on either end. We see from Fig. 5.9b that the controller attenuates this disturbance just as it did the harmonic disturbance.

5.2.2 Force Feedback Through Classical Compensators

The second control technique used for vibration isolation is a classical compensator in the force feedback path. The first compensator used has the form

$$\frac{V_{in}}{f_t} = \frac{s+10}{s^2+\omega_d^2} \tag{5.1}$$

In this work, the compensator is explicitly placed in the feedback loop, and not formed through a method such as higher harmonic control, as has been done before [Scribner, 1989]. This eliminates the need for the system model. Even though this compensator has no guarantee of stability, it was not found to cause stability problems in any of the cases tried in this work. That may have been due to the fact that high gains are not needed for the proper performance of this controller. High gains are provided at the frequencies of interest by the lightly damped poles in the denominator of Eq. 5.1.

Applying this compensator to our example system, with the same harmonic disturbance as before, gives the results shown in Fig. 5.10. We see that the transmitted force approaches zero in steady-state, just as with the high-gain feedback case. There is a slow decay in the transmitted force in this case which was not seen before. This is believed to be a period when proper phasing is achieved between the transmitted force and the control voltage (as the compensator gain is increased, this decay becomes faster). Note that the control voltage (Fig. 5.10b) slowly increases in this case, whereas in the high-gain case there is a spike in the control voltage just as the control turns on. That spike allows the active mount to very quickly

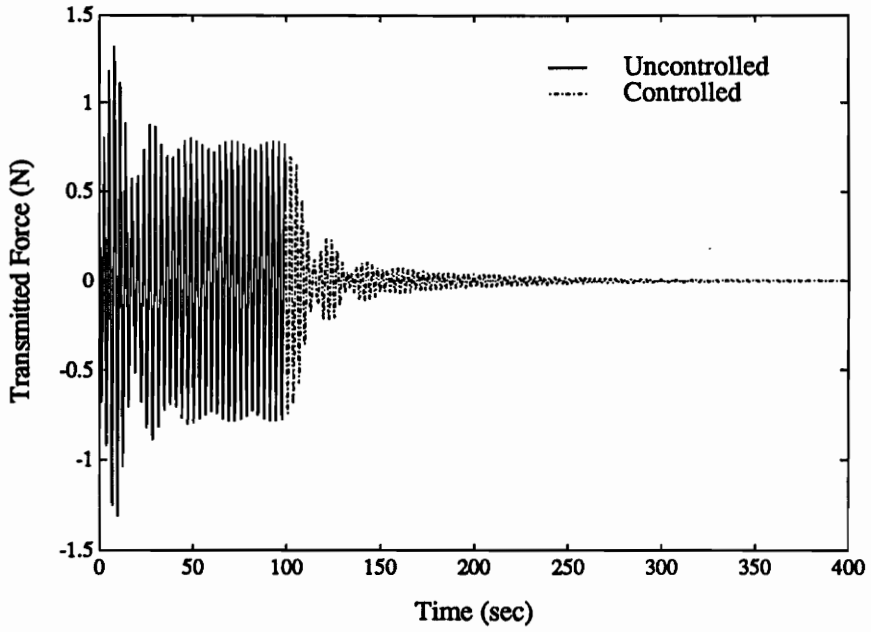

a. Transmitted force.

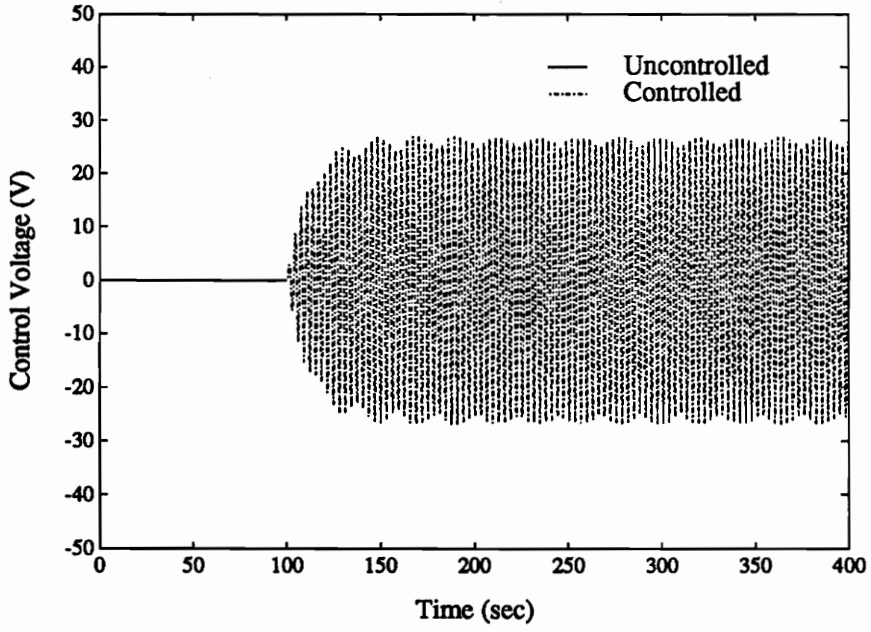

b. Control voltage.

Figure 5.10: Transmitted force and control voltage for classical compensator where disturbance is harmonic.

achieve proper phasing. The steady-state control voltage is shown to be much like the voltages required for high-gain feedback, which brings up an important point. The use of very high gains for force feedback conjures up images of high control efforts being requested by the system. In the classical case shown here, however, there is essentially an infinite feedback gain at the disturbance frequency (since the compensator poles are undamped), but we see relatively small control voltage required. The point is that control saturation, if it occurs, is no more a problem for one control technique than it is for any other.

It would seem likely that static loads would not be a problem for this compensator, since the high gain only occurs at the disturbance frequency. Static components are not, however, completely filtered out of the transmitted force measurement before reaching the control signal because the compensator does have a dc gain. If we apply a disturbance with a dc offset, as before, we see that drift again occurs in the active mount. Figure 5.11a shows the length of the active mount. The magnitude of the drift, however, is much lower than in the high-gain case. If the restrictions on mount length are not too high, then the low authority link control (to prevent offsets from the harmonic input) should be sufficient to provide a "stiff" mount for static loads as well. If the link control is not enough, then the methods discussed earlier of subtracting the dc offset from the force measurement should be used.

Note that the compensator used above has one more pole than it has zeros, so if the actuator or sensor dynamics have an excess of at least two poles, the system will be guaranteed to be unstable for some gain. In very lightly damped systems, this gain could be very low. To avoid that problem, a compensator of the form shown in Eq. 5.2 could be used.

$$\frac{V_{in}}{f_t} = \frac{s^2 + 2\zeta_o\omega_o s + \omega_o^2}{s^2 + \omega_d^2} \tag{5.2}$$

The zeros of the compensator are placed near the poles to attempt to preserve

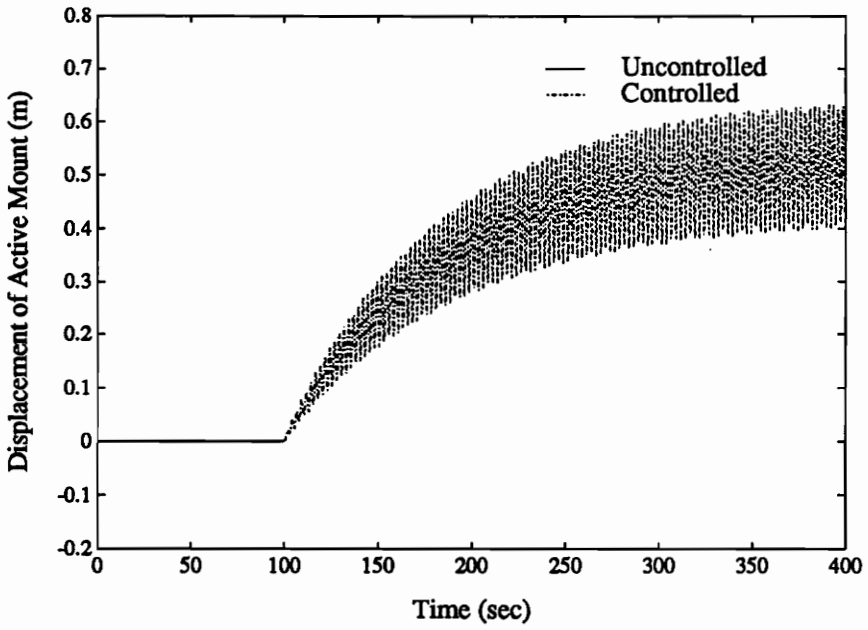

a. Active mount displacement.

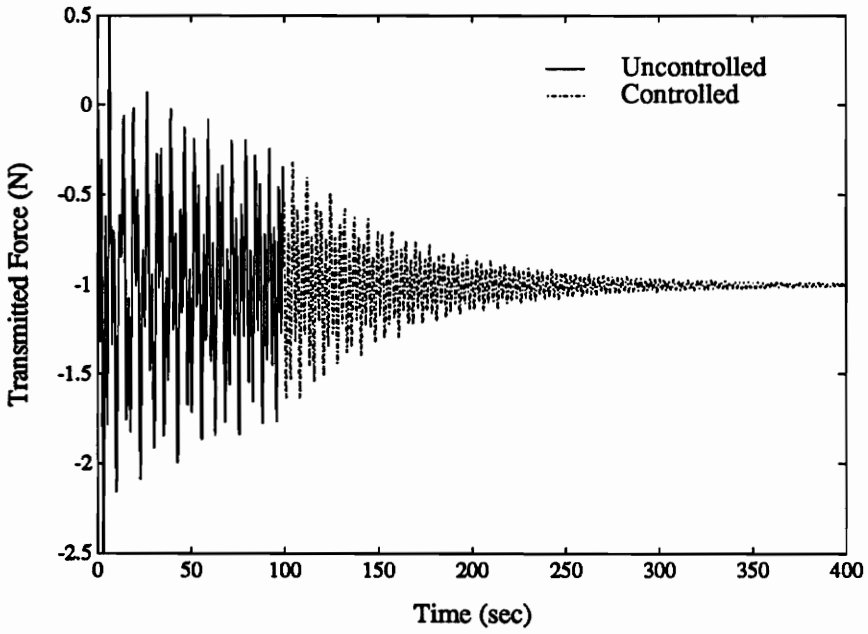

b. Transmitted force.

Figure 5.11: Transmitted force and active mount displacement for classical compensator where disturbance is harmonic with offset.

the alternating pole-zero pattern that leads to a stable feedback method. If the zeros are too close to the poles, then performance suffers (consider that a pole-zero cancellation provides no performance, other than unity gain). Damping is provided in the numerator to separate the pair along the real axis, but to keep them closely-spaced in frequency. In this example, for a disturbance frequency of 2 rad/sec, the numerator parameters are chosen to be $\zeta_o = 0.1$, and $\omega_o = 2.5$ rad/sec. The results for this compensator are shown in Fig. 5.12. It is shown that both the transmitted force and the control voltage are comparable to the previous results.

In order to perform broadband or transient vibration isolation with this type of scheme, more complex compensators (or multiple compensators of the same type) would be necessary. Since stability is not guaranteed for even the simplest of these compensators, adding more poles would seem only to leave the stability issue on even shakier ground.

5.2.3 LQR/LQG Controllers

The final control scheme to be used is the linear quadratic regulator technique discussed in Chapter 2. In this case, we assume that we have an accurate model of the system, and we use that information to provide a stable gain set for feedback, as well as to provide estimates of the unmeasurable system states. The reason for using this method is to try to achieve the same type of compensator as in the previous section, which provided good performance with low overall gains, but to guarantee stability in the process. The price for these benefits is the necessity for an accurate system model.

Recall from Chapter 2 that a typical cost function for this problem contains penalties on the states of the form

$$\mathbf{Q} = \mathbf{C}_o'\mathbf{C}_o \tag{5.3}$$

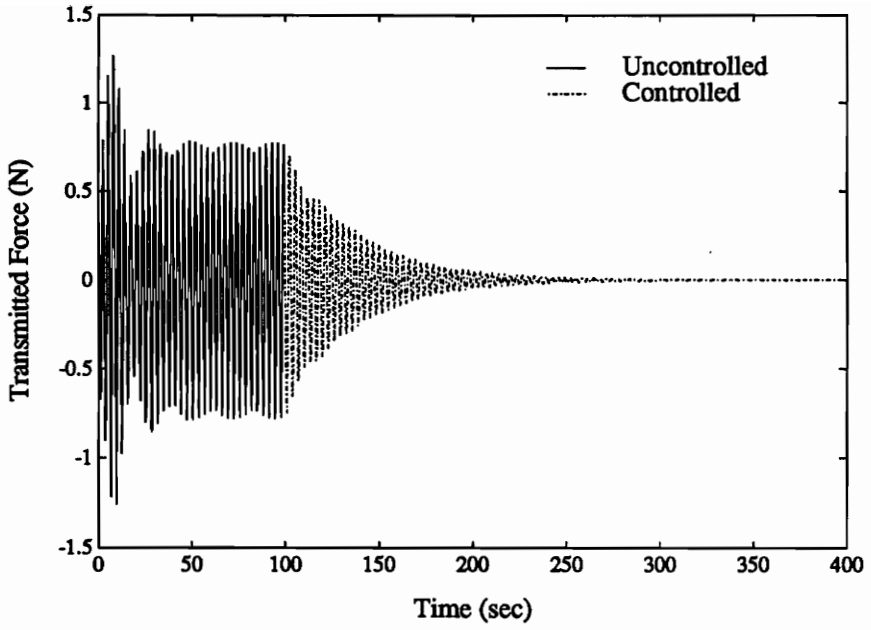

a. Transmitted force.

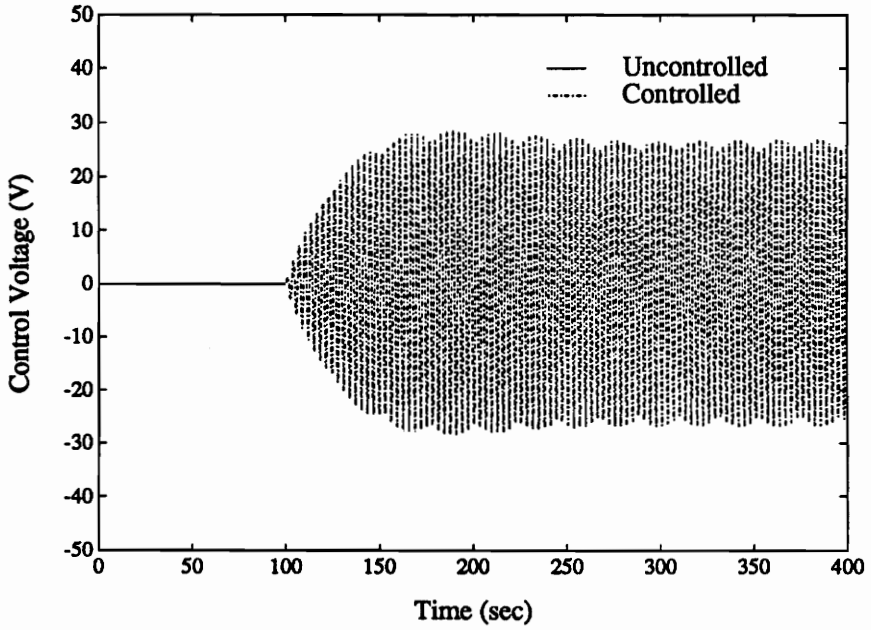

b. Control voltage.

Figure 5.12: Transmitted force and control voltage for classical compensator with feedthrough of force measurement where disturbance is harmonic.

where $\mathbf{C}_o$ is the output matrix for the system. This is useful if we want to regulate all the outputs of the system. The resulting gain set, then, tends to cause damping to be added. It has been mentioned before, though, that using our active mount for damping degrades the isolation performance. We do not care to regulate all the states in the system, only those states associated directly with the force transmitted across the mount. In the penalty matrix, then, we will use a $\mathbf{C}_o$ which is a measure of the transmitted force. We will also include a measure of the active link length so that some low authority control will be provided to the mount itself.

Given the system shown in Fig. 5.1, the state vector can be written as

$$\mathbf{x} = \begin{bmatrix} x_1 & x_2 & x_3 & x_4 & x_5 & \delta & \dot{x}_1 & \dot{x}_2 & \dot{x}_3 & \dot{x}_4 & \dot{x}_5 & \dot{\delta} \end{bmatrix}' \tag{5.4}$$

The assumed output matrix, then, for deriving the isolation cost function, can be written as

$$\mathbf{C}_o = \begin{bmatrix} 0 & -k_2 & k_2 & 0 & 0 & -k_2 & 0 & -c_2 & c_2 & 0 & 0 & -c_2 \\ 0 & 0 & 0 & 0 & 0 & 1 & 0 & 0 & 0 & 0 & 0 & 0 \end{bmatrix} \tag{5.5}$$

where it is assumed that we would like to measure only transmitted force and active mount displacement. The penalties used in the cost function are $\mathbf{Q} = 1000\mathbf{C}_o'\mathbf{C}_o$ and $\mathbf{R} = 10^{-2}$.

Applying the LQR/LQG controller to our example system provides the results shown in Fig. 5.13. We see that we do get suppression of the transmitted force, although it is not as good as what was achieved using the previous two methods. Notice also that similar control voltages are required. The best explanation for why the performance is not as good as that of the other methods is that the LQR approach has added some damping to the system which is compromising the isolation performance. It is also difficult to place a disturbance rejection notch in this system using the cost function chosen here. A notch can be placed, but not always at the

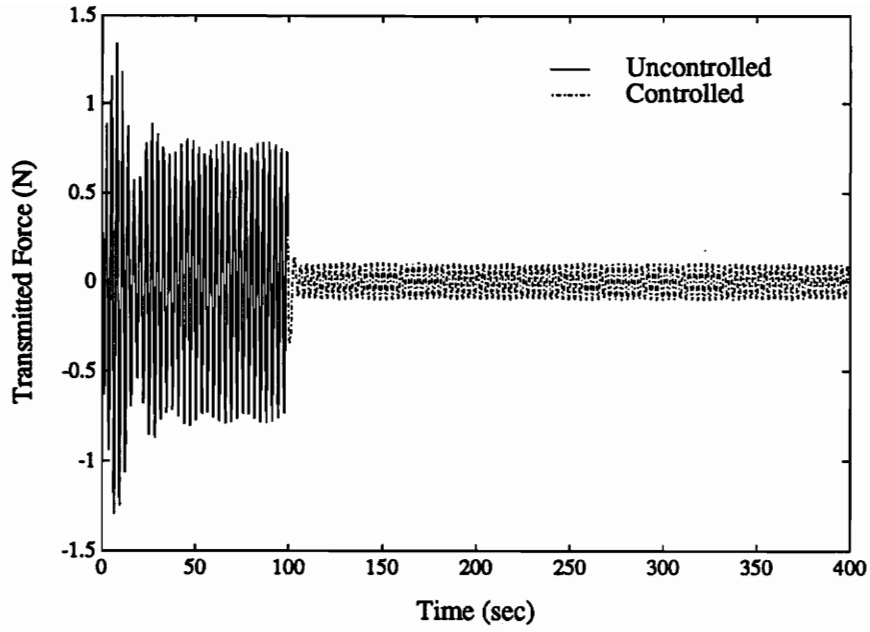

a. Transmitted force.

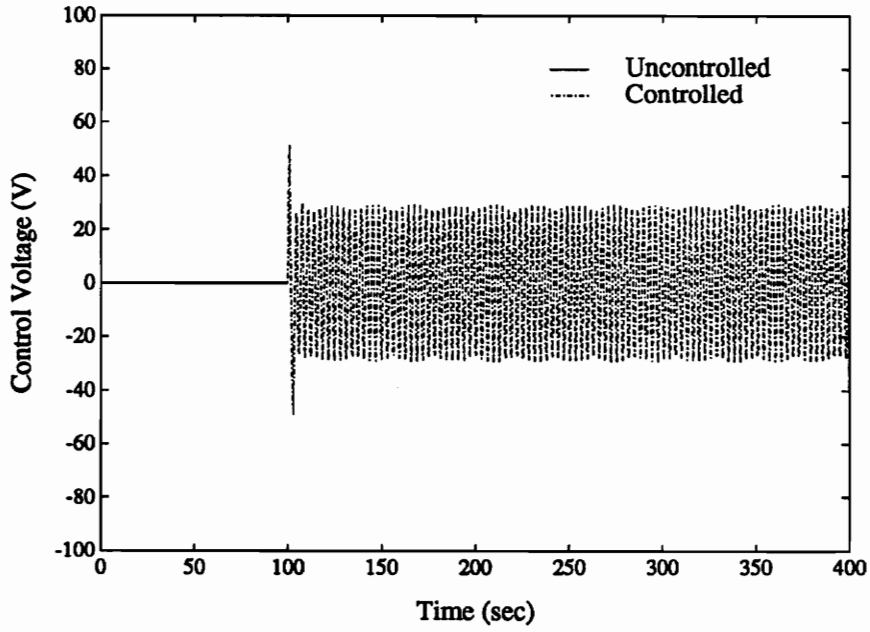

b. Control voltage.

Figure 5.13: Transmitted force and control voltage for LQR control where disturbance is harmonic.

correct location in frequency, so the majority of the isolation effort comes from the transient feedback gains.

In building a narrowband controller (such as this method and the classical compensator shown before), there is always the possibility that the controller may not be designed at the proper frequency. If the disturbance frequency actually occurs away from the design point of the LQR controller, then all is not lost, because the estimator can track the disturbance, and still provide some isolation. This is shown in Fig. 5.14 where the actual disturbance has a frequency of 3 rad/sec while the controller is designed at 2 rad/sec. Good performance away from the design point is something that the classical compensator cannot provide.

The estimator may not be the only factor in the LQR method's good performance away from the design point. The LQR method provides relatively high gains on the transmitted force as compared to all the other gains. In applying the LQR method, with high penalties, we seem to have come full-circle, back to the simple high-gain case we started with at the beginning of this chapter. The overhead required to do so, though, in terms of the system model, is high.

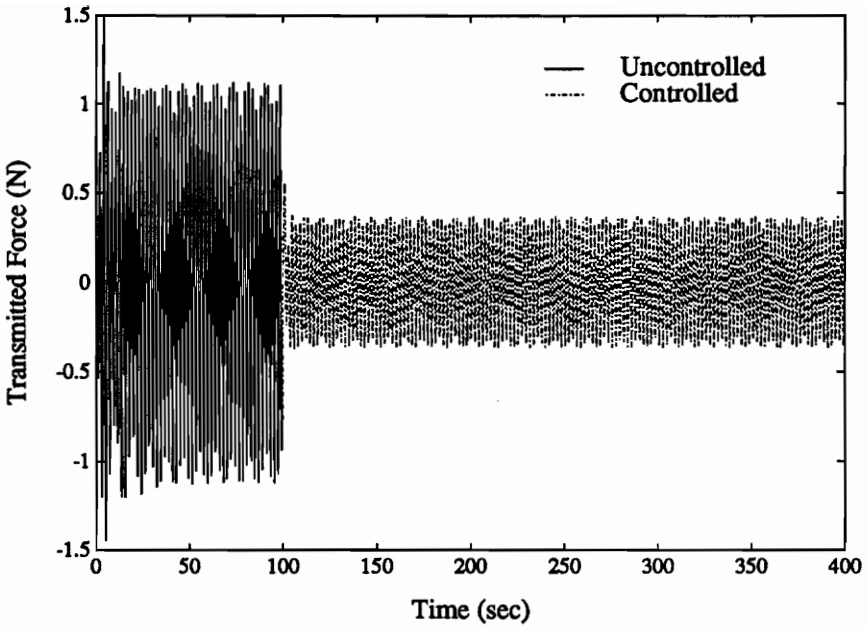

a. Transmitted force.

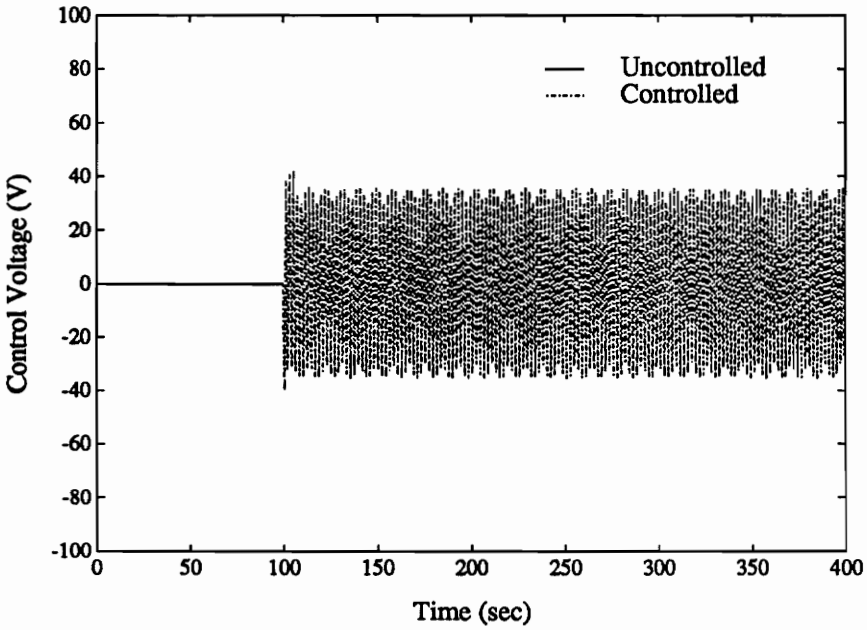

b. Control voltage.

Figure 5.14: Transmitted force and control voltage for LQR where disturbance is harmonic but away from design point.

Chapter 6

Vibration Isolation With an Adaptive Truss

The previous chapter discussed the application of three control laws to a system with a single active mount. This chapter takes up the case where a mount is an adaptive truss which is made up of more than one actuator.

A schematic diagram of the adaptive truss with two attached beams is shown in Fig. 6.1. The truss is a five link mechanism. It is placed at the base of the two beams and at no point is the system fixed to ground. In general, the system represents any two flexible structures connected with an adaptive truss with the required degrees of freedom necessary for vibration isolation. (In this case, three degrees of freedom are necessary, because the system has three rigid-body modes.) Links 1, 2 and 3 are extensible, controlling links (the active mounts) whereas links 4 and 5 are connected to beams A and B, respectively. The extensible links are made up of motor/ballscrew combinations, and each is identical to the active mount configuration discussed in section 4.3.

The joints of this truss are designed as pinned connections, so it is assumed that no moments are carried in the truss' extensible links. Each link, then, is considered to be a two-force member, and the control laws are concerned with minimizing this

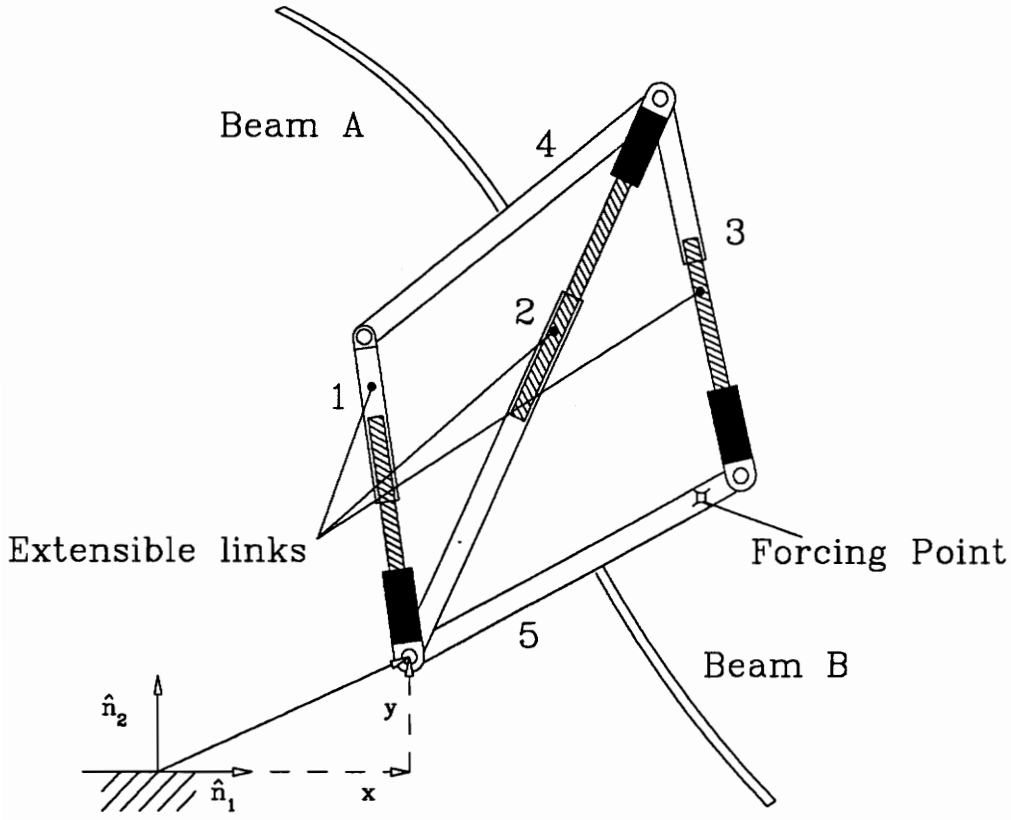

Figure 6.1: Illustraion of adaptive truss with two beams attached.

axial force in each link. In the experiment, the links are massive in comparison with the attached flexible structure, and there is a significant moment generated (as a result of the link's own inertial loading) as a link is rotated through an angle. This moment causes difficulties in measuring transmitted forces in the link, as will be discussed later. Moments such as this are not expected to be a problem in actual practice, where the ratio of structural mass to truss mass will be the opposite of what it is here.

6.1 Derivation of System Equations of Motion

This section presents an overview of the derivation of equations of motion for the system. These equations will later be used to simulate the system response. A variational approach is used to derive the truss and the two beam equations of motion independently. Expressions for the kinetic and potential energies are first written; then Lagrange's equations are applied to form a set of governing differential equations. The beams' equations are derived using a 3-mode Ritz approximation of the beam continua. The three systems (two beams and truss) are combined and the motor equations of section 4.3 are included to generate the total system equations of motion.

6.1.1 Truss Equations of Motion

A lumped mass approach is used to derive the equations of motion of the active truss. The truss is separated into individual links and the energies are written for each and then summed. Figure 6.2 shows that the truss is free to move as a rigid body through global displacements x, y, and α. The truss is also free to change its configuration through the extensible links.

As shown in Fig. 6.2, six coordinate systems are used in the modelling process.

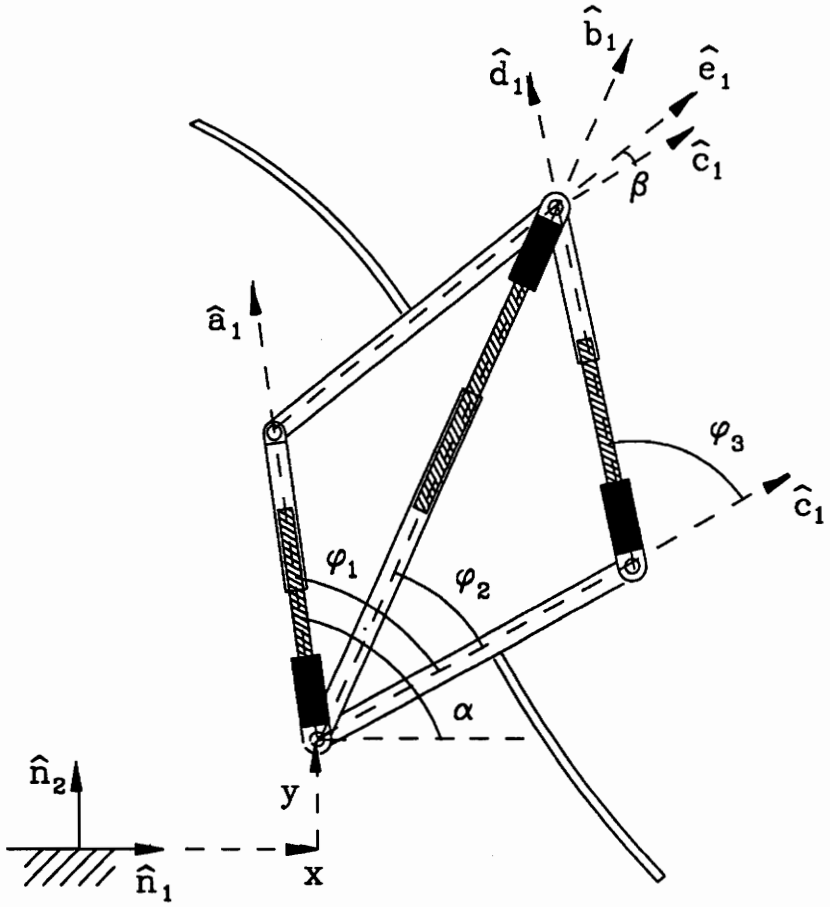

Figure 6.2: Coordinate systems used in modelling the adaptive truss.

They are related to one another through the following transformations:

$$[\hat{\mathbf{a}}] = [c_3(\alpha)]\,[\hat{\mathbf{n}}] \tag{6.1}$$

$$[\hat{\mathbf{b}}] = [c_3(\psi_2)]\,[\hat{\mathbf{c}}] \tag{6.2}$$

$$[\hat{\mathbf{c}}] = [c_3(-\psi_1)]\,[\hat{\mathbf{a}}] \tag{6.3}$$

$$[\hat{\mathbf{d}}] = [c_3(\psi_3)]\,[\hat{\mathbf{c}}] \tag{6.4}$$

$$[\hat{\mathbf{e}}] = [c_3(\beta)]\,[\hat{\mathbf{c}}] \tag{6.5}$$

where

$$[c_3(\cdot)] = \begin{bmatrix} \cos(\cdot) & \sin(\cdot) & 0 \\ -\sin(\cdot) & \cos(\cdot) & 0 \\ 0 & 0 & 1 \end{bmatrix} \tag{6.6}$$

As an example of the modelling process, the kinetic energy for link 1 of the truss will be derived. Figure 6.3 shows link 1 of the truss with the pertinent coordinates. If we consider each extensible link to be an active mount, then recall from Fig. 4.3 that the link can be lumped into three masses which are independent of one another. One mass accounts for the motor and ballscrew, the second accounts for the "moveable" part of the link where the ballscrew nut is attached, and the third is included to allow for a force measurement in the link.

In general, the kinetic energy can be written as

$$T = \frac{1}{2}M(\dot{\mathbf{R}} \cdot \dot{\mathbf{R}}) + \frac{1}{2}\omega \cdot J \cdot \omega \tag{6.7}$$

A position vector to the center of each mass in Fig. 6.3 can be written as

$$\begin{aligned} \mathbf{R}_{m1} &= x\hat{\mathbf{n}}_1 + y\hat{\mathbf{n}}_2 + r_a\hat{\mathbf{a}}_1 \\ &= (x + r_a\cos\alpha)\hat{\mathbf{n}}_1 + (y + r_a\sin\alpha)\hat{\mathbf{n}}_2 \end{aligned} \tag{6.8}$$

$$\begin{aligned} \mathbf{R}_{m2} &= x\hat{\mathbf{n}}_1 + y\hat{\mathbf{n}}_2 + r_b\hat{\mathbf{a}}_1 \\ &= (x + r_b\cos\alpha)\hat{\mathbf{n}}_1 + (y + r_b\sin\alpha)\hat{\mathbf{n}}_2 \end{aligned} \tag{6.9}$$

$$\begin{aligned} \mathbf{R}_{m3} &= x\hat{\mathbf{n}}_1 + y\hat{\mathbf{n}}_2 + (r_b + r_c)\hat{\mathbf{a}}_1 \\ &= [x + (r_b + r_c)\cos\alpha]\hat{\mathbf{n}}_1 + [y + (r_b + r_c)\sin\alpha]\hat{\mathbf{n}}_2 \end{aligned} \tag{6.10}$$

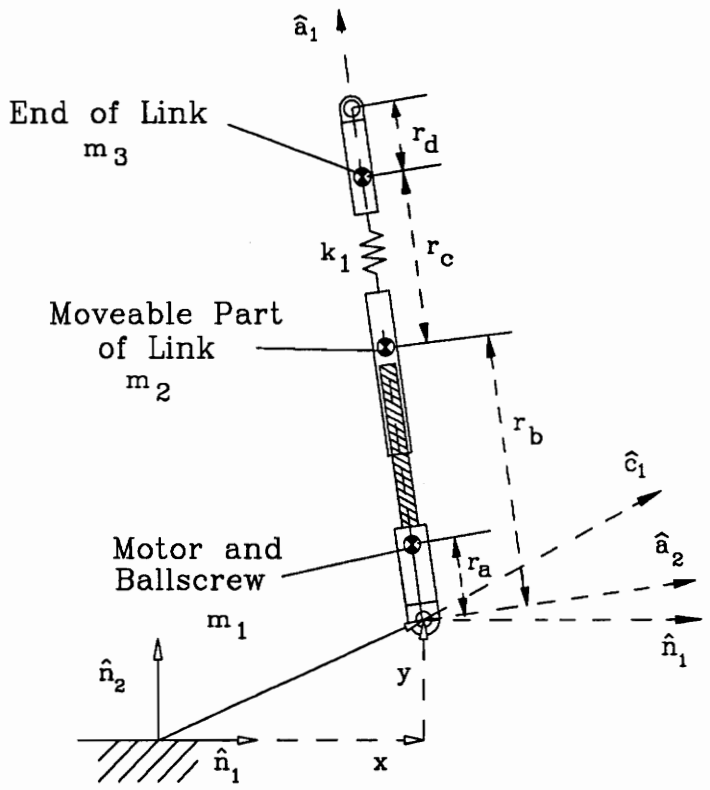

Figure 6.3: Link one of the truss shown with coordinate systems used to derive its equations of motion.

differentiating,

$$\dot{\mathbf{R}}_{m1} = (\dot{x} - r_a\dot{\alpha}\sin\alpha)\hat{\mathbf{n}}_1 + (\dot{y} + r_a\dot{\alpha}\cos\alpha)\hat{\mathbf{n}}_2 \tag{6.11}$$

$$\dot{\mathbf{R}}_{m2} = (\dot{x} - r_b\dot{\alpha}\sin\alpha + \dot{r}_b\cos\alpha)\hat{\mathbf{n}}_1 + (\dot{y} + r_b\dot{\alpha}\cos\alpha + \dot{r}_b\sin\alpha)\hat{\mathbf{n}}_2 \tag{6.12}$$

$$\begin{aligned}\dot{\mathbf{R}}_{m3} \;=\; & [\dot{x} - (r_b + r_c)\dot{\alpha}\sin\alpha + (\dot{r}_b + \dot{r}_c)\cos\alpha]\hat{\mathbf{n}}_1 + \\ & [\dot{y} + (r_b + r_c)\dot{\alpha}\cos\alpha + (\dot{r}_b + \dot{r}_c)\sin\alpha]\hat{\mathbf{n}}_2\end{aligned} \tag{6.13}$$

The dot products become

$$\begin{aligned}\dot{\mathbf{R}}_{m1}\cdot\dot{\mathbf{R}}_{m1} \;=\; & \dot{x}^2 + r_a^2\dot{\alpha}^2\sin^2\alpha - 2\dot{x}\dot{\alpha}r_a\sin\alpha + \\ & \dot{y}^2 + r_a^2\dot{\alpha}^2\cos^2\alpha + 2r_a\dot{y}\dot{\alpha}\cos\alpha\end{aligned} \tag{6.14}$$

$$\begin{aligned}\dot{\mathbf{R}}_{m2}\cdot\dot{\mathbf{R}}_{m2} \;=\; & \dot{x}^2 + r_b^2\dot{\alpha}^2\sin^2\alpha - 2r_b\dot{x}\dot{\alpha}\sin\alpha + \\ & 2\dot{x}\dot{r}_b\cos\alpha - 2r_b\dot{r}_b\dot{\alpha}\cos\alpha\sin\alpha + \\ & \dot{y}^2 + r_b^2\dot{\alpha}^2\cos^2\alpha + 2r_b\dot{y}\dot{\alpha}\cos\alpha + \\ & 2\dot{y}\dot{r}_b\sin\alpha + 2r_b\dot{r}_b\dot{\alpha}\sin\alpha\cos\alpha + \\ & \dot{r}_b^2\sin^2\alpha + \dot{r}_b^2\cos^2\alpha\end{aligned} \tag{6.15}$$

$$\begin{aligned}\dot{\mathbf{R}}_{m3}\cdot\dot{\mathbf{R}}_{m3} \;=\; & \dot{x}^2 + (r_b + r_c)^2\dot{\alpha}^2\sin^2\alpha - 2(r_b + r_c)\dot{x}\dot{\alpha}\sin\alpha + \\ & 2\dot{x}(\dot{r}_b + \dot{r}_c)\cos\alpha - 2(r_b + r_c)(\dot{r}_b + \dot{r}_c)\dot{\alpha}\cos\alpha\sin\alpha + \\ & \dot{y}^2 + (r_b + r_c)^2\dot{\alpha}^2\cos^2\alpha + 2(r_b + r_c)\dot{y}\dot{\alpha}\cos\alpha + \\ & 2\dot{y}(\dot{r}_b + \dot{r}_b)\sin\alpha + 2(r_b + r_c)(\dot{r}_b + \dot{r}_c)\dot{\alpha}\sin\alpha\cos\alpha + \\ & (\dot{r}_b + \dot{r}_c)^2\sin^2\alpha + (\dot{r}_b + \dot{r}_c)^2\cos^2\alpha\end{aligned} \tag{6.16}$$

Eliminating terms greater than second order (to retain linear equations of motion) the kinetic energy becomes

$$\begin{aligned}T_1 \;=\; & \tfrac{1}{2}M_{m1}(\dot{x}^2 + \dot{y}^2 + r_a^2\dot{\alpha}^2 + 2r_a\dot{y}\dot{\alpha}) + \\ & \tfrac{1}{2}M_{m2}(\dot{x}^2 + \dot{y}^2 + r_b^2\dot{\alpha}^2 + 2r_b\dot{y}\dot{\alpha} + 2\dot{x}\dot{r}_b + \dot{r}_b^2) + \\ & \tfrac{1}{2}M_{m3}(\dot{x}^2 + \dot{y}^2 + (r_b + r_c)^2\dot{\alpha}^2 + 2(r_b + r_c)\dot{y}\dot{\alpha} + 2\dot{x}(\dot{r}_b + \dot{r}_c) + (\dot{r}_b + \dot{r}_c)^2) \\ & + \tfrac{1}{2}J_{m1}\dot{\alpha}^2 + \tfrac{1}{2}J_{m2}\dot{\alpha}^2 + \tfrac{1}{2}J_{m3}\dot{\alpha}^2 + \tfrac{1}{2}J_{ls}\frac{\dot{\theta}_m^2}{G_m^2}\end{aligned} \tag{6.17}$$

where the last term appears from the rotation of the ballscrew about its longitudinal axis.

In the control problem, we are only concerned with the change in length of the links from their nominal lengths, so

$$r_b = l_1 + l_{1_0} \tag{6.18}$$

$$r_c = l_{1k} + l_{1k_0} \tag{6.19}$$

and

$$\dot{r}_b = \dot{l}_1 \tag{6.20}$$

$$\dot{r}_c = \dot{l}_{1k} \tag{6.21}$$

where l_1 and l_{1k} represent the change in length of the leadscrew and the flexible link, respectively, and l_{1_0} and l_{1k_0} are fixed lengths which make up the nominal length of the link. Substituting into Eq. 6.17 yields

$$\begin{aligned} T_1 = & \tfrac{1}{2}M_{m1}(\dot{x}^2 + \dot{y}^2 + r_a^2\dot{\alpha}^2 + 2r_a\dot{y}\dot{\alpha}) + \\ & \tfrac{1}{2}M_{m2}(\dot{x}^2 + \dot{y}^2 + l_{1k_0}^2\dot{\alpha}^2 + 2l_{1k_0}\dot{y}\dot{\alpha} + 2\dot{x}\dot{l}_{1k} + \dot{l}_{1k}^2) + \\ & \tfrac{1}{2}M_{m3}(\dot{x}^2 + \dot{y}^2 + (l_{1_0} + l_{1k_0})^2\dot{\alpha}^2 + 2(l_{1_0} + l_{1k_0})\dot{y}\dot{\alpha} + 2\dot{x}(\dot{l}_1 + \dot{l}_{1k}) + (\dot{l}_1 + \dot{l}_{1k})^2) \\ & + \tfrac{1}{2}J_{m1}\dot{\alpha}^2 + \tfrac{1}{2}J_{m2}\dot{\alpha}^2 + \tfrac{1}{2}J_{m3}\dot{\alpha}^2 + \tfrac{1}{2}J_{ls}\tfrac{\dot{\theta}_m^2}{G_m^2} \end{aligned} \tag{6.22}$$

The dependent coordinates for link 1, then, are x, y, α, l_1, and l_{1k}.

The kinetic energy for all other links of the truss can be derived similarly, and the total kinetic energy for the truss can be written as

$$T_{truss} = \sum_{i=1}^{5} T_i \tag{6.23}$$

Note that when the kinetic energies of the other links of the truss are found, they will be written in terms of the angular coordinates, ψ_1, ψ_2, ψ_3, and β. These are not independent of the link length coordinates, l_1, l_{1k}, l_2, l_{2k}, l_3, and l_{3k}. A transformation must be developed, then, with which to write the angles as a function of the link lengths. Considering the truss shown in Fig. 6.4, we can write two loop-closure equations around different paths in the truss. The primes in Fig. 6.4 denote an offset link length (for example, L_1 is the nominal length of link 1, and L_1' is its length after some control input has been applied.)

Loop 1 gives us

$$L_1' e^{j\psi_1} + L_4 e^{j\beta} - L_2' e^{j\psi_2} = 0 \tag{6.24}$$

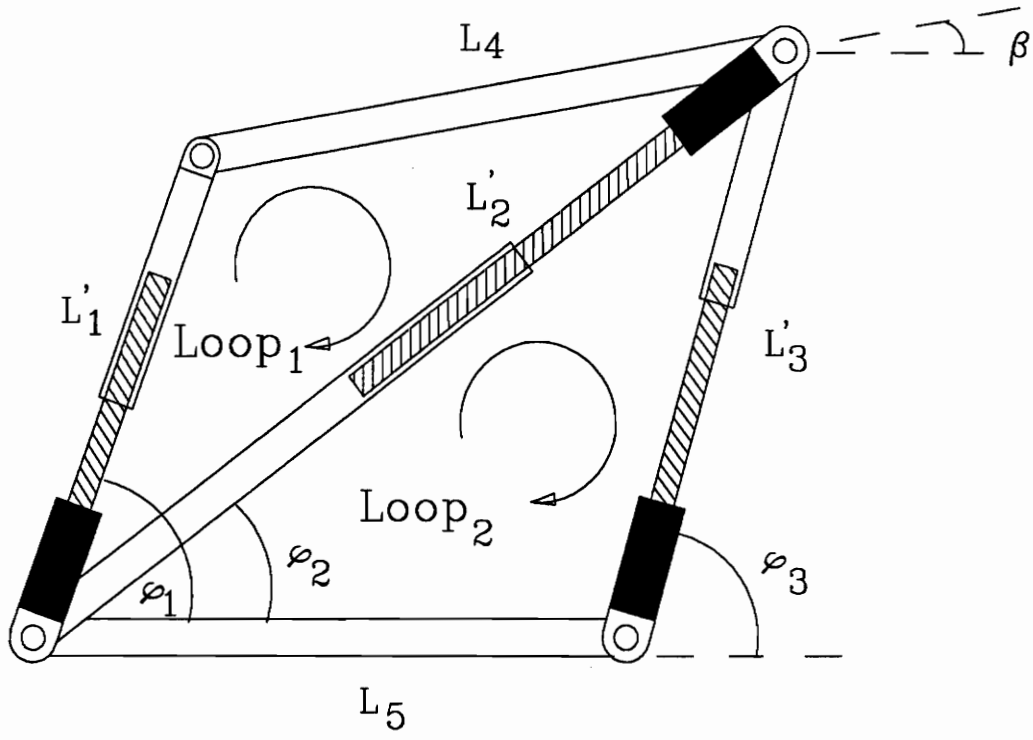

Figure 6.4: Truss shown with paths used for loop closure equations.

and loop 2 provides

$$L_2' e^{j\psi_2} - L_3' e^{j\psi_3} - L_5 = 0 \tag{6.25}$$

Applying Euler's identity, these can be written as (separating real and imaginary parts)

$$L_1' \cos\psi_1 + L_4' \cos\beta - L_2' \cos\psi_2 = 0 \tag{6.26}$$

$$L_1' \sin\psi_1 + L_4' \sin\beta - L_2' \sin\psi_2 = 0 \tag{6.27}$$

$$L_2' \cos\psi_2 - L_3' \cos\psi_3 - L_5' = 0 \tag{6.28}$$

$$L_2' \sin\psi_2 - L_3' \sin\psi_3 = 0 \tag{6.29}$$

These equations may be linearized about the nominal angles ($\psi_1 = 90°$, $\psi_2 = 45°$, $\psi_3 = 90°$, and $\beta = 0°$) and the nominal link lengths, and then rearranged to write the angles in terms of the link lengths. The result is

$$\psi_1 = \frac{707(l_2 + l_{2k}) - 500(l_3 + l_{3k}) - 500L_4}{500L_1} + \frac{\pi}{2} \tag{6.30}$$

$$\psi_2 = \frac{707(l_2 + l_{2k}) - 1000(l_3 + l_{3k})}{707L_2} + \frac{\pi}{4} \tag{6.31}$$

$$\psi_3 = \frac{707(l_2 + l_{2k}) - 500(l_3 + l_{3k})}{500L_3} + \frac{\pi}{4} \tag{6.32}$$

$$\beta = \frac{l_1 + l_{1k} + l_3 + l_{3k}}{L_4} \tag{6.33}$$

Now the total kinetic energy for the truss can be derived, and written as

$$T_{truss} = \dot{\mathbf{v}}_\mathbf{t}'(t)\mathbf{M}_{\mathbf{truss}}\dot{\mathbf{v}}_\mathbf{t}(t) \tag{6.34}$$

where

$$\mathbf{v_t} = \begin{bmatrix} x & y & \alpha & l_1 & l_2 & l_3 & l_{1k} & l_{2k} & l_{3k} \end{bmatrix}^t \tag{6.35}$$

and $\mathbf{M}_{truss}$ is the mass matrix for the truss.

Potential energy is found only in the force-measuring coordinate, l_{ik}, and can be written as

$$V = \sum_{i=1}^{3} \frac{1}{2} k_i l_{ik}^2 \tag{6.36}$$

The other parts of the truss are assumed to be rigid.

The equations of motion can be obtained by applying Lagrange's equation (see Meirovitch [1970])

$$\frac{\partial}{\partial t} \frac{\partial L}{\partial \dot{v}_{t_i}} - \frac{\partial L}{\partial v_{t_i}} = Q_i - D_i \tag{6.37}$$

where L is defined as

$$L = T - V \tag{6.38}$$

and v_{t_i} are the generalized coordinates (elements of $\mathbf{v_t}$), Q_i are the generalized force inputs, and D_i are damping terms.

Recall from the discussion in section 4.3 that because of the gear ratios involved, the motor equations are assumed to be independent of the other coordinates of the system. That is true for the truss as well, so the motor coordinates, l_1, l_2, and l_3, are assumed to provide kinematic inputs to the other system equations. For that reason, Eq. 6.37 is applied only to the the coordinates x, y, α, l_{1k}, l_{2k}, and l_{3k}. The remaining three equations are equivalent to Eq. 4.16.

The equations of motion become

$$\mathbf{M}_{truss}\ddot{\mathbf{v}}_t + \mathbf{C}_{truss}\dot{\mathbf{v}}_t + \mathbf{K}_{truss}\mathbf{v}_t = \mathbf{F}_m\mathbf{V}_m + \mathbf{F}_d f(t) \tag{6.39}$$

where $\mathbf{V}_m$ is the vector of motor input voltages, and $\mathbf{F}_m$ is a matrix of coefficients that describe how the voltages are transformed into forces and enter the system (see Eq. 4.16). The vector $\mathbf{F}_d$ is included to account for disturbance forces, $f(t)$, entering the system.

6.1.2 Frequency Response of the Adaptive Truss

Once the truss model was complete, it was important to know how well it actually represented the real system so that later simulations would have meaning. This was done by comparing the frequency responses of the analytical and experimental systems.

The adaptive truss, equipped with force sensors in the links, is a multi-input multi-output system, with 3 inputs and 3 outputs. There is a possibility of nine transfer functions in this system. We will look at only two of these transfer functions, to provide an understanding of how well the model compares to the physical system.

Figure 6.5 shows the frequency response from link 2 input to the force measurement in link 2. Note that the plots show the existence of 3 natural frequencies in the truss, as we would expect for the three degree of freedom system. Note also that the plots show an alternating pole-zero pattern for this colocated actuator/sensor pair. This is one of the "best" comparisons of the nine frequency response plots. Figure 6.6 shows the frequency response of the force measured in link 1 given an excitation in link 3. This is one of the poorer comparisons of the group.

The measure of goodness of comparison was somewhat subjective, and was based on how well the two plots matched in amplitude, how well the resonant frequencies agreed, and how well the character of the poles and zeros compared. To help in this decision, the difference between the magnitudes of the frequency responses was found, and plotted in Fig. 6.7. We see that the for the link 2-to-2 frequency response, the differences are an order of magnitude less than the magnitudes themselves, while for the link 3-to-1 plots, they are in general the same order. In all the cases the general character of each plot is accurate.

To correct the errors in the model, perhaps the most productive approach would

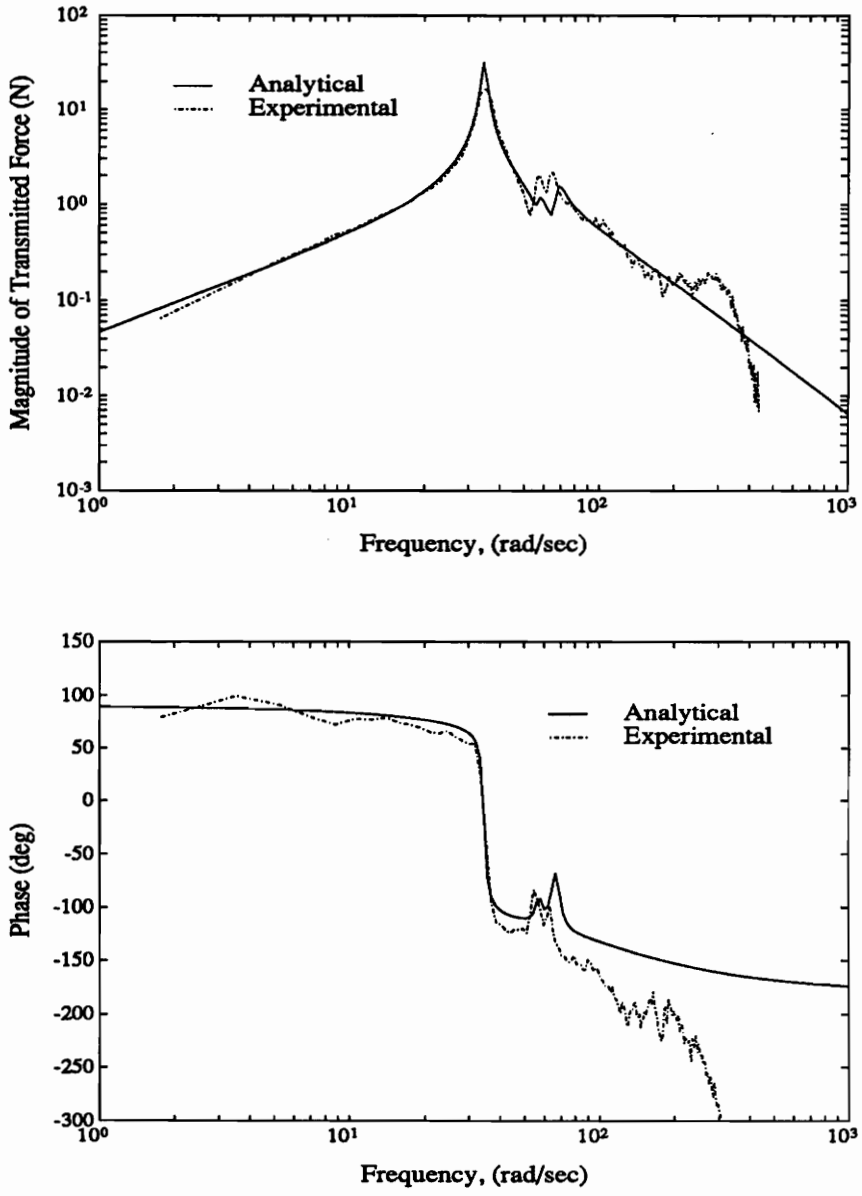

Figure 6.5: Frequency response from link 2 input to link 2 transmitted force output.

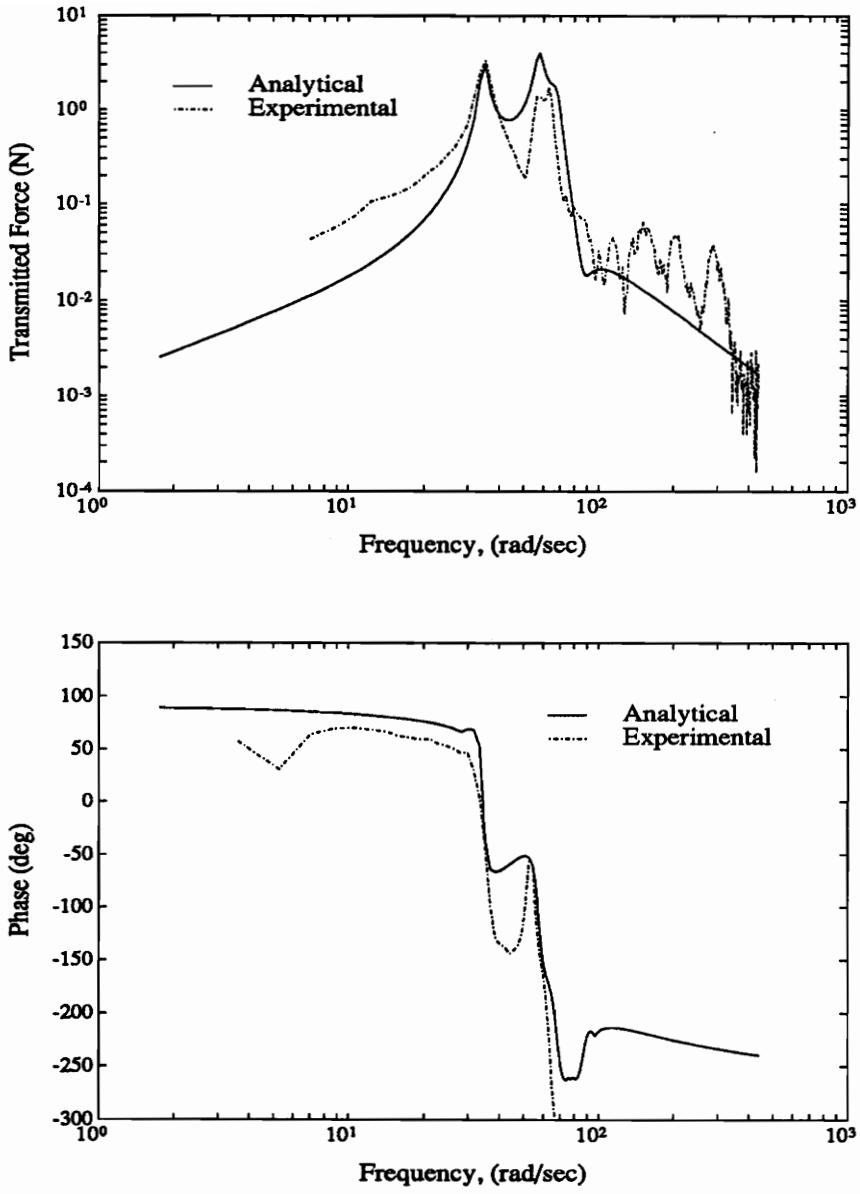

Figure 6.6: Frequency response from link 3 input to link 1 transmitted force output.

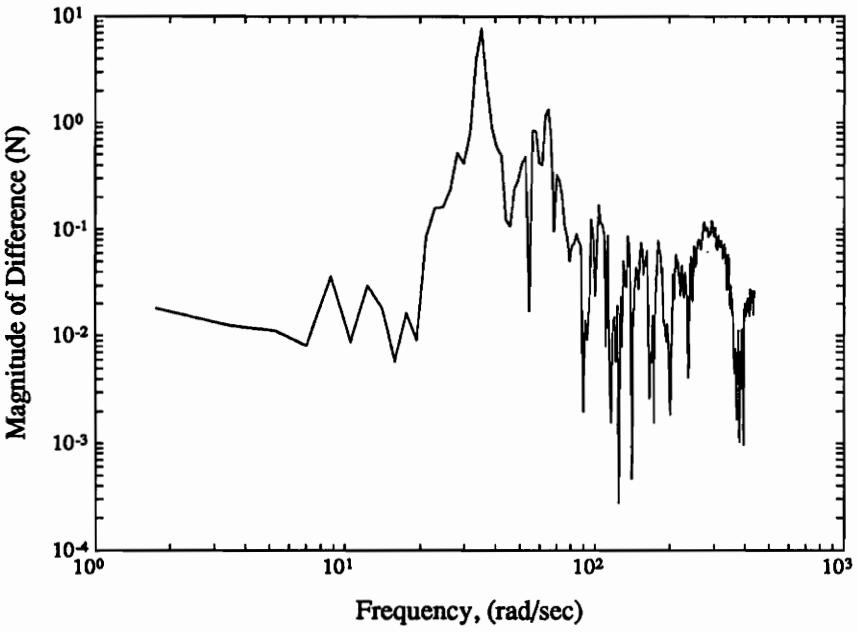

a. Difference for link 2 to 2 frequency response.

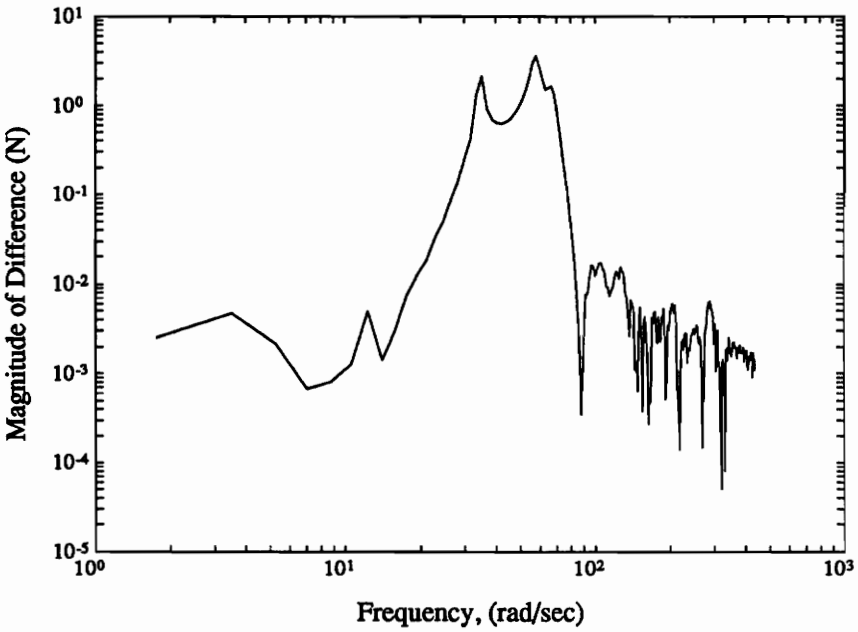

b. Difference for link 3 to 1 frequency response.

Figure 6.7: Differences in the magnitudes of the frequency response plots to show errors in the analytical model.

be to adjust the stiffnesses (and damping) in each of the links. It was assumed here that the stiffnesses are identical, which may not be the case in the real system. Another approach would be to reevaluate the distribution of the masses in the truss model.

6.1.3 Beam Equations

The potential and kinetic energies for the beam will be written using a three-mode Ritz approximation (this is a common approach and can be found in Thomson [1981], for example). Lagrange's equations are then applied to form a set of governing equations. Figure 6.8 shows a schematic of the beam to be modelled.

The kinetic energy of the beam can be found by locating a differential element of mass along the beam (Fig. 6.8) with a vector $\mathbf{R}$. This is shown for both beam A and B as

$$\mathbf{R}_A = x\hat{\mathbf{n}}_1 + y\hat{\mathbf{n}}_2 + L_1'\hat{\mathbf{a}}_1 + \frac{L_4}{2}\hat{\mathbf{e}}_2 + \hat{x}\hat{\mathbf{e}}_1 - w(\hat{x},t)\hat{\mathbf{e}}_2 \tag{6.40}$$

$$\mathbf{R}_B = x\hat{\mathbf{n}}_1 + y\hat{\mathbf{n}}_2 + \frac{L_5}{2}\hat{\mathbf{c}}_1 - \tilde{x}\hat{\mathbf{c}}_2 + w(\tilde{x},t)\hat{\mathbf{c}}_1 \tag{6.41}$$

The lateral beam deflection, $w(\hat{x},t)$ is approximated by

$$w(\hat{x},t) = \sum_{i=1}^{n} \phi_i(\hat{x}) q_i(t) \tag{6.42}$$

where ϕ_i represents the assumed mode shapes and q_i represents the modal coefficients. The equations describing the mode shapes can be written as

$$\phi_i(\hat{x}) = A_i\left[\cosh\beta_i\hat{x} - \gamma_i \sinh\beta_i\hat{x} - \cos\beta_i\hat{x} + \gamma_i \sin\beta_i\hat{x}\right] \tag{6.43}$$

where Table 6.1 defines the constants in Eqn. 6.43. The first three mode shapes, ϕ_1, ϕ_2, and ϕ_3, (normalized to 1.0 m end deflection) for clamped-free beam are used in this model.

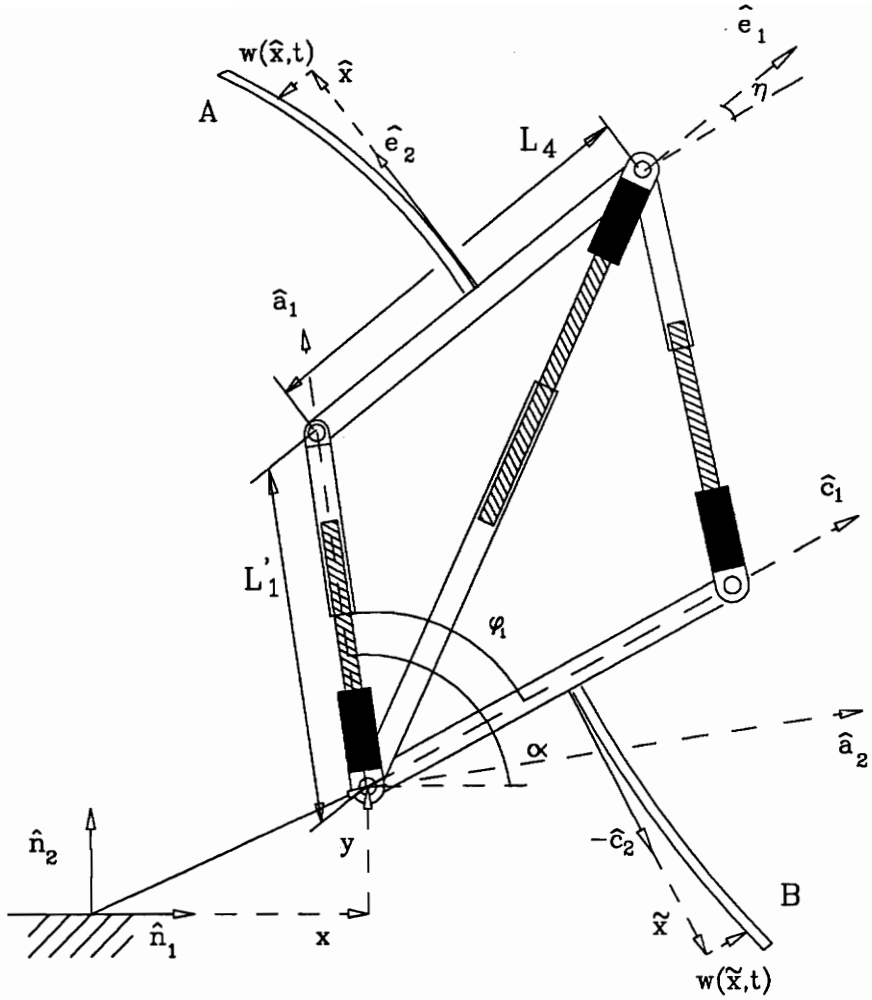

Figure 6.8: Coordinate systems used in modelling the flexible beams.

Table 6.1: Clamped-Free Ritz Parameters

i	A_i	γ_i	$L \cdot \beta_i$
1	0.5	0.7348	1.8762
2	-0.5	1.0186	4.6904
3	0.4921	0.9992	7.8549

The kinetic energy for each beam can then be formed from the equation

$$T = \frac{1}{2}\int_m \left(\dot{\mathbf{R}} \cdot \dot{\mathbf{R}}\right) dm = \frac{\xi}{2}\int_0^l \left(\dot{\mathbf{R}} \cdot \dot{\mathbf{R}}\right) d\hat{x} \tag{6.44}$$

where ξ is the beam's mass per unit length and l is the length of the beam. A second-order linearization of the kinetic energy can be performed, keeping in mind the transformations from angles to link-length coordinates derived earlier.

Next the potential energy of the beam, linearized to second-order, is written. The potential energy is written as strain energy,

$$V = \frac{EI}{2}\int_0^l \left[w''(\hat{x})\right]^2 d\hat{x} \tag{6.45}$$

where E represents Young's modulus, I is the beam's area moment of inertia, and $w''(\hat{x}) = \frac{d^2w}{d\hat{x}^2}$.

Modal damping was added to the beam based on experimental data. A logarithmic decrement of first mode was done to find first mode damping. This provided a factor which could be used, assuming structural damping, to find the damping of higher modes [Wie, 1981]. The damping coefficients for the first three modes of the beam were found to be 0.01, 0.02, and 0.04, respectively.

The equations of motion for each beam become

$$\mathbf{M}_{beam}\ddot{\mathbf{v}}_b + \mathbf{C}_{beam}\dot{\mathbf{v}}_b + \mathbf{K}_{beam}\mathbf{v}_b = \mathbf{0} \tag{6.46}$$

where $\mathbf{v}_b$ contains the coordinates used to describe the beam's motion. Note that motor coordinates are included here, but only as kinematic inputs.

6.1.4 Combination of the Models

The beam and truss equations will now be combined. First the coordinate vectors in Eqs. 6.39 and 6.46 must be augmented to account for additional states in both the beam and truss models. This process consists of adding rows and columns of zeros to the appropriate mass, stiffness, or damping matrices. When this is done the system consists of 15 independent coordinates; 3 global coordinates (x, y,and α), 3 truss coordinates (l_{ik}), 3 coordinates for each beam (q_i), and 3 motor coordinates (l_i). Now the three sets of equations of motion are simply added to form a new set of equations describing the total system. The resulting equations of motion become

$$[\mathbf{M}_{tot}]\,\ddot{\mathbf{v}} + [\mathbf{C}_{tot}]\,\dot{\mathbf{v}} + [\mathbf{K}_{tot}]\,\mathbf{v} = \mathbf{FV} \tag{6.47}$$

These equations can then be written in state space form as

$$\dot{\mathbf{x}} = \mathbf{Ax} + \mathbf{Bu} \tag{6.48}$$

where $\mathbf{x}$ is the vector of states ($\mathbf{v}$ and its derivatives), $\mathbf{u}$ is the vector of motor inputs, to be determined by a control law, and $\mathbf{A}$ and $\mathbf{B}$ are defined as

$$\mathbf{A} = \begin{bmatrix} \mathbf{0} & \mathbf{I} \\ -\mathbf{M}_{tot}^{-1}\mathbf{K}_{tot} & -\mathbf{M}_{tot}^{-1}\mathbf{C}_{tot} \end{bmatrix} \tag{6.49}$$

$$\mathbf{B} = \begin{bmatrix} \mathbf{0} \\ \mathbf{M}_{tot}^{-1}\mathbf{F} \end{bmatrix} \tag{6.50}$$

6.2 Experimental Setup

As has been mentioned, the test article for this work was a planar adaptive truss with a beam attached to either end, Fig. 6.1. The two beams were identical in shape and material, (both were steel with dimensions of 0.10x.91x0.00079m), and their first three natural frequencies (for lateral vibrations) were approximately 1, 5,

and 14 Hz. These beams were attached to the truss so that their end conditions were clamped-free. The truss was supported on a test-bed by custom-designed air bearings to provide as frictionless a support as possible.

The link forces (the transmitted forces in the system) were determined through the use of a strain-sensing device which was placed in-line with the active link. Figure 6.9a shows a diagram of the force gage used. The gage is made up of a small piece of aluminum (0.5 in. wide and 0.031 in. thick) which is clamped on either end. Each clamped end of the gage is rigidly attached to one end of the active link as shown in Fig. 6.9b. When an axial load is applied to the link, the gage undergoes bending, which is sensed by the strain gages mounted at one end of the clamped-clamped aluminum "beam." There are four strain gages mounted on the beam, two on either side. Each gage makes up one arm of a Wheatstone bridge, and they are arranged to provide the maximum sensitivity to bending, but to cancel torsional loads which may be seen in the force gage [Beckwith, 1982].

The equivalent stiffness of the gage was derived by considering it to be a clamped-clamped beam in bending [Beer, 1981], and was found to be

$$k_{eq} = \frac{12EI}{l^3} \tag{6.51}$$

where E and I are the modulus of elasticity and moment of inertia of the force gage, and l is the gage's length. Similarly, the relationship between measured strain and force was found to be

$$f = \frac{4EI\epsilon}{lh} \tag{6.52}$$

where h is the thickness of the gage-beam.

It was mentioned earlier that bending loads arising in the structure are not supported by the links of the adaptive truss because of the pinned connections. There are, however, bending loads which come about as a result of the link's inertial

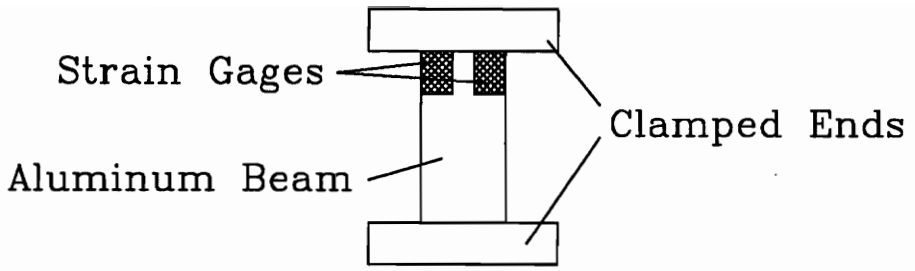

a. Force gage used in the active links.

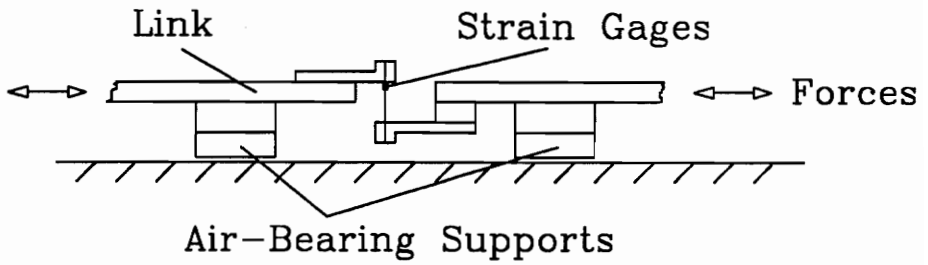

b. Side view of active link with force gage.

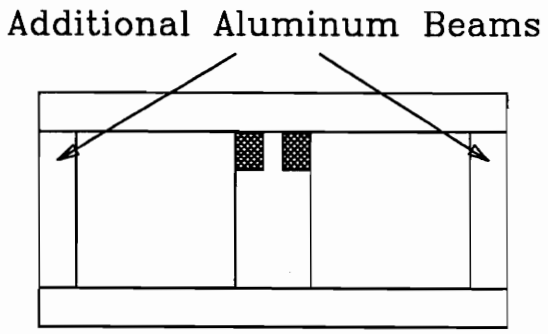

b. Force gage shown with increased thickness to reduce torsional effects.

Figure 6.9: Diagrams of force gage used in the active links.

loading. These loads play an important role in the choice and design of the force gage. First of all, the bending loads ruled out the use of common, piezoelectric force gages, because the measurement errors caused by the bending loads were larger than the force measurement itself. The bending loads also governed certain aspects of the strain-gage design as well. It was desirable to use a beam that was as narrow as possible to increase the sensitivity of the force gage, but decreasing the width of the beam caused the torsional displacements to increase. A compromise was made between the two factors. The actual gage has two additional beams, placed relatively far off the neutral axis (see Fig. 6.9c), which serve to increase the effective width of the beam (and thus reduce torsional effects) by only slightly changing the force sensitivity.

It is assumed that in actual practice, an alternative, and perhaps more versatile form of force-sensing technology will be used. A possibility may be thick-film polymer, force-sensing resistors which could be imbedded in the active mount [Interlink Electronics, 1991]. This would work well for measuring compressive loads, but sensing tensile loads as well will be more difficult. A preloaded link which carries all the load through the sensor is an appealing solution, but one which will be difficult to build.

The other instrumentation in the experimental system includes strain gages on the beams to provide information on the vibration isolation performance, or in the case of the LQR control law, to provide necessary information for the model-based controller. On each beam, strain gages are placed at three locations (at each location there is a full bridge, just as in the force gage). From the strain information, the three modal displacements of each beam could be inferred by applying a strain-to-mode transformation.

The lengths of the links of the adaptive truss were measured using linear poten-

tiometers. Feeding back this information allowed us to maintain a nominal truss position. Recall from section 4.4 that position feedback is required to maintain a zero-mean link displacement if a periodic control signal is applied.

The control laws were implemented using an 80286-based digital computer equipped with Data Translation 2821 A/D boards. Depending on the application, this hardware provided a sample and control frequency of up to 250 Hz.

6.3 Results of Vibration Isolation with an Adaptive Truss

This section presents the results of simulations of the adaptive truss/beam system in response to a forced input. Just as in the previous chapter, three control methods are used to perform active vibration isolation.

The force input to the system is applied at the location marked in Fig. 6.1. In the actual experiment, the force is applied through a rotating unbalance shaker which is placed at that point in the system. In order to properly model this force input, which is an internal force in the system, an extra mass is added at that location. A new equation of motion is derived for this new, "proof" mass, which is coupled to the other equations. The disturbance force is then applied between the "proof" mass and the truss. The forcing vector for our system equations of motion ($\mathbf{F}_d$ in Eq. 6.39) can be filled in by finding the generalized forces for each coordinate. Each generalized force can be written as [Meirovitch, 1970]

$$Q_i = \sum_{j=1}^{n} \mathbf{F}_j(t) \cdot \frac{\partial \mathbf{R}_j}{\partial v_i} \tag{6.53}$$

where $\mathbf{F}_j(t)$ are all the forces applied to the system, and $\mathbf{R}_j$ are the vectors describing the point of application of each force. In this case, there are two applied forces in the system, the force applied to the truss, and its equal and opposite reaction force

applied to the proof mass. It is assumed that the forces are applied only in the $\hat{\mathbf{n}}_2$ direction. (The force is actually applied in the $\hat{\mathbf{c}}_2$ direction, but since the angle $\alpha - \phi_1$ is negligible for all cases performed in this work, this assumption is valid.) The generalized forces from the rotating unbalance shaker can be written as

$$Q_i = f_d(t)\hat{\mathbf{n}}_2 \cdot \frac{\partial(x\hat{\mathbf{n}}_1 + y\hat{\mathbf{n}}_2 + l_{f_d}\hat{\mathbf{c}}_1)}{\partial v_i} - f_d(t)\hat{\mathbf{n}}_2 \cdot \frac{\partial(x\hat{\mathbf{n}}_1 + y\hat{\mathbf{n}}_2 + l_{f_d}\hat{\mathbf{c}}_1 + x_p\hat{\mathbf{c}}_2)}{\partial v_i} \quad (6.54)$$

where x_p is the proof mass coordinate. This simplifies to

$$Q_i = -f_d(t)\hat{\mathbf{n}}_2 \cdot \frac{\partial x_p \hat{\mathbf{c}}_2}{\partial v_i} \quad (6.55)$$

By applying the relationship between the $\hat{\mathbf{n}}$ and $\hat{\mathbf{c}}$ coordinate systems (Eqs. 6.1 and 6.3) and taking the dot product, this can be further simplified to

$$Q_i = -f_d(t)\frac{\partial x_p \cos(\alpha - \phi_1)}{\partial x_i} \quad (6.56)$$

For very small angles, the generalized force becomes

$$Q_i = -f_d(t)\frac{\partial x_p}{\partial x_i} \quad (6.57)$$

which is nonzero only if $x_i = x_p$. The disturbance forcing vector, then, only contains a term of -1 on the x_p coordinate.

6.3.1 High-Gain Force Feedback

As before, the first control law applied to the system is feedback of the link forces through a high gain. Even though we are now dealing with a multi-input, multi-output system, this control method acts locally. In other words, each link receives a control signal based only on its own transmitted force. Stability of this method holds, because each link is still a colocated actuator-sensor pair. Even though we have added new poles for the dynamics of the additional actuators, we have not altered the root locus for any given link. The transfer function from any actuator

to its sensor sees pole-zero cancellations for the added actuators (one actuator is cannot affect another).

Figures 6.10 - 6.13 show the results of applying this control technique when a harmonic disturbance of 2 Hz and amplitude of 1 N is applied to the truss. A gain of 1000 is used for each of the links (a link-length gain of 5 is also used). Figures 6.10a through 6.12a show that the forces in each of the links is suppressed. The control voltage required for this performance is shown in Figs.6.10b through 6.12b, and is not found to be excessive. Notice that the transmitted force is highest in link 3, as we would expect, since the disturbance is applied closest to that link in the truss. Also note that the control voltage is proportional to the respective transmitted forces, and it also is highest for link 3. With that in mind, we will only show the responses for link 3 from here on, since this proportionality holds for all the remaining results.

Before moving on to other cases, we will also look at the response of the beams in the system, Fig. 6.13, since the end goal is to reduce the response on the clean side. When the control is begun, the response of beam A (on the clean side) diminishes since it no longer sees a disturbance after the transmitted forces are suppressed. The slow decay is a result of the light damping in the beam. Figure 6.13b shows the (first mode) response of beam B, which is on the dirty side. The response on this side of the system increases, as we would expect since much of the system mass (which sees the disturbance) has been effectively removed.

It was shown in Chapter 5 that the high-gain force feedback technique is not restricted to a particular type of disturbance. This is demonstrated, as before, by applying a broadband disturbance to the truss. Figure 6.14 shows the response of the transmitted force and the required control voltage for link 3 when a disturbance is applied which ranges in frequency from 2 Hz to 10 Hz. The transmitted force is

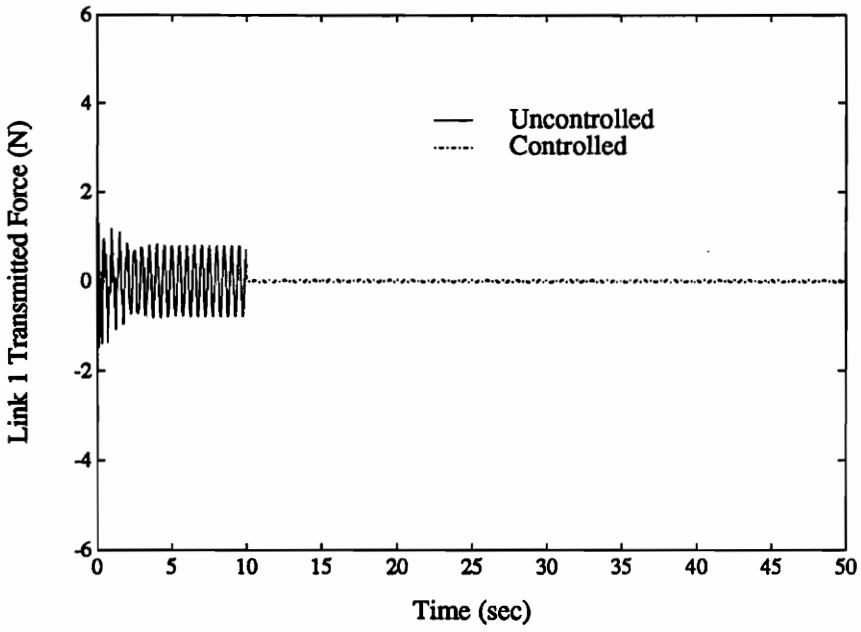

a. Transmitted force in link 1.

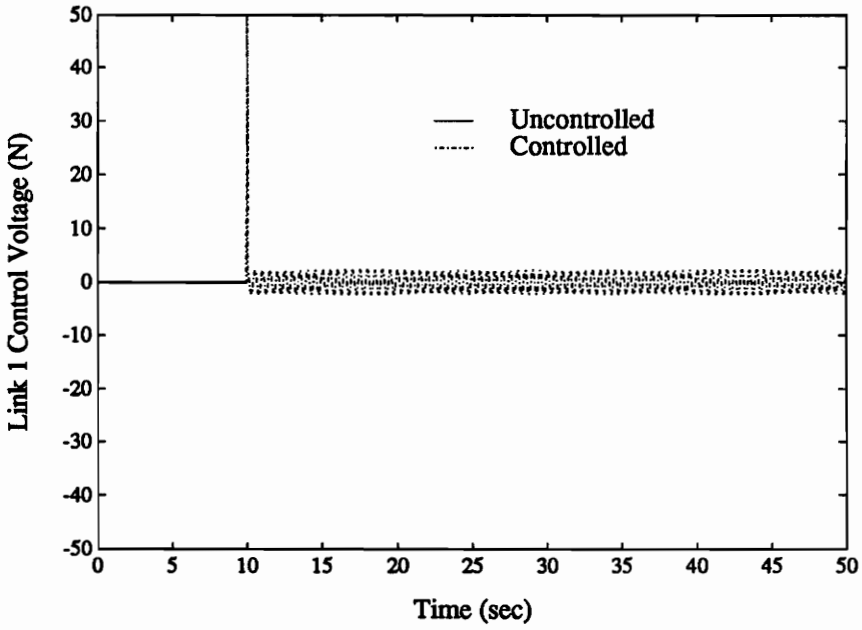

b. Control voltage for link 1.

Figure 6.10: Transmitted force and control voltage for link 1 of the adaptive truss for high-gain force feedback where disturbance is harmonic.

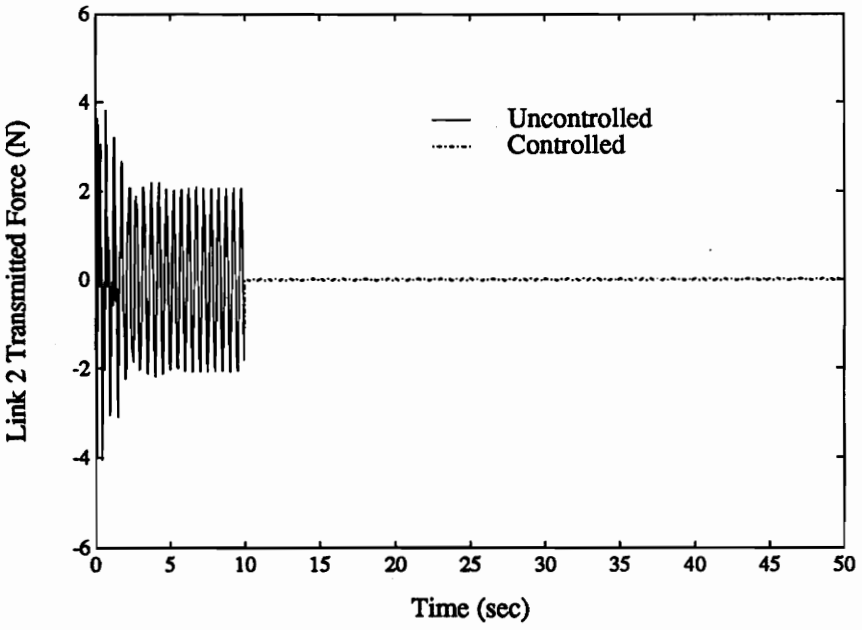

a. Transmitted force in link 2.

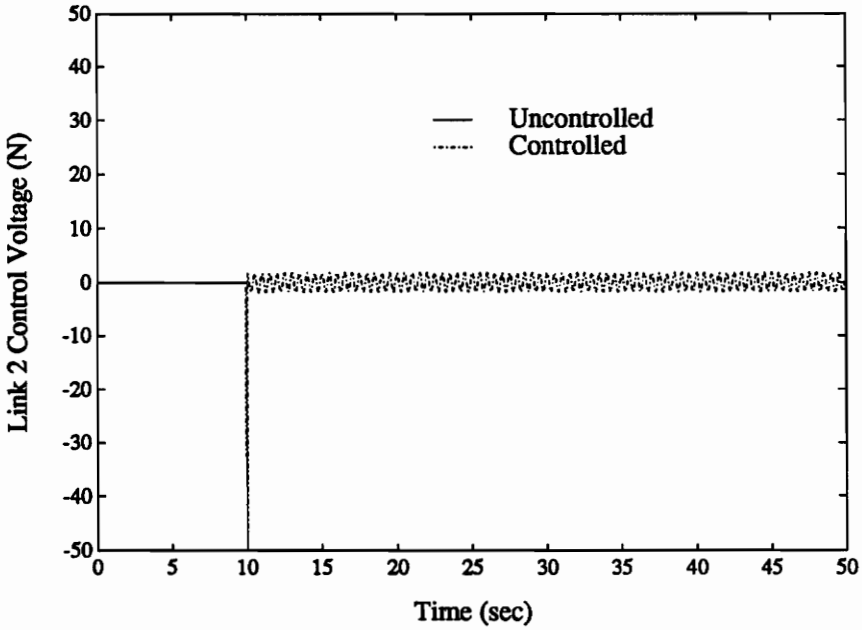

b. Control voltage for link 2.

Figure 6.11: Transmitted force and control voltage for link 2 of the adaptive truss for high-gain force feedback where disturbance is harmonic.

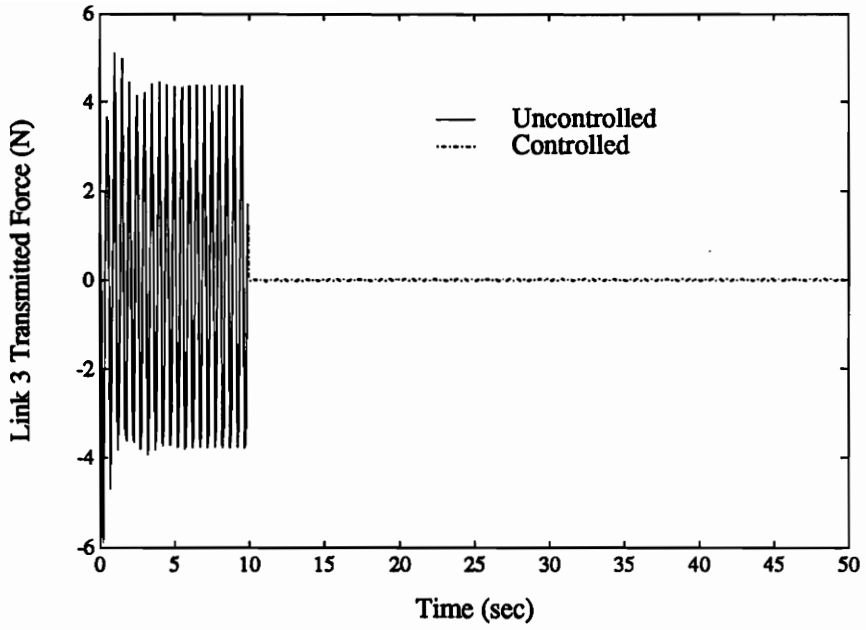

a. Transmitted force in link 3.

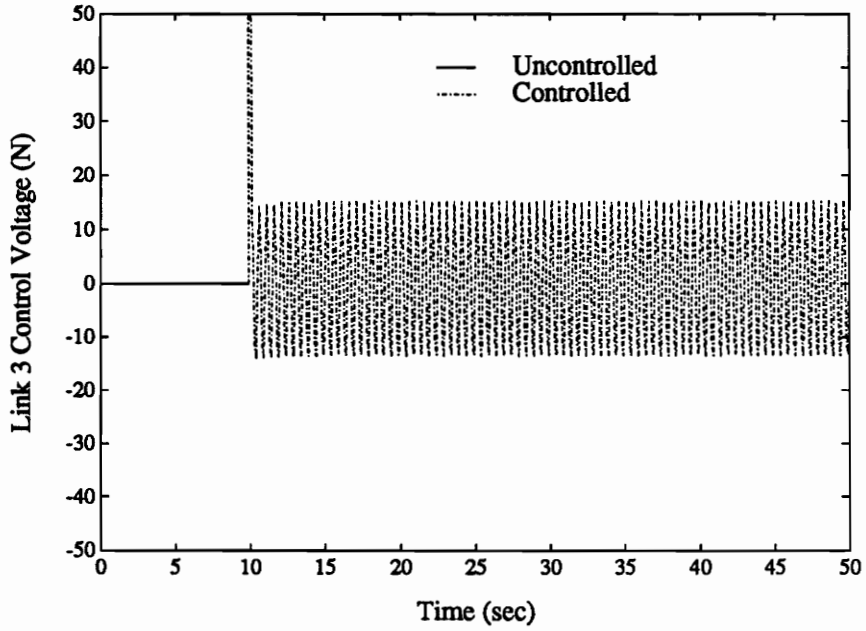

b. Control voltage for link 3.

Figure 6.12: Transmitted force and control voltage for link 3 of the adaptive truss for high-gain force feedback where disturbance is harmonic.

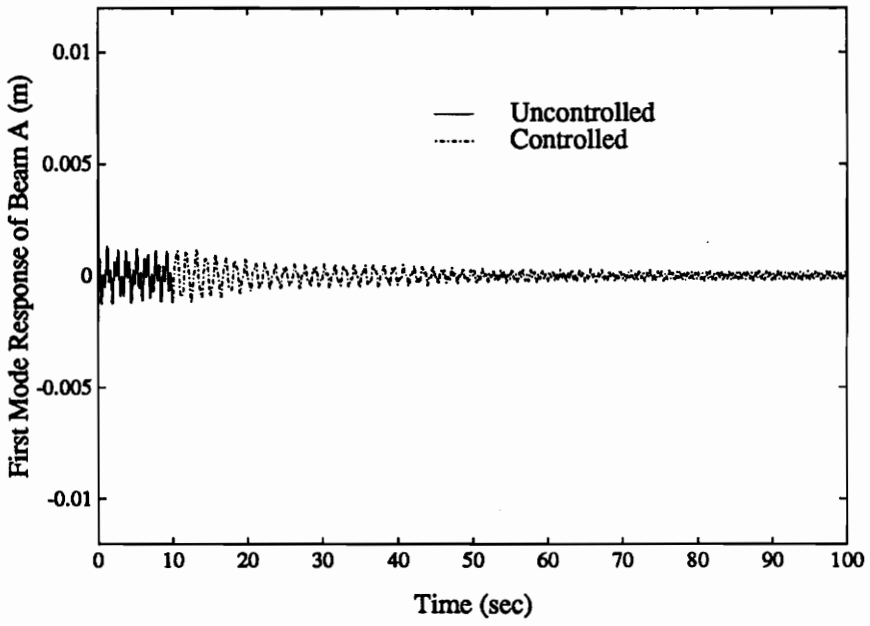

a. Mode 1 displacement of beam A.

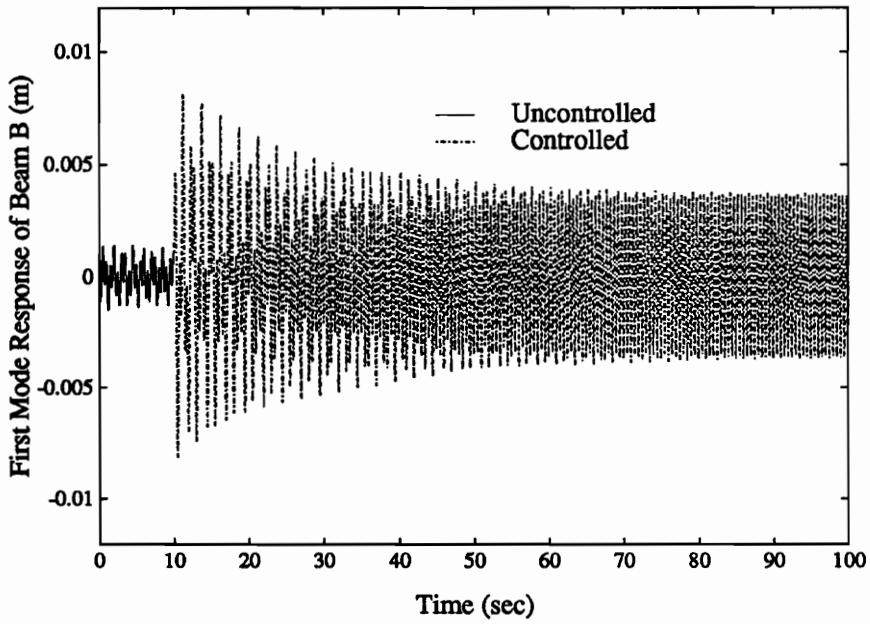

b. Mode 1 displacement of beam B.

Figure 6.13: Beam displacements for high-gain force feedback where disturbance is harmonic.

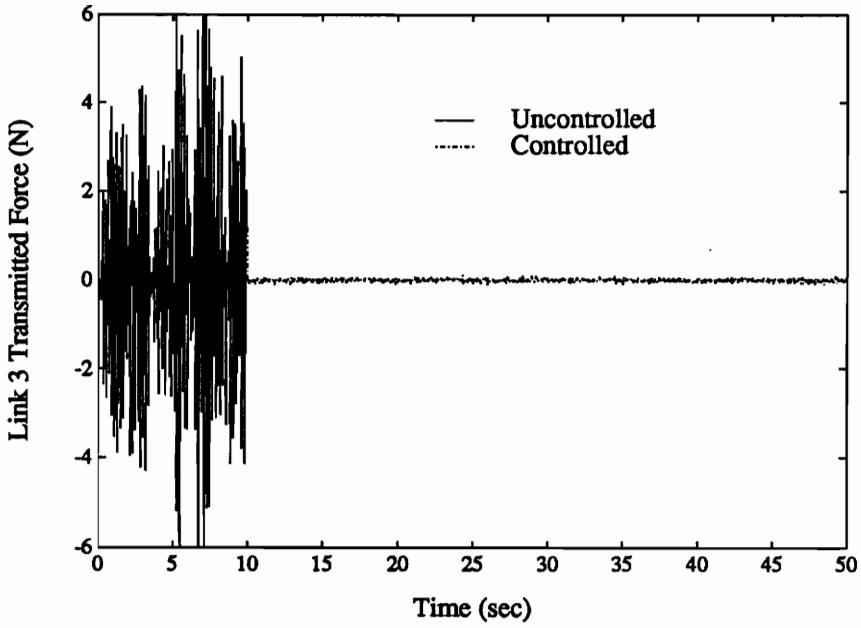

a. Transmitted force in link 3.

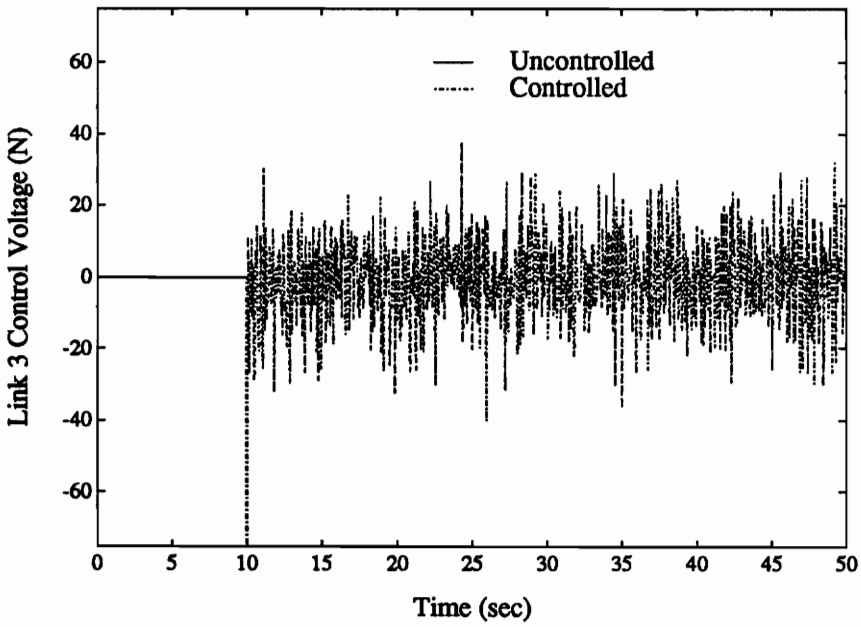

b. Control voltage for link 3.

Figure 6.14: Transmitted force and control voltage for link 3 of the adaptive truss for high-gain force feedback where disturbance is broadband.

suppressed just as for the harmonic case.

6.3.2 Force Feedback Through Classical Compensators

To demonstrate the use of classical compensators for isolation in an adaptive truss, we will use the compensator shown in Eq. 5.2. Each link will have its own controller; the control for any given link will be that link's transmitted force passed through the compensator. Again, stability has not changed now that we are dealing with a multi-input, multi-output system, but remember that stability is not guaranteed for the classical compensators.

Figure 6.15 shows the transmitted force and control voltage for link 3 of the truss. These results are similar to what was found in Chapter 5. The transmitted force is suppressed in steady-state, but has a period of slow decay. The control voltage is similar to that found for the high-gain controller.

6.3.3 LQR/LQG Controllers

The LQR control technique is a true multi-input, multi-output control method. In this case, we develop a cost function based on what we would like to minimize in the system, the transmitted forces, and not based on the system outputs. The assumed output, for cost function purposes, is just like that shown in Eq. 5.5, but it contains two new transmitted forces and two new link length outputs. The resulting gain set is used for control.

Figure 6.16 shows the transmitted force and control voltage for link 3 of the truss when the LQR controller is used for active isolation. We see a suppression of the transmitted force, but, just as in the single mount case, it is not as good as the other two methods. It seems that the LQR controller is attempting to add damping to the system which is hindering the isolation performance. The control voltage

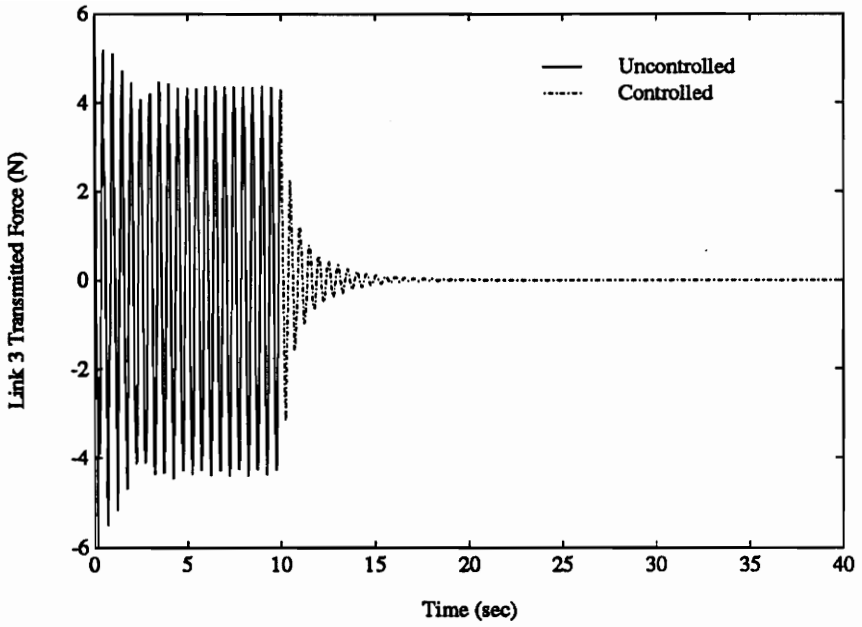

a. Transmitted force in link 3.

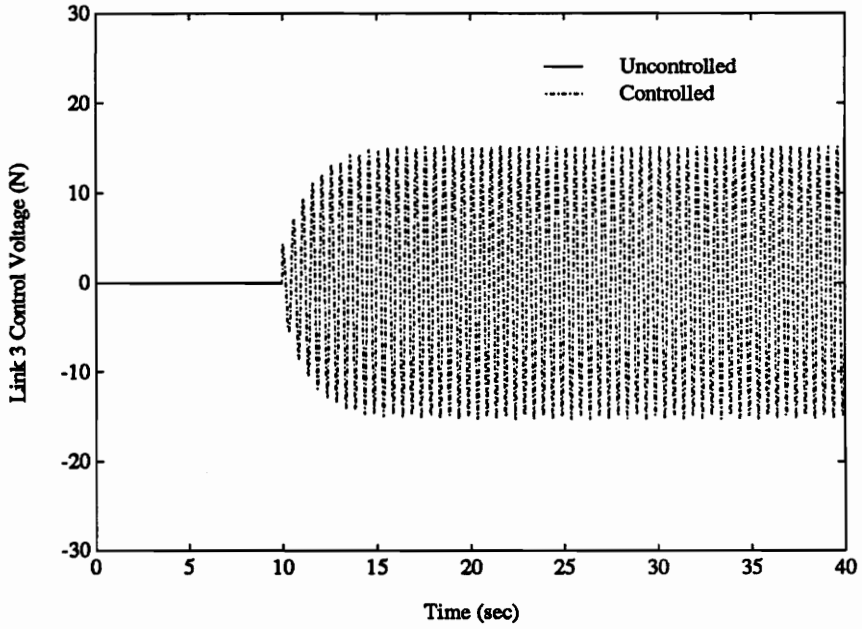

b. Control voltage for link 3.

Figure 6.15: Transmitted force and control voltage for link 3 of the adaptive truss for classical compensation where disturbance is harmonic.

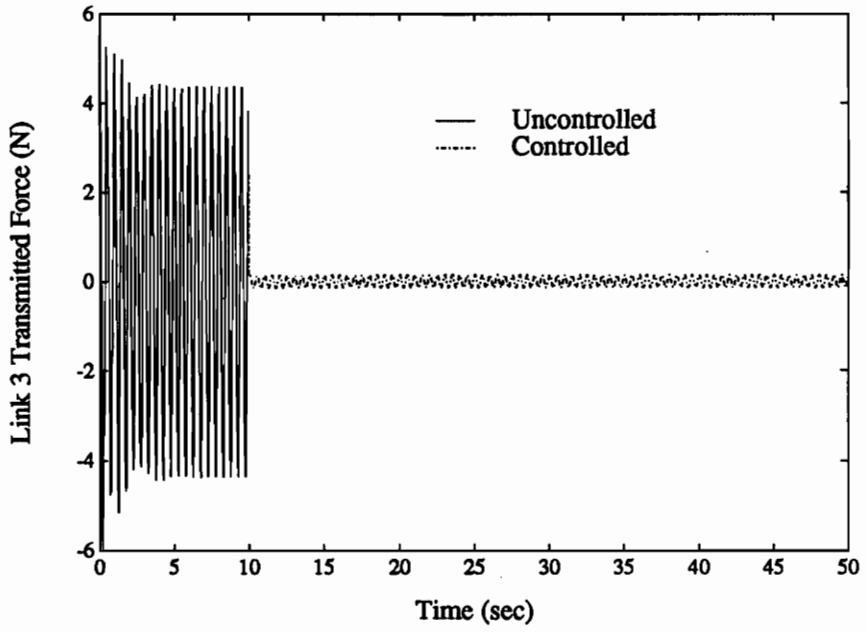

a. Transmitted force in link 3.

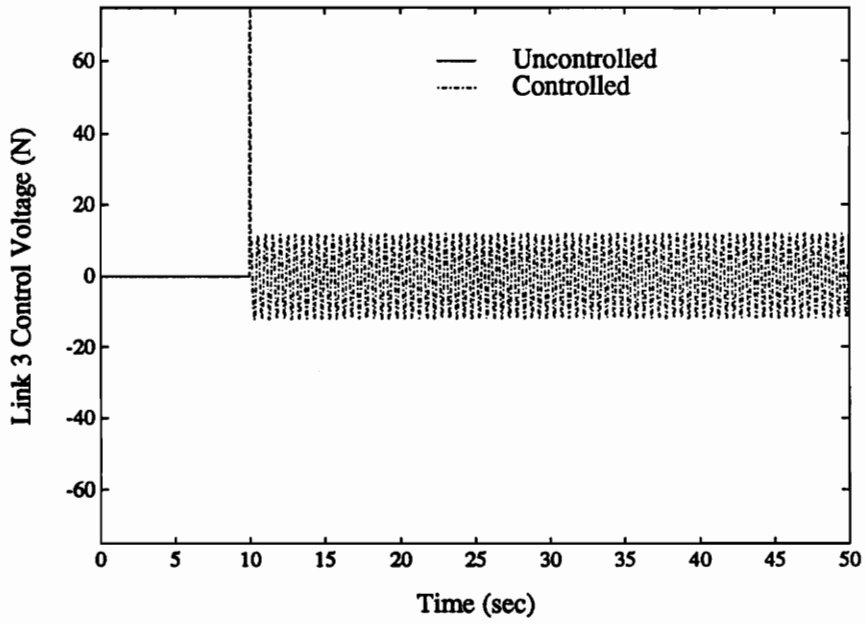

b. Control voltage for link 3.

Figure 6.16: Transmitted force and control voltage for link 3 of the adaptive truss for the LQR technique where the disturbance is harmonic.

required is comparable to the previous two examples.

6.4 Experimental Results

Force feedback was applied to the experimental system using a simple gain applied to each link force. Figures 6.17-6.19 show the resulting link forces. Each figure contains the experimental as well as the corresponding analytical results. The force feedback gains were 1.3, 1.3, and 2.0 V/N (these gains are as high as the links would allow, for reasons discussed below) in links 1, 2, and 3, respectively, and the disturbance was at a frequency of 4.5 Hz and amplitude of approximately 5.8 N. In the experimental results we see reductions in the transmitted force of 66%, 70%, and 55% in the respective links. This can be compared to the analytical results in each figure which show reductions of 72%, 79%, and 60%.

Figure 6.20 shows that the amplitude of vibrations of the beam on the clean side of the system is reduced. This is shown by plotting the root strain of beam A as a function of time (the plot is for longer time than the previous plots to more clearly show the decay in the beam). When the control is turned on, we see that the beam vibrations begin to decrease.

Based on the results shown here, and on the analytical results shown earlier for high-gain force feedback, it would seem reasonable that we should be able to improve the isolation performance by increasing the feedback gains. In the experimental system, however, we cannot increase the gains much beyond what was used to produce Figs. 6.17-6.19. There is a backlash nonlinearity in the motor/ballscrew actuator which is limiting the capability of this system. As the gain becomes higher, an oscillation appears in the motor which causes an oscillation in the force signal that has higher amplitude than the transmitted force from the disturbance. The frequency of the oscillation is the same as that of the axial mode of the link and

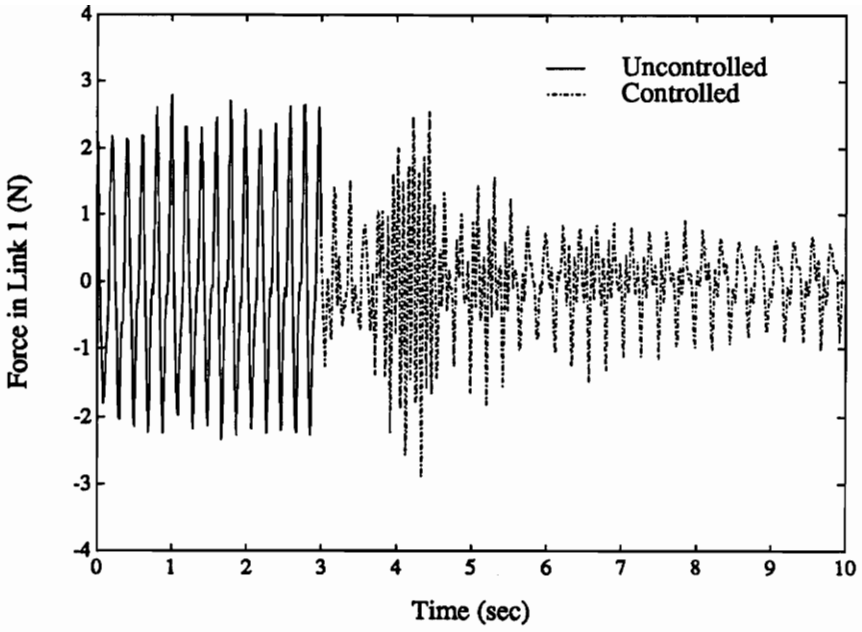

a. Experiment.

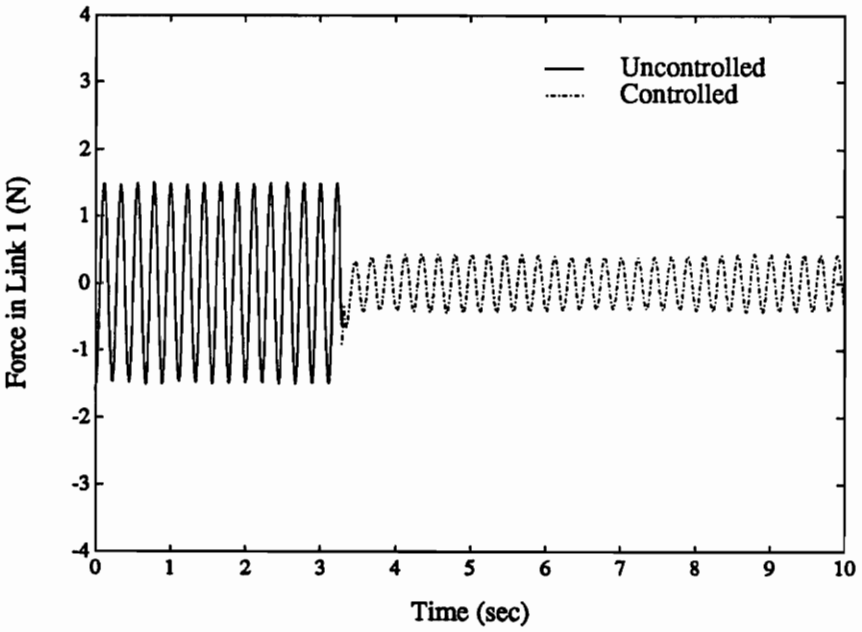

b. Simulation.

Figure 6.17: Experimental and simulated transmitted force in link 1 of the adaptive truss.

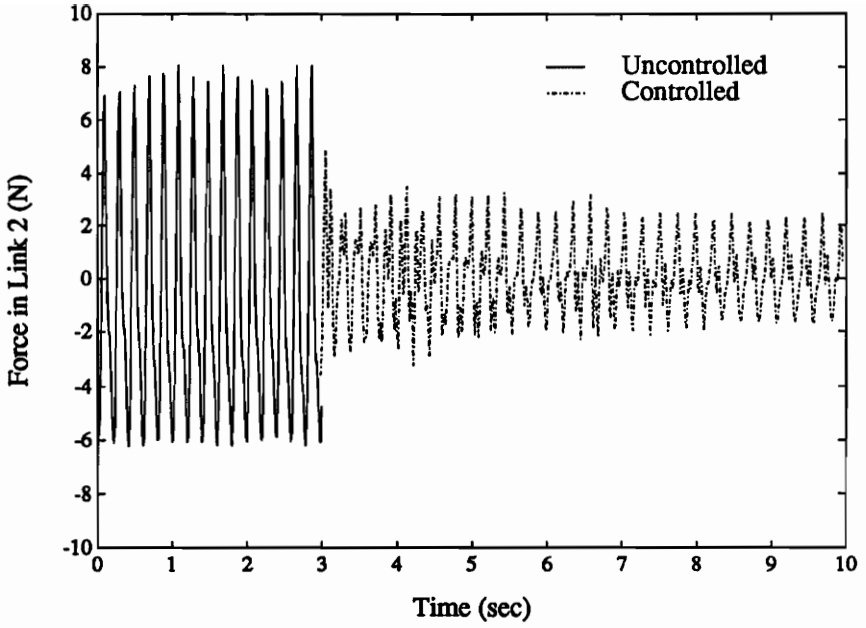

a. Experiment.

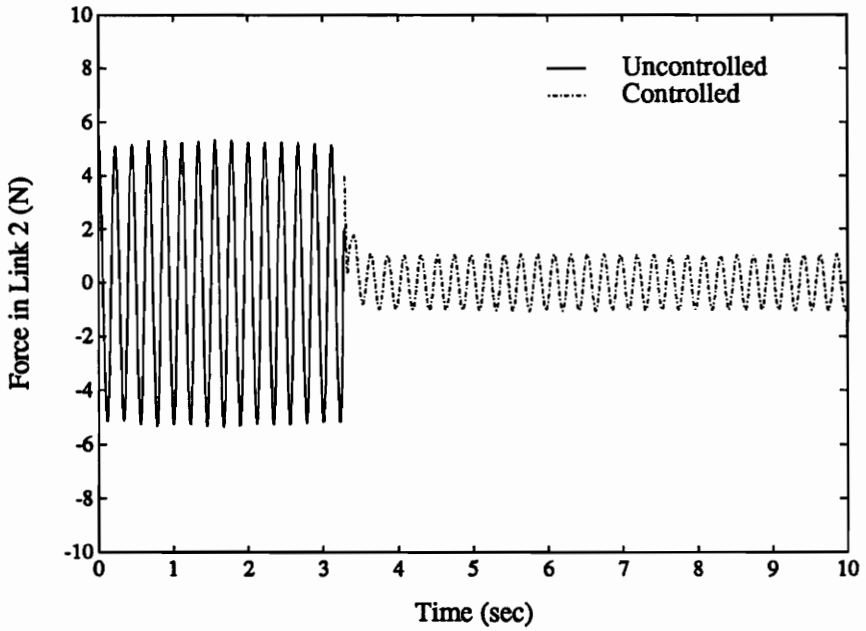

b. Simulation.

Figure 6.18: Experimental and simulated transmitted force in link 2 of the adaptive truss.

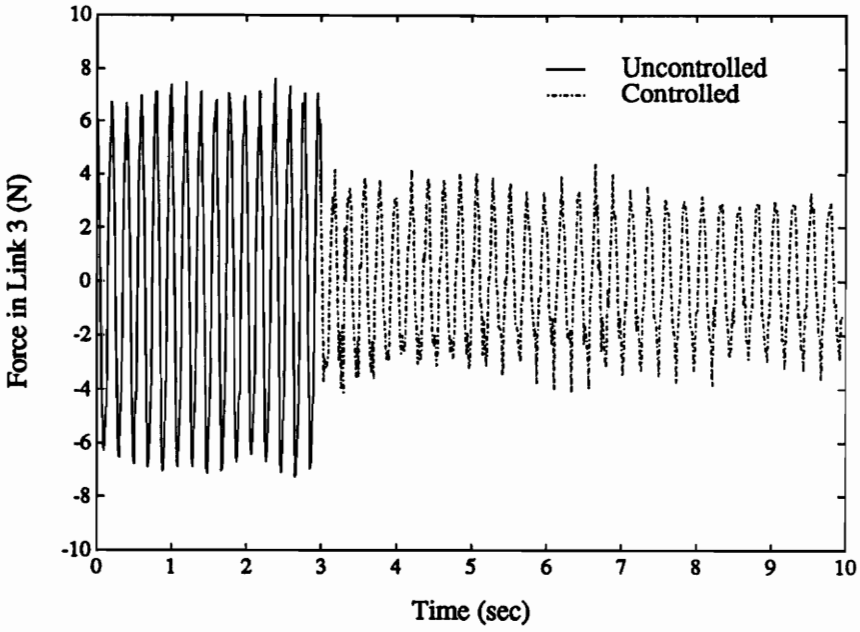

a. Experiment.

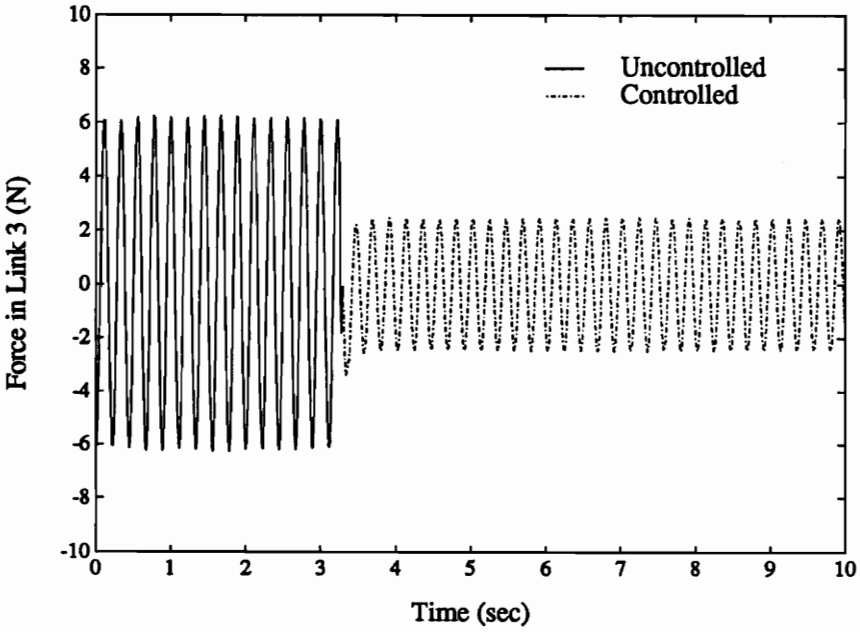

b. Simulation.

Figure 6.19: Experimental and simulated transmitted force in link 3 of the adaptive truss.

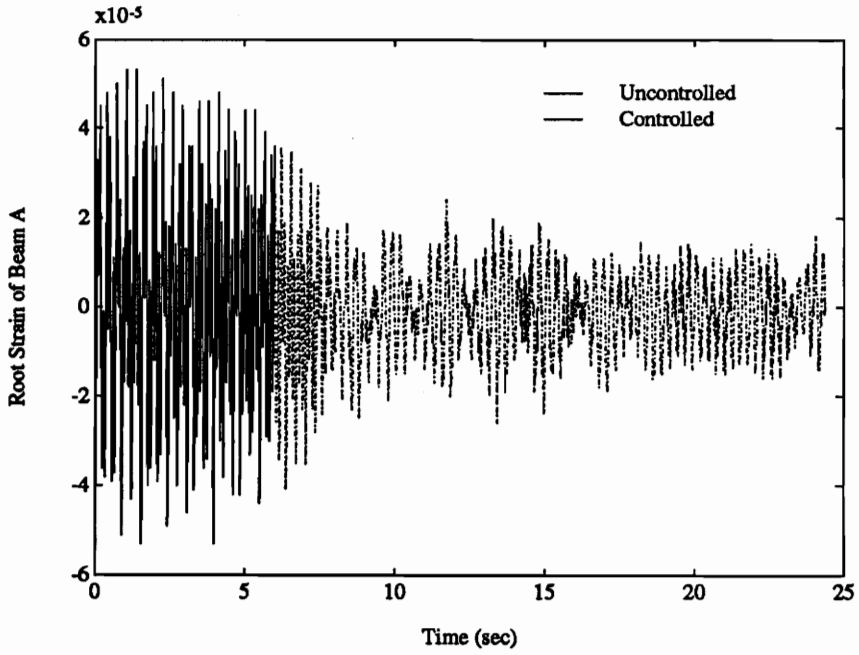

Figure 6.20: Experimental root strain for beam A with harmonic disturbance input.

appears to be due to backlash in the actuator sustaining the transient vibrations of the link's mode.

A backlash nonlinearity would have the effect of applying an impulse-type excitation to the system each time the actuator changes directions. Such an impulse would be repetitive if we were isolating a transient mode of the structure, and would occur at a frequency of the given mode. The fourier series for this type of periodic excitation has harmonics at integer multiples of the fundamental frequency [James, 1989]. So, if we were to look at the frequency content of the transmitted force in the link when this oscillation was occuring, we would expect it to contain peaks evenly spaced in frequency. This is just what we see in Fig. 6.21 which shows the power spectrum of the transmitted link force when the oscillation is occurring (the force-feedback gain is approximately 4 V/N). The fundamental frequency shown in Fig. 6.21 is 40 Hz (which is the natural frequency of the link's axial mode), and the other peaks shown are integer multiples of that frequency.

To show that there is, in fact, a noticeable nonlinearity in the active link, Fig. 6.22 shows the time history of the transmitted force generated in the link when the motor is driven with a 1.5 Hz harmonic input (with amplitude of 2.5 volts). The resulting output is quite a bit different from the sine-wave voltage input. The two plots are out of phase by about 90°, because of the actuator dynamics. We see that as the voltage is changing signs, the transmitted force signal receives some type of transient input, most likely an impulsive-type input from backlash.

When direct feedback of the transmitted force is used for control, the backlash seems to be sustaining the transient oscillations of the link. Each time the motor moves to eliminate the transient forces in the link, it applies another impulse and excites the transient mode again. The resulting forces become higher than the disturbance forces in the mount.

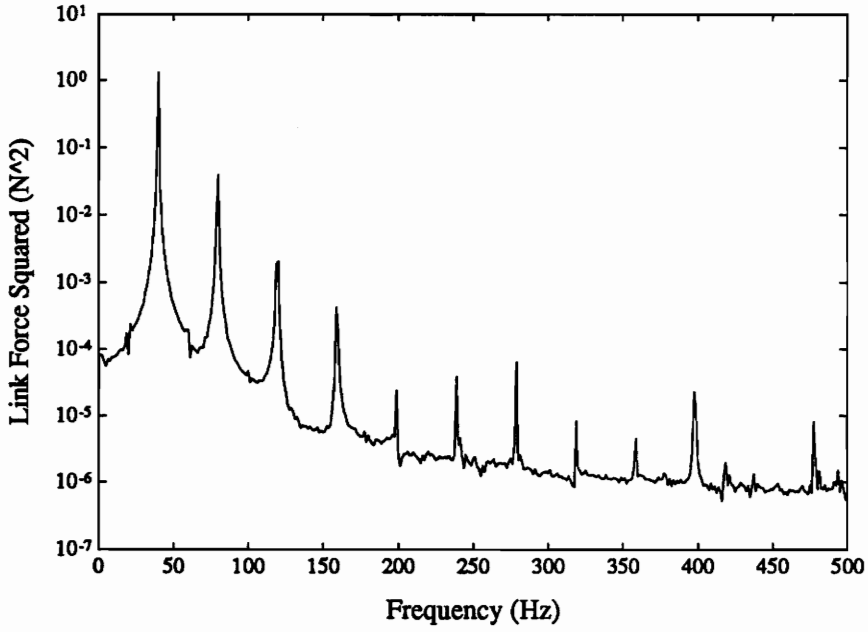

Figure 6.21: Power spectrum of the transmitted force with sustained motor oscillation.

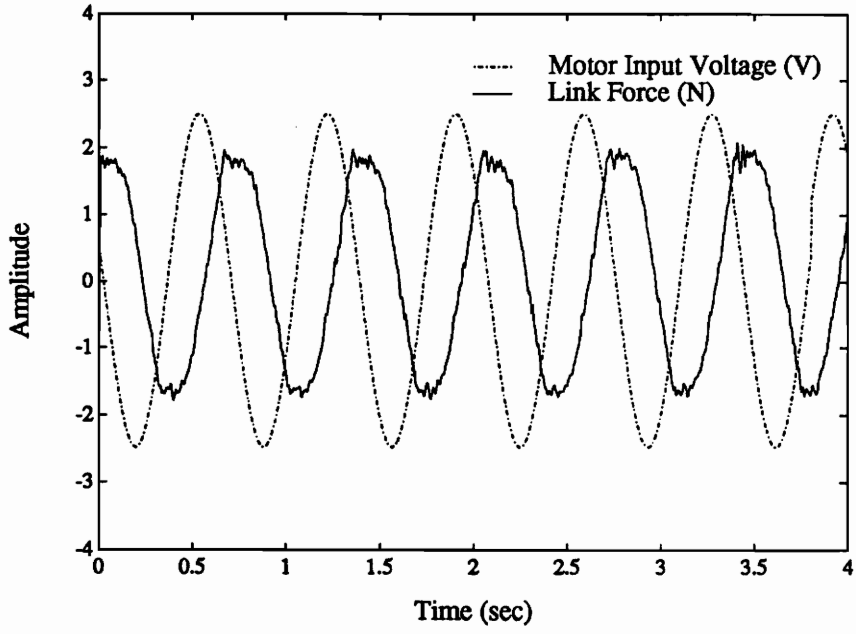

Figure 6.22: Transmitted force output for voltage input to active link showing non-linear effect.

It is not clear how to solve this problem so that higher gains may be used for vibration isolation. "Tightening" the existing system to eliminate the backlash would seem to be an appropriate place to start, or a better approach may be to use an actuator which contains no mechanical backlash.

Chapter 7

Conclusions and Recommendations

7.1 Conclusions

The goal of this work was to find control methods with which to use adaptive trusses for vibration isolation. It began as an investigation into previous techniques presented in the literature for active vibration isolation, to see how these techniques may be extended to the multi-input multi-output application of adaptive trusses. The focus was on techniques which do not require detailed knowledge of the disturbance (assuming no disturbance measurement is available), and if possible, limited knowledge of the system. This ruled out the possibility of feedforward techniques such as the LMS algorithm, which has been documented for its performance in active vibration isolation, but which requires a measure of the disturbance. So the investigation centered around feedback techniques.

It was shown that force feedback can be used to provide complete vibration isolation (with the proper control method) in two directions across an active mount. The analysis was shown to be independent of the type of active mount used, whether it is in serial or parallel with the passive mount, or whether the actuator is displacement- or force-commanded. The actual choice of actuator and mount arrangement will de-

pend on the physical requirements of the system. It was shown, however, that the analysis of the control system may provide some guidance in the design of the passive mount.

The first techniques studied were classical compensation methods introduced by Sievers and von Flotow (for a vibration isolation application) and which have been implemented in the past using Shaw's HHC controller. Two forms of classical compensators are presented in this work, and are implemented explicitly in the feedback loop. The first has the same form as that produced by the HHC method, while the second is an extension of the first where feedthrough of the output is added to provide another zero in the compensator. These methods, when implemented explicitly, require no system model, and only require knowledge of the disturbance frequency. They provide excellent performance, if they are placed correctly in the frequency domain, but neither is guaranteed to be stable. An additional benefit of these compensators is that since they provide high gain over a small portion of the frequency domain, there is less amplification of noise in the measurement which may occur at frequencies away from the disturbance. These types of compensators are useful only for disturbances which are harmonic, or which are narrowband in nature. Extension of these compensators to address broadband disturbances, or disturbances with multiple harmonics, is difficult to do with limited system knowledge, primarily because stability begins to break down even further.

In studying the various forms of classical compensators which could be used for vibration isolation, it was found that the best compensator is also the simplest, a gain. This is the most important contribution of this work. It was shown that force feedback with a simple gain in the loop provides excellent vibration isolation performance, is guaranteed to be stable, requires no model of the system, requires no knowledge of the applied disturbance, is not restricted to any given type of

disturbance, and is easily implemented in an adaptive truss.

The disadvantages to high-gain force feedback are both rooted in the fact that such a high gain is required for good performance. If a static load is a requirement of the active mount, then care must be taken to eliminate the dc component from the force measurement so that it does not enter the control. There is also a possibility of amplifying noise in the signal. It has been discussed here that noise may be addressed, while maintaining stability, through the use of filters made up entirely of real poles and zeros.

The third technique presented here is the LQR method, with disturbance modelling, a technique which has been used in the past for vibration control. A method is presented here for using the LQR method for vibration isolation. The idea is to attempt to achieve, with guaranteed stability, the excellent performance of the classical techniques, while keeping the loop gains low. The overhead for these benefits is, of course, an accurate system model. It was shown that this method works, however the performance is not as good as expected. It is believed that the difference in performance is due to an increase in active damping which is inadvertently provided by the LQR method, as well as the difficulty in properly placing a notch in the system's frequency response. It is interesting to note, though, that as the penalties are increased in the LQR formulation, the resulting gain set begins to look more and more like simple high-gain feedback.

Each of the active vibration isolation methods mentioned above are implemented on a model of a real flexible structure through an adaptive truss. The modelling procedure was developed from standard energy methods, and incorporated both the dynamics and kinematics of the flexible truss. The resulting model agreed favorably with experimental data from the actual system. Even though the procedure is quite cumbersome, the results are good enough to warrant further investigation of this

technique for modelling other (more complicated) adaptive trusses.

Finally, it was shown that force feedback through a gain provided vibration isolation when implemented experimentally in an adaptive truss. The experimental results agreed with those of the analysis. It was found, though, that mechanical backlash in the active links of the adaptive truss limited the performance of the high-gain force feedback method.

7.2 Recommendations

It seems appropriate that at the "end" of a project such as this, there would be just as many (if not more) unanswered questions as there were at the beginning. It is not that we take away from the knowledge of the world, or even call it a draw, but rather through the progress of the work, we begin to see more clearly the correct questions to ask. So it is with this work. Below is a summary of the recommendations for extensions to this work, based on the conclusions presented above.

It was concluded that the best method, in terms of simplicity and stability, for using force feedback for active vibration isolation is to apply a high feedback gain. This method works if the actuator and sensor are colocated, a requirement which is met when adaptive trusses are used. Not all isolation applications, however, lend themselves to this discretization of the actuator. Consider, for example, the transmission of forces from a bearing into the structure in which it is mounted. The forces in such a case will be distributed around the bearing, and not restricted to the axial forces of a truss' members. Force feedback could be useful in such a situation, but questions would need to be answered such as: How do the colocated results apply to the distributed input/output case? How can we implement a distributed actuator and sensor? Would it be better to break up the problem into many, very small, actuator/sensor pairs? How effective could a low number of discrete actuators

be in such a case?

An important issue in all of the controllers used in this work is stability. For the case of high-gain force feedback, stability was shown to hold based on discussions of the characteristics of the undamped system. To the author's knowledge, stability for colocated actuator/sensor pairs has never been shown for damped systems. This question can be extended if we consider the effect of real axis poles and zeros. Based on the examples considered in this work, it seems that stability is not adversely affected by real axis poles and zeros, but this needs to be addressed. Since many controllers today are implemented with digital computers, it would seem pertinent to address these issues in the z-plane as well.

This work focused on the use of force feedback for vibration isolation. It is possible to use other measures, such as acceleration, to drive a feedback controller. Even though it was discussed here how acceleration measurements provide "one-way" isolation as opposed to the "two-way" isolation of force feedback, there are instances where one-way isolation is sufficient. It seems that acceleration measurements could be used in feedforward control schemes for vibration isolation. There are questions of how to do this, as well as when the dynamics on the clean side become great enough to cause the feedforward acceleration signal to act like feedback, a potentially destabilizing situation.

It seems that improvements could be made to the method presented for using the LQR technique for vibration isolation. There should be some way to pose the cost function, perhaps in terms of the accelerations in the system rather than the forces, to derive better performance from the method. The reason for lack of performance should be investigated, and if it is found to be because of damping added by the controller, then methods should be addressed to keep that from happening.

Finally, before the full potential of the high-gain method is realized, the problem

of mechanical backlash in the actuator must be overcome. The motor/ballscrew actuator should be investigated to determine the source of the backlash, and to find a way to eliminate it. Other active mount designs should be investigated to find those which do not contain this backlash problem.

References

1. Anton, H., *Elementary Linear Algebra*, John Wiley & Sons, Inc., New York, NY, 1981.

2. Astrom, K.J., and B. Wittenmark, "On Self Tuning Regulators," *Automatica*, Vol. 9, pp. 185-199, 1973.

3. Astrom, K.J., and B. Wittenmark, *Adaptive Control*, Addison-Wesley Publishing Company, Reading, MA, 1989.

4. Beckwith, T.G., N.L. Buck, and R.D. Marangoni, *Mechanical Measurements*, Addison Wesley Publishing Company, Reading, MA, 1982.

5. Beer, F.P. and E.R. Johnston, Jr., *Mechanics of Materials*, McGraw-Hill Book Company, New York, NY, 1981.

6. Chalam, V.V., *Adaptive Control Systems Techniques and Applications*, Marcel Dekker, New York, NY, 1987.

7. Cheok, K.C., H.X. Hu, and N.K. Loh, "Discrete-Time Frequency-Shaping Parametric LQ Control with Application to Active Seat Suspension Control," *IEEE Transactions on Industrial Electronics*, Vol. 36, No. 3, August 1989, pp. 383-390.

8. Clark, W.W., H.H. Robertshaw, and T.J. Warrington, "A Comparison of Actuators for Vibration Control of the Planar Vibrations of a Flexible Cantilevered Beam," *Journal of Intelligent Material Systems and Structures*, Vol. 1, No. 3, July 1990, pp. 289-308.

9. Clark, W.W., B. Kimiavi, and H.H. Robertshaw, "Control of Flexible Beams Using a Free-Free Active Truss," *Adaptive Structures*, ASME, edited by B.K. Wada, 1989, pp. 61-68.

10. Crosby, M.J., and Karnopp, D.C., "The Active Damper – A New Concept for Shock and Vibration Control," *43rd Shock and Vibration Bulletin*, Part H, 1973.

11. Den Hartog, J.P., *Mechanical Vibrations*, Dover Publications, Inc. New York, NY, 1985.

12. Elliot, S.J., I.M. Strothers, and P.A. Nelson, "A Multiple Error LMS Algorithm and Its Application to the Active Control of Sound and Vibration," *IEEE Transactions on Acoustics, Speech, and Signal Processing*, Vol. Assp-35, No. 10, pp. 1423-1434, 1987.

13. Electro-Craft Corporation, *DC Motors, Speed Controls, and Servo Systems*, Electro-Craft Corporation, Hopkins, MN, 1980.

14. Eyerman, C.E., "A Systems Engineering Approach to Disturbance Minimization for Spacecraft Utilizing Controlled Structures Technology," M.S. Thesis, Massachusetts Institute of Technology, June 1990.

15. Fuller, C.R., R.J. Silcox, V.L. Metcalf, and D.E. Brown, "Experiments on Structural Control of Sound Transmitted Through An Elastic Plate," *Proceedings of the American Control Conference*, Pittsburgh, PA, 1989, pp. 2079-2084.

16. Fuller, C.R., C.H. Hansen, and S.D. Snyder, "Experiments on Active Control Of Sound Radiation From A Panel Using A Piezoceramic Actuator," submitted for publication to *Journal of Sound and Vibration*, 1989.

17. Gevarter, W.B., "Basic Relations for Control of Flexible Vehicles," *AIAA Journal*, vol. 8, no. 4, pp. 666-672, 1970.

18. Gupta, N.K., "Frequency-Shaped cost functionals: extension of linear quadratic gaussian design methods," *Journal of Guidance and Control*, vol. 3, no. 6, pp. 529-535, 1980.

19. Gupta, N.K. and R.W. Du Val, "A New Approach for Active Control of Rotorcraft Vibration", *Journal of Guidance and Control*, vol. 5, no. 2, pp. 143-150, 1982.

20. Hall, S.R. and N.M. Werely, "Linear Control Issues in the Higher Harmonic Control of Helicopter Vibrations," *Proceedings of the 45th Annual Forum of the American Helicopter Society*, pp. 955-971, 1989.

21. Interlink Electronics, Technical Data on Force Sensing Resistors, Interlink Electronics, Carpinteria, CA, 1991.

22. Jacobs, O.L.R., "Introduction to Adaptive Control," *Self-Tuning and Adaptive Control: Theory and Applications*, H. Nicholson and B.H. Swanick, Eds., Peter Peregrinus Ltd., London, UK, 1981.

23. James, M.L., G.M. Smith, J.C. Wolford, and P.W. Whaley, *Vibration of Mechanical and Structural Systems: With Microcomputer Applications*, Harper & Row, Publishers, New York, NY, 1989.

24. Johnson, W. "Self-tuning regulators for multicyclic control of helicopter vibration," NASA Technical Paper 1996, 1982.

25. Kaplow, C.E., and J.R. Velman, "Active Local Vibration Isolation Applied to a Flexible Space Telescope," *Journal of Guidance and Control*, Vol. 3, No. 3, 1980, pp. 227-233.

26. Karnopp, D.C., "Active and Passive Isolation of Random Vibration," *Isolation of Mechanical Vibration, Impact, and Noise*, ASME Design Engineering Conference, Cincinnati, OH, 1973, pp. 64-68.

27. Kwakernaak, H. and R. Sivan, *Linear Optimal Control Systems*, Wiley Interscience, New York, 1972.

28. Laskin, R.A., J.M. Estus, Y.H. Lin, J.T. Spanos, and C.M. Satter, "NASA Office of Space Science and Applications study on space station attached payload pointing," *Proceedings of the AIAA Guidance, Navigation, and Control Conference*, pp. 430-443, 1988.

29. Maciejowski, J.M., *Multivariable Feedback Design*, Addison-Wesley Publishing Company, Wokingham, England, 1989.

30. Martin, G.D., "On the Control of Flexible Mechanical Systems," Ph.D. Thesis, Stanford University, 1978.

31. Meirovitch, L. *Methods of Analytical Dynamics*, McGraw-Hill Book Company, New York, NY, 1970.

32. Miller, S.K., "Adaptive Filtering for Active Isolation of Machinery," M.S. Thesis, Massachusetts Institute of Technology, May 1989.

33. Scribner, K. B., "Active Narrow Band Vibration Isolation of Machinery Noise from Resonant Substructures," M.S. Thesis, Massachusetts Institute of Technology, September, 1990.

34. Shaw, J. and N. Albion, "Active Control of Helicopter Rotor for Vibration Reduction," *Journal of the American Helicopter Society*, vol. 26, no. 3, pp. 32-39, 1981.

35. Shaw, J., N. Albion, E.J. Hanker, and R.S. Teal, "Higher harmonic control: wind tunnel demonstration of fully effective vibratory hub force suppression," *Journal of the American Helicopter Society*, vol. 34, no. 1, pp. 14-25, 1989.

36. Sievers, L.A., and A.H. von Flotow, "Linear Control Design for Active Vibration Isolation of Narrow Band Disturbances," Proceedings of the 27th Conference on Decision and Control, December, 1988, pp. 1032-1037.

37. Sievers, L.A. and A.H. von Flotow, "Comparison and extensions of control methods for narrowband disturbance rejection," Presented at the 1990 ASME Winter Annual Meeting, November 1990.

38. Sunwoo, M., K.C. Cheok, and N.J. Huang, "Application of Model Reference Adaptive Control To Active Suspension Systems," *Proceedings of the 1990 American Control Conference*, May 1990, pp. 1340-1346.

39. Sunwoo, M., and K.C. Cheok, "An Application of Explicit Self-Tuning Controller To Vehicle Active Suspension Systems," *Proceedings of the 29th Conference on Decision and Control*, December, 1990, pp. 2251-2257.

40. Thompson, A.G., "An Active Suspension with Linear Optimal State Feedback," *Vehicle System Dynamics*, Vol. 5, 1976, pp. 187-203.

41. Thomson, William T. *Theory of Vibration with Applications*, Second Ed., Prentice Hall, Englewood Cliffs, NJ, 1981.

42. von Flotow, A.H., "An Expository Overview of Active Control of Machinery Mounts," *Proceedings of the 27th Conference on Decision and Control*, pp. 2029-2032, December, 1988.

43. Warrington, T.J., W.W. Clark, and H.H. Robertshaw, "The Analysis and Large-Angle Control of a Flexible Beam Using an Adaptive Truss," Proceedings of the 1990 American Control Conference, San Diego, CA, 1990, pp. 2190-2196.

44. Widrow, B., P. Mantley, L Griffiths, and B. Goode, "Adaptive antenna systems," *Proc. IEEE*, vol. 55, pp. 2143-2159, December, 1967.

45. Widrow, B., "Adaptive Filters," *Aspects of Network and System Theory*, R. Kalman and N Declaris, Eds., Holt, Rinehart, and Winston, 1971, pp. 563-587.

46. Widrow, B., et. al., "Adaptive noise cancelling: principles and applications," *Proceedings of the IEEE*, vol. 63, no. 12, pp. 1692-1716, 1975.

47. Widrow, B., S.D. Stearns, *Adaptive Signal Processing*, Prentice-Hall, Englewood Cliffs, NJ, 1985.

48. Wie, B., and A.E. Bryson, Jr., "Modelling and Control of Flexible Space Structures," Proceedings of the 3rd VPI&SU/AIAA Symposium on Dynamics and Control of Large Flexible Spacecraft, Blacksburg, VA, 1981, pp. 153-174.

49. Wynn, R.H. Jr. and H.H. Robertshaw, "The Control of Flexible Structure Vibrations Using a Cantilevered Adaptive Truss," Proceedings of the 32nd Structures, Structural Dynamics, and Materials Conference, Baltimore, MD, 1991, pp. 2280-2289.

Vita

The author was born in Clifton Forge, Virginia on April 10, 1963, and grew up on a beef farm in Bath County. He was drawn to the field of Engineering partly through his fascination of the workings of agricultural machinery. He received a Bachelor of Science degree in Mechanical Engineering from VPI&SU in 1986, followed by a Master of Science degree in Mechanical Engineering from VPI&SU in 1988. He is about to begin a new phase of his life as he will soon become an Assistant Professor of Mechanical Engineering at the University of Pittsburgh, and a few short months later, Lord willing, a father. We can never be certain about the future, but if all goes well, the circle will be completed and the author and his wife will eventually find themselves back on the farm bringing calves into the world.